NOTICE

The quality of this microform is heavily dependent upon the quality of the original thesis submitted for microfilming. Every effort has been made to ensure the highest quality of reproduction possible

If pages are missing, contact the university which granted the degree.

Some pages may have indistinct print especially if the original pages were typed with a poor typewriter ribbon or if the university sent us an inferior photocopy.

Reproduction in full or in part of this microform is governed by the Canadian Copyright Act, R.S.C. 1970, c. C-30, and subsequent amendments.

AVIS

La qualité de cette microforme dépend grandement de la qualité de la thèse soumise au microfilmage. Nous avons tout fait pour assurer une qualité supérieure de reproduction.

S'il manque des pages, veuillez communiquer avec l'université qui a conféré le grade.

La qualité d'impression de certaines pages peut laisser à désirer, surtout si les pages originales ont été dactylographiées à l'aide d'un ruban usé ou si l'université nous a fait parvenir une photocopie de qualité inférieure.

La reproduction, même partielle, de cette microforme est soumise à la Loi canadienne sur le droit d'auteur, SRC 1970, c. C-30, et ses amendements subséquents.

Canada

Vibration Analysis of Rotary Arm Actuator and Rotor in Computer Hard Disk Drive

Muhammad Babar Khan

A Thesis

in

The Department

of

Mechanical Engineering

Presented in Partial Fulfillment of the Requirements
for the Degree of Master of Engineering at
Concordia University
Montreal, Quebec, Canada

February 1989

ISBN 0-315-51398-5

ABSTRACT

Vibration Analysis of Rotary Arm Actuator and Rotor in Computer Hard Disk Drive

Muhammad Babar Khan

The objective of this thesis is to study the dynamic behavior of swinging arm actuator and the rotor in a computer hard disk drive. The swinging arm actuator is used for head positioning in magnetic disk storage devices. The rotor consists of a series of circular hard disks mounted on a shaft, which in turn is supported on ball bearings at its ends. During the read/write operation, the head mounted on the swinging arm is subjected to step displacement in moving between tracks and a sinusoidal track runout, which triggers the servomechanism controlling the actuator to correct the head position.

The system equations, which takes into consideration the pivot clearance and the pivot bearing elasticity, are solved using matrix exponential technique. The time variation of the head positioning error, and bearing response, are presented and discussed. A parametric study is carried out to find the effect of various parameters on system stability.

Finite element modelling is carried out for a swinging arm structure. Natural frequencies and mode shapes for such a structure are determined.

Dynamic behaviour of the disk rotating mechanism is studied by solving the equations of motion. The natural frequencies and mode shapes are obtained by solving the homogeneous form of the equations. The response of the system is obtained by solving the non homogenous problem using modal analysis.

ACKNOWLEDGEMENT

The author is sincerely grateful to his thesis supervisor Dr. R. B. Bhat for his excellent guidance, help, and continuous encouragement during the course of this work.

The help and assistance provided by friends and colleagues, espacially by Mr. Ashok Kaushal and Mr. Vineet Gupta is gratefully acknowledged. Special thanks are due to Dr. Santosh Neriya for his suggestions and guidance.

Finally, the author is grateful to his parents for their abundant moral support and understanding throughout the course of this investigation.

TABLE OF CONTENTS

NOMENCLATURE

a	amplitude of track runout
c	damping coefficient of the pivot bearing
[C]	damping matrix
E	Young's modulus of elasticity
E_h	head positioning error
F	contact force at the pivot
F_m	driving force
G	modulus of rigdity or shear modulus
h	thickness of beam
I	moment of inertia of beam cross-section
I_1 to I_8	moment of inertia of disks
J	moment of inertia of rotary actuator
K	radial spring constant
K_1 & K_2	constants of servo mechanism
k_1 to k_8	shaft stiffnesses
L	length of beam
l	moving carriage length
M	mass
m_1 to m_8	mass of disks
m_1e_1 to m_8e_8	mass unbalances
P_h	head position

P	pivot bearing center
P_c	drive point
$[P]$	principal coordinate
R	amplitude ratio
r	radial clearance
T_m	motor torque
$[X]$	generalized coordinate
$x_1 \quad x_8$	displacement
y_g	parallel displacement component of moving carriage
Y_h	head displacement
Y_p	bearing displacement
y_{tr}	track displacement (track runout)
Y_{kmax}	bearing minimum elastic deformation
$y_1 \quad y_8$	displacement
Z_1	displacement of centriod
Z_2	velocity
Z_3	relative displacement of head w.r.t centriod
Z_4	velocity
ω	rotational speed
ν	Poisson's ratio
ρ	density of the material
Ω	non-dimensional angular velocity
ζ	damping ratio

θ	angular displacement component of moving carriage
λ_i	eigen value
$[\phi]$	eigen vector
θ_1 to θ_8	angle of twist due to torque acting on the shaft

LIST OF FIGURES

LIST OF TABLES

CHAPTER 1

INTRODUCTION, LITERATURE REVIEW AND OBJECTIVES

CHAPTER 1

INTRODUCTION, LITERATURE SURVEY AND OBJECTIVES

1.1 General

Data storage devices play a vital role in every computer based system. Magnetic hard disk storage is widely used for this purpose. This consists of an enclosure which has one or several disks mounted on a vertical spindle supported on bearings. Rotary actuators read the data which is stored in concentric circles on the disks, called servo tracks. The widespread use of the hard disk drives by microcomputers has resulted in several technological innovations in this field. This type of storage provides definite advantages over the traditional diskette drives, such as higher access speeds, much greater storage capacity, less cost per kilobyte and overall convenience.

Data processing applications of computers have a significant influence in our society. Early data processing systems used magnetic tapes as a principal storage medium. Processing was batch sequential on a job-by-job basis. The data processing systems of today, which allow many different jobs to run concurrently and require very large capacity on-line magnetic storage. Improvements in cost, capacity, and performance of on-line magnetic storage is thus necessary.

Magnetic disk storage consists of stacked magnetic disks, a spindle, a head positioning actuator and an air cleaning system as shown in Fig.1.1. The function of a rotary actuator is to bring the arm on the desired track. Air cleaning system prevents any

outside air from entering the disk enclosure, and the disk rotating mechanism containing disks which are supported on spindle. The main performance measures in magnetic disk storage are access time and areal recording density. Inorder to achieve this, a proper understanding of the dynamic behaviour of the mechanisms in a hard disk drive must be gained through a dynamic analysis.

1.2 Literature Survey

1.2.1 The Evolution of Magnetic Storage

Three distinct periods can be identified which indicated a gradual change in this technology. During the first stage i.e. the early years from 1953 to 1962, tape drive served as a storage medium. High cost, limited capacity, and difficulty of use were some of the features of the computer of that era. The next period, from 1963 to 1966, known as the transition years, removed some of the constraints which existed during first era. The third period is considered as the growth age towards the improvement of this technology. During this stage there was a tremendous progress. It came with improved system software and above all, the disk storage devices became far cheaper. Disk capacity per system has been thousand times greater than that of the main memory since 1973.

The arm of the rotary actuator on which the read/write heads are mounted rotates in a ball bearing about a pivot shaft. A radial clearance exists between the pivot shaft and the inner race of the bearing. A radial preload is used inorder to reduce the pivot clearance but it cannot be eliminated entirely. Although the

pivot clearance is very small, it is about one order of magnitude larger than the sub-micron accuracy required for head positioning. Moreover, due to manufacturing errors, the center of the circular servo track may not coincide with the axis of rotation. This offset is termed as track runout which has a frequency corresponding to the shaft rotational speed. Kakizaki [1] modelled the rotary actuator taking into account bearing elasticity and damping and pivot clearance, and obtained the response with the track runout as input to the system using the Runge-Kutta method. Khan, et al [2], modelled the rotary actuator taking into account this clearance, and obtained the response due to sinusoidal track runout and step input resulting from searching from track to track.

Two kinds of actuators are in general use: Linear and Rotary [3]. The main difficulty with the conventional wheel or ball supported linear actuator carriage is in providing a single degree of freedom of movement with minimum friction. To overcome this problem a swinging arm actuator concept was proposed in which the heads move in arc approximately radially across the disk. The rotary actuator which uses a swinging motion around a pivot shaft for positioning, has a lower effective mass and greater structural simplicity compared to the linear actuator. It has several advantages which are listed below.

1. Increased reliability through long life rated bearings and reduced bearing motion.

2. Low inertia.

3. Negligible friction and associated servo off-sets.

4. A balanced assembly insensitive to translational machine vibration.

5. Reduced cost.

Two requirements dominate the design of the moving part of the actuator mechanism. The first is to minimize the ratio of the available torque to inertia inorder to give the shortest motion time interval for the track seeking operation. The second is to achieve a structure permitting maximum possible band width for the position servo loop, to give the shortest possible settling time after the search. A high bandwidth is also desirable to minimize the position error of the servo head in the presence of vibrations and external forces. The band width of a head positioning servo is limited by the need to maintain stability in the presence of mechanical structural resonances [4].

Kakizaki, T., et al [5] reports the design of a high performance and compact rotary actuator for a large capacity magnetic disk storage. FEM, Modal Analysis, and other dynamic analysis techniques were utilized for designing the actuator. Stiffness and damping for the pivot bearing were considered.

1.2.2 Clearances

The presence of clearances in the joints and connections of mechanisms and electromechanical systems has been recognised as a source of deterioration of the dynamic performance of these machines [6]. This deterioration usually takes the form of increased noise and vibration, amplification of internal forces

and stresses. The analytical methods for predicting the effects of clearances and backlash in complex systems are usually beyond the analytical capabilities of most industrial facilities. The results are often either inadequate designs with early failure or poor performance or cases of over design with both economic and engineering wastes [7].

Many studies and discussions have been carried out on non-uniform motion mechanisms. There is a need for high precision. However most of them are kinematic and static analysis and syntheses phenomena associated with the elasticities of members and clearances of pairs are not yet clarified in detail. [8]

The principle of conservation of momentum togather with the coefficient of restitution is used to analyze the impact phenomenon of pairing elements of plane linkages [9]. The dynamics of four-bar mechanisms has been discussed by various authors assuming that the pairing elments keep contact with each other [10].

The dynamic characteristics of a slider-crank mechanism with a clearance have been theoretically and experimentally analyzed, revealing the influence of the clearances and the crank speed upon the relative motions between the pairing elements, input torque and output displacement [12,13].

The effects of numbers and positions of clearance connections upon the relative motions of pairing elements, the output displacement and the input torque about the plane crank and rocker mechanism has been discussed by Funabashi et al [11].

1.2.3 Other Studies

One of the main goal of the computer manufacturer is to increase areal density without much increase in cost of the equipment. One approach to a disk store design was an exploratory development under the direction of Walter S. Buslik in which a low-mass, low load recording head was used on a single disk surface to give a store approximately five million bytes capacity. In this design the drive was to be packaged as a sealed self-contained unit, because the very low flying height of the head (25 μ in), demanded high levels of cleanliness obtainable only by a sealed enclosure or by expensive filtered purging facilities.

Advances in disk areal density and capacity per disk spindle offered customer reduced cost per mega byte of on-line data. Increase in data rate, reduction in access motion and rotational delay, and improved reliability have enhanced system performance and availability. High performance and lower cost per Mbyte, however have been more difficult to achieve in small and intermediate-sized disk drives. This development work is discussed in some detail by Mulvany [14].

Douglas, F., et al., [15] used finite element approach in the development of rotary actuator. Several parameters were varied and their effect on mechanical frequencies were observed. Radwan ,H. R., and Chokshi, J. V., [16] discussed the use of non-contact measurements for modal analysis of disk drive components. Five different non-contact measurement devices were

considered for use in testing the gimbal component, namely: laser, optical, eddy current, capacitance, and fiber optics. The problem associated with the non-contact measurement for modal analysis are discussed. Radwan, H. R., et al., [17] analysed the servo system instability in recent disk actuator design and suggested appropriate modifications with minimum structural changes and iterations.

The effects of various flow patterns on disk stability, the parameters that influence non uniform fl o w are reported by Lannenman [18]. Bouchard, G., et al [19] discussed recent disk drives which have slider bearings that maintain a head-to-disk spacing. Such close head-to-disk spacings have t o be maintained otherwise contact can result in damage to the magnetic coating of the disk. This is also known as "head crashing". The study of stability of head under steady operating conditions is compared between a 5 1/4-inch and two different 8-inch "Winchester" drives.

Mulvany, R. B., and Thompson, L. V., [20] discussed the important innovations in disk file manufacturing at IBM over the last twenty-five years. The authors showed how the technology advanced in the key components of disk file and resulted in increase in areal recording density. Design features of a large capacity memory device having random access to information stored magnetically on rotating disks, the mechanical arrangement of an array of 50 disks, access mechanism, and the timing system for positioning the heads on the disk tracks are described by Noyes, T., and Dickinson, W. E. [21]. Ciskowski, R. D., et al

[22] describe the use of System Identification which provides information about system parameters, useful in predicting behaviour and evaluating performance. More sophisticated techniques for system identification have been developed that can simultaneously estimate many parameters accurately and repeatedly.

Mizochita, Y., et al [23] present a method for measuring the head slider flying height fluctuation caused by disturbances on the disk and head arm vibration. The effect of flying height variation on the off track data rate is discussed by Morris and Chou [24]. Design concepts of the mechanical and servo system of a newly-developed compact disk drive with its own closed self circulating air system is designed to minimize undesired vibration and a rotary actuator to achieve fast, precise positioning is discussed by Mizochita, et al [25].

A novel magnetic design permits placement of the actuator between the disks, thus eliminating the massive and vibration-prone comb structure used in conventional linear actuators. The technology and system advantages of a high performance magnetic recording head disk file actuator are reported by Scranton et al [26]. Naruse, et al [27] discuss the design of a disk drive which accomodates two rotary actuators. Since mechanical vibration is quite significant in such drives, analysis of mechanical vibration in these units is reported. Winfrey et al, [28] describe the design of a rotary positioner for a 14-inch, mid-range magnetic disk memory while retaining traditional advantages. Tagawa, et al [29] describe sub-micron

spacing dynamics for total flying head slider mechanisms, considering suspension gimbal spring and actuator arm mechanism as well as the air bearing slider.

The progress of the disk file industry has been fueled by an evergrowing demand for on-line storage with improved price and performance. The single most important factor in meeting this demand has been the increased areal storage density permitted by the advances in basic recording technology discussed by Harker, Brede, Pattison, Santana, and Taft [30].

State Space technique can be used in the prediction of dynamic responses of structures. The Matrix Exponential technique was used by Bahar [31] to obtain the dynamic response of structures when excited by deterministic sources. He found the method was stable and accurate and it compared well with the Wilson method [32]. The Wilson method is based on introducing a simple relationship between displacement, velocity, and acceleration which may be assumed to be valid for a short increment of time, which is then used to convert simultaneous differential equations of motion into simultaneous algebric equations.

Kaneko and Yoshi [33] discuss about a large capacity disk storage with a high areal recording density. By setting the moisture absorption mechanism and the air filtering mechanism in the disk enclosure, the disk enclosure can be operated with no scheduled maintenance for more than five years. Takanami, Komachiya, and Matsumoto [34], discuss storage control, which has

lower cost and small size. It has less than half the previously used main parts through using many L.S.I circuits and large scale printed circuit cards. Moreover, the storage control contains two paths, called storage detectors, for executing channel commands and transferring data between channels and disk devices. Different techniques are shown by Nakanishi, Koshmoto, and Ouara [35] by which high areal recording density is achieved. Kogure, Kita, and Fubi [36] describe how high linear density in magnetic disk storage is affected by head slider flying height.

Mitsuva, Kogure, and Oguchi [37] describe the disk drive assembly comprising a disk rotating mechanism, a head positioning actuator and an air cleaning system. They compared it with conventional large capacity disk storages formerly in use. Disks, heads, and the head carriage with a moving coil are contained in a sealed catridge. Ito, Tanaka, and Matsumoto [38] outline a magnetic disk storage system with 800 MB/spindle, satisfying large capacity and low price requirement. High recording density is achieved by means of a thinly coated recording medium and contact start/stop read/write head with narrow track width. Fast seek time and high data transfer rate are achieved by lightweight head positioning mechanism. For achieving higher recording density and higher reliability, Head-Disk mechanism with a new air flow system, high performance positioning control and a new signal handling are discussed by Keneko, Takanami, and Nakanishi [39].

1.3 Scope of the Present Investigation

The objectives of the present investigation are:

i) To study the effect of pivot clearance on head positioning of a rotary actuator for magnetic disk storage.

ii) To study the response of a servomechanism controlled rotary actuator subjected to step input and a sinusoidal track runout. To carry out a parametric study to find the effect of variousparameters on system stability.

iii) To obtain the natural frequency and mode shapes of the arm structure using finite element approach.

iv) To study the dynamic response of a disk rotating mechanism containing eight disks supported on a vertical spindle and driven by a D.C. motor. In this investigation torsional and flexural degrees of freedom of the spindle are considered. Also the system natural frequencies and mode shapes are obtained.

Chapter 2 deals with the non-linear dynamic analysis of a rotary actuator for head positioning in magnetic disk storage. The response of the rotary actuator subjected to a step and a sinusoidal track run-out is obtained by solving the equations of motion using a Matrix Exponential technique. The results are compared with Runge-Kutta-Gill method. Also the stability study of the rotary actuator is carried out by varying the values of servo-constants, radial stiffness, and damping co-efficient to see

how it reacts to such a change. The equations of motion which take pivot clearance and pivot bearing elasticity into account is derived for a track following servo-controlled actuator. During read/write operation, the head is subjected to a step displacement in moving between tracks and a sinusoidal track runout, which triggers the actuator mechanism to correct the head position.

Chapter 3, presents the finite element model of the arm structure. A general purpose finite element package 'ANSYS' is utilized to model this structure. The natural frequencies and mode shapes are obtained.

Chapter 4, describes the dynamic response of a disk rotating mechanism containing eight disks supported on a vertical shaft and driven by a D.C. motor. The sources of excitations are in the form of mass unbalance and fluctuation in torque. The spindle is considered flexible in bending and torsion, the effects being studied separately. Modal analysis is used to obtain the response.

Finally, conclusions and recommendations for future work are presented in chapter 5.

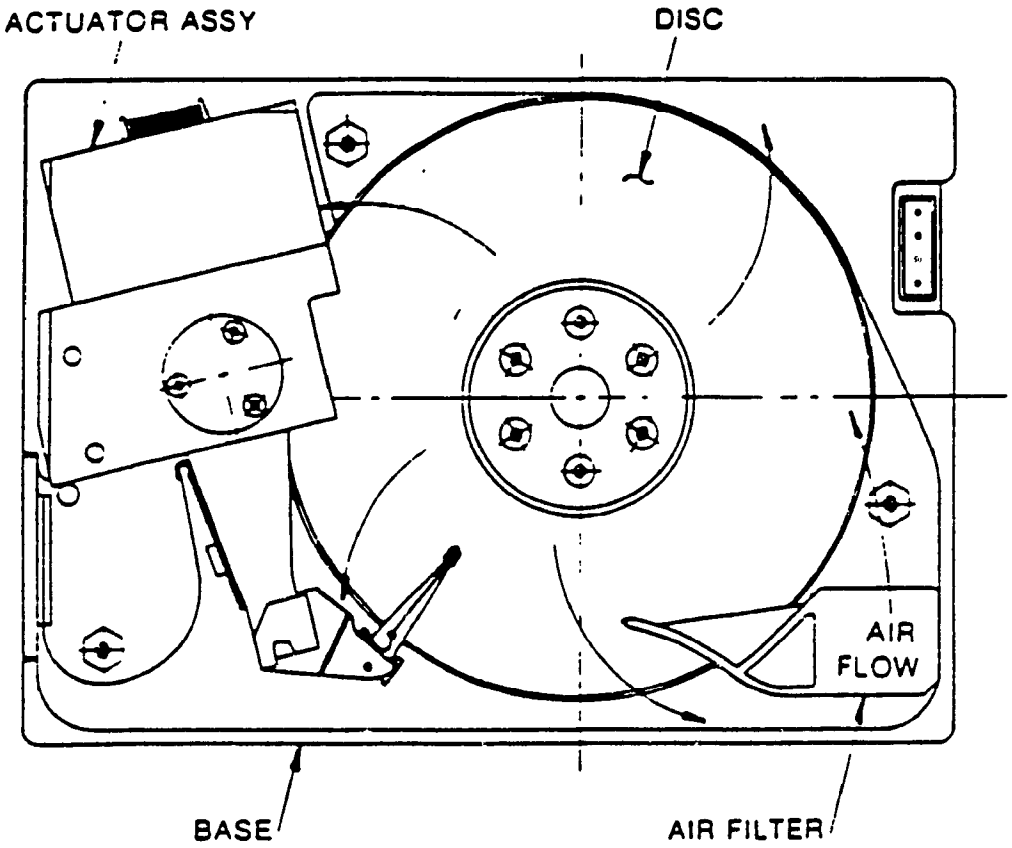

Fig. 1.1 Magnetic Disk Storage

CHAPTER 2

NON-LINEAR DYNAMIC ANALYSIS OF A ROTARY ACTUATOR

CHAPTER 2

NON-LINEAR DYNAMIC ANALYSIS OF A ROTARY ACTUATOR

2.1 Introduction

In information processing systems, magnetic disk storage is the main online file and acts like a large-capacity random access memory. Data is stored in concentric circles called servo tracks. The main performance measures in magnetic disk storage are access performance and areal recording density. Higher speed and higher densities can be achieved by improving the performance of the head positioning actuator mechanism. A rotary actuator which uses a swinging motion around a pivot shaft for positioning, has lower effective mass and greater structural simplicity compared to the linear actuator. However, mechanical vibrations due to elasticity, inertia and damping in the rotary actuator mechanism degrade its dynamic performance. Hence a dynamic analysis would provide a better understanding of the parameters influencing this degradation in performance and means to improve it. The rotary actuator mechanism shown in Fig. 2.1 consists of a rotary actuator supported on precision ball bearings on which the read/write heads and servo head are mounted. A radial clearance called the pivot clearance, exist between the pivot shaft and the inner race of the bearing. A radial preload is used in order to reduce the pivot clearance but it can not be eliminated entirely. Although the pivot clearance is very small, it is about one order of magnitude larger than the sub-micron accuracy required for head

positioning. Moreover, due to errors in manufacturing, the center of the circular servo tracks may not coincide with the axis of rotation. This offset is termed as track runout at a frequency corresponding to the shaft rotational speed. Kakizaki [1] modelled the rotary actuator taking into account this clearance and obtained the response due to a track runout using the Runge-Kutta method.

In this chapter, the rotary actuator is modelled as a rigid link taking into account the flexibility of the bearing and the pivot clearance. A closed loop servo system is used to determine the driving force required to rotate the actuator for head positioning. The track runout which is sinusoidal in nature superimposed on a step displacement due to searching of the tracks is assumed as the input excitation to the arm. The resulting non-linear equations of motion are solved using the Matrix Exponential Technique [31].

2.2 Analysis

The schematic model of the actuator is shown in Fig. 2.2, where P_h, G, P, and P_c denote head position, center of gravity, pivot bearing center, and drive point respectively. The pivot portion consists of a pivot bearing tightly attached to the moving part and a pivot shaft whose axis center is located at O, as shown. A radial pivot clearance between the pivot shaft and the inner race of bearing is called a pivot clearance. The analysis is carried out under the following assumptions.

i) Both the moving part and pivot shaft are rigid.

ii) The pivot bearing is a linear spring with viscous damping.

iii) The parallel displacement component Y_g and the angular displacement component θ of the moving carriage are small.

For small motions, the equation of motion of the rotary actuator are:

$$M \ddot{Y}_g = F + F_m \tag{2.1}$$

$$J \ddot{\theta} = F l_2 + F_m l_3 \tag{2.2}$$

where M and J are the mass and moment of inertia of rotary actuator, respectively. θ is assumed very small in this analysis. F and F_m are the contact forces at the pivot and the servomechanism, respectively. Bearing displacement y_p and head displacement $\bar{y}_h$ can be expressed as follows:

$$y_p = y_g + l_2\theta \tag{2.3}$$

$$\bar{y}_h = l_1\theta - y_g \tag{2.4}$$

The contact force at the pivot, F, is non-linear function of clearance, given by

$$F = \{ - k(y_p + \lambda r) - c\dot{y}_p \} \delta \tag{2.5}$$

where k and c are the radial stiffness and damping co-efficient of bearing. The co-efficients δ and λ are given by

$$\begin{array}{lll} \delta = 1 & \lambda = 1 & y_p \leq -r \\ \delta = 0 & \lambda = 0 & |y_p| < r \\ \delta = 1 & \lambda = -1 & y_p \geq r \end{array} \qquad (2.6)$$

where r is radial clearance. The driving force F_m applied by the servomechanism depends on the track displacement Y_{tr}, and is expressed as

$$F_m = K_1(y_{tr} - y_h) + K_2(\dot{y}_{tr} - \dot{y}_h) \qquad (2.7)$$

where K_1 and K_2 are the constants of servo mechanism.

Due to manufacturing errors, the center of the circular servo track may not coincide with the axis of rotation, therefore the track displacement is assumed as

$$y_{tr} = a + d \sin \omega t \qquad (2.8)$$

where ω is the frequency of the track runout, which is the rotational frequency of the disk.

Substituting the values of F and F_m in Equation (2.1), we get

$$M \ddot{Y}_g = \{ -k (y_p + \lambda r) - c y_p \} \delta + K_1 (y_{tr} - \bar{y}_h) + K_2 (\dot{y}_{tr} - \dot{\bar{y}}_h) \qquad (2.9)$$

From Eqn's (2.3), (2.4), (2.8), and (2.9), results in

$$M \ddot{Y}_g = \{ -k (y_g + l_2\theta + \lambda r) - c (\dot{y}_g + l_2\dot{\theta}) \} \delta +$$

$$K_1 (a \sin\omega t - l_1\theta + y_g) + K_2 (a \omega \cos\omega t - l_1\dot{\theta} + \dot{y}_g)$$

$$\ddot{Y}_g = -\frac{k\,\delta}{M}\{ y_g + l_2\,\theta + \lambda r\} - \frac{c\,\delta}{M} -\{ \dot{y}_g + l_2\dot{\theta} \}$$

$$+ \frac{K_1}{M}\{ a \sin \omega t - l_1\,\theta + y_g \}$$

$$+ \frac{K_2}{M}\{ a\,\omega \cos \omega t - l_1\,\dot{\theta} + \dot{y}_g \} \qquad (2.10)$$

Similarly Equation (2.2) results in

$$\ddot{\theta} = -\frac{k\,\delta\,l_2^2}{J}\{ y_g + l_2\,\theta + \lambda r \}$$

$$-\frac{c\,\delta\,l_2}{J}\{ \dot{y}_g + l_2\,\dot{\theta} \}$$

$$+\frac{K_1\,l_3}{J}\{ a \sin \omega t - l_1\,\theta + y_g \}$$

$$+\frac{K_2\,l_3}{J}\{ a\,\omega \cos \omega t - l_1\,\dot{\theta} + \dot{y}_g \} \qquad (2.11)$$

The following nondimensional quantities are introduced:

$$z_1 = \frac{y_g}{a} \qquad (2.12)$$

$$L_1 = \frac{l_1}{l} \qquad (2.13)$$

$$\Omega_1^2 = \frac{4\,\pi^2\,K}{M\,\omega^2} \qquad (2.14)$$

$$z_2 = \frac{dz_1}{d\tau} \qquad (2.15)$$

$$L_2 = \frac{l_2}{l} \qquad (2.16)$$

$$\Omega_2^2 = \frac{4\,\pi^2\,K_1}{M\,\omega^2} \tag{2.17}$$

$$z_3 = \frac{l\ \theta}{a} \tag{2.18}$$

$$L_3 = \frac{l_3}{l} \tag{2.19}$$

$$\eta_1 = \frac{2\ \pi\ c}{M\ \omega} \tag{2.20}$$

$$z_4 = \frac{dz_3}{d\tau} \tag{2.21}$$

$$R = \frac{r}{a} \tag{2.22}$$

$$\eta_2 = \frac{2\ \pi\ K_2}{M\ \omega} \tag{2.23}$$

$$\tau = \frac{\omega t}{2\pi} \tag{2.24}$$

$$\alpha = \frac{J}{M\,l^2} \tag{2.25}$$

Use of the nondimensional quantities, from Eqns. (2.12) to (2.25), in Eqns (2.10) and (2.11), results in

$$\begin{aligned} \dot{Z}_2\ a = &- \Omega_1^2\ \delta\ \{\ Z_1\ a + L_2\ Z_3\ a + \lambda\ R\ a\ \} \\ &- \eta_1\ \delta\ \{\ Z_2\ a + L_2\ Z_4\ a\ \} \\ &+ \Omega_2^2\ \{\ a \sin \omega t - L_1\ Z_3\ a + Z_1\ a\ \} \\ &+ \eta_2\ \{\ a\ \omega \cos \omega t - L_1\ Z_4\ a + Z_2\ a\ \} \end{aligned}$$

$$\dot{Z}_2 = -\Omega_1^2 \delta \{ Z_1 + L_2 Z_3 + \lambda R \}$$
$$- \eta_1 \delta \{ Z_2 + L_2 Z_4 \}$$
$$+ \Omega_2^2 \{ \sin \omega t - L_1 Z_3 + Z_1 \}$$
$$+ \eta_2 \{ \omega \cos \omega t - L_1 Z_3 + Z_2 \} \qquad (2.26)$$

Using nondimensional quantities in Equation (2.11)

$$\dot{Z}_4 = - \frac{\Omega_1^2 \delta}{\alpha} -\{ Z_1 L + L_2^2 Z_3 + \lambda R L_2 \}$$
$$- \frac{\eta_1 \delta}{\alpha} \{ Z_2 L_2 + Z_4 L_2^2 \}$$
$$+ \frac{\Omega_2^2}{\alpha} \{ L_3 \sin \omega t - L_1 L_3 Z_3 + L_3 Z_1 \}$$
$$+ \frac{\eta_2}{\alpha} -\{ 2\pi \cos \omega t * L_3 - L_1 L_3 Z_4 + L_3 Z_2$$

Equations (2.26) and (2.27) can be transformed into the matrix form as:

$$\{ \ddot{Z} \} + [C] \{ \dot{Z} \} + [K] \{ Z \} = \{ f(t) \} \qquad (2.28)$$

The equations of motion described by Eq. (2.28) are recast into state space form using,

$$\{ X \} = \begin{Bmatrix} Z \\ \dot{Z} \end{Bmatrix}$$

inorder to predict the dynamic response using the matrix exponential method.

The equations of motion can be cast into a system of first order differential equation of the form,

$$\{ \dot{Z} \} = [A] \{ Z \} + \{ B \} \qquad (2.29)$$

The elements a_{nk} , b_{nk} of matrices [A] and [B] are given in appendix I.

2.3 Solution Procedure

The numerical solution of Eq. (2.29) can be obtained by the corresponding equivalent discrete-time system model,

$$Z (t_{i+1}) = \phi (t_{i+1} , t_i) Z (t_i) + b_d (t_i) \qquad (2.30)$$

where, the state transition matrix is given by:

$$\phi (t_{i+1} , t_i) = \exp [A (t_{i+\frac{1}{2}}) \Delta T] \qquad (2.31)$$

where,

$$\Delta T = t_{i+1} - t_i$$

The Matrix Exponential technique, widely used in modern control theory, is adopted as an integration procedure for predicting the dynamic response of the system subjected to deterministic input. This state space method is stable and accurate. It is also less sensitive to an increase in the time step [31].

The discrete-time forcing vector $b_d (t_i)$ is given by

$$b_d (t_i) = \int_{t_i}^{t_{i+1}} \phi (t_{i+1}, \tau) B (\tau) \, d\tau \qquad (2.32)$$

If the time increment ΔT is chosen to be sufficiently small as compared to the time constants of the system, the vector $[B(\tau)]$ in Eq. (2.31) can be considered to be constant during that time increment and can be represented by $B(t_i)$, its value during the

preceding instant. Bahar [31] showed that Eq. (2.32) can be rewritten as

$$b_d(t_i) = \sum_{n=0}^{\infty} \frac{A\left(t_{i+\frac{1}{2}}\right)^n (\Delta T)^{n+1}}{(n+1)!} B(t_i) \qquad (2.33)$$

For bearing displacement and head positioning error the following nondimensional quantities are introduced.

Bearing displacement $$Y_p = \frac{y_p}{a} \qquad (2.34)$$

Head Positioning Error $$E_h = \frac{y_{tr} - \bar{y}_h}{a} \qquad (2.35)$$

2.4 Results and discussion

2.4.1 Effect of Clearance on Bearing Displacement and Head Positioning error

The details of the rotary actuator system used to obtain the numerical results are given in Table 2.1.

Bearing displacement and head positioning error are obtained for different values of clearance. The results are plotted, which shows how it can play a significant role. The results are obtained using a Matrix Exponential technique.

Figs. 2.3 to 2.11 show that mechanical vibration acting on pivot shaft can degrade the dynamic performance of the actuator. Although the pivot clearance is very small but it still can affect the head positioning mechanism. We are encountering three kinds of vibrartions. The first is when there is no pivot clearance i.e R=0. both bearing displacement and head positioning error exhibit

a sinusoidal response and it is known as sinusoidal vibration. By giving a certain value of clearance we can see the impact of pivot bearing against the pivot shaft but the head positioning error show the same response as in case of no clearance. It is known as fundamental impact vibration. As we increase the value of clearance the bearing makes multiple bounces against the pivot shaft very frequently and correspondingly large head positioning error. This is reffered as high frequency impact vibration.

The response of the system to bearing displacement and head positioning error is observed by giving the same value of clearance.

Figs. 2.3 and 2.4 shows bearing displacement Y_p and head positioning error E_h when there is no clearance. It can be seen that both Y_p and E_h exhibit a vibration of first kind.

From Figs. 2.5 to 2.8 it can be seen that vibration is caused by the impact of pivot bearing against the pivot shaft but E_h shows the same response as in case of no clearance. This attributes to the vibration of second kind.

It can be seen from Figs. 2.9 to 2.10 that as the value of clearance increases the bearing hits the pivot shaft in quick succession and results in high frequency impact vibration and head positioning error.

2.4.2 Effect of Pivot Bearing Damping

Figs. 2.11 to 2.13 show the bearing displacement plotted as a function of bearing damping. It can be seen from these plots as

damping increases the period of impact increases and as a result maximum deformation decreases.

2.5 Numerical Results and Discussion

The method was applied on a rotary actuator system with the parameters shown in Table 2.1. These values are chosen as the base configuration in the parametric study. The results of the parametric study are shown in Figures 2.14 to 2.31. In all these cases, the actuator arm is assumed to move through tracks, one after the other, in search of information.

The effect of radial clearance on the bearing displacement, (y_p/a), and head positioning error, $(y_{tr} - y_h)/a$, are shown in Figures 2.14, 2.15, 2.16, and 2.17. Figures 2.14 and 2.15 show bearing displacement and head positioning error, respectively, for $R = 10^{-2}$ and Figures 2.16 and 2.17 for $R = 10^{-3}$. The initial transient due to the step displacement in moving from one track to another and gradual change towards a steady behaviour until the next step displacement can be clearly seen in all the figures. As the radial clearance is decreased it is seen that there is a significant reduction in the vibration amplitude

The effect of stiffness of the rotary arm on the bearing displacement and head positioning error are shown in Figures 2.18, 2.19, 2.20, and 2.21. The periodic nature of the response due to successive track searching can be seen clearly. The frequency of the response increases with arm stiffness.

The effect of increasing the damping in the rotary arm is

shown in Figures 2.22 and 2.23. The damping reduces the vibration amplitude as should be expected.

The effect of the servo constant which provides displacement proportional force, K_1, is shown in Figures 2.24, 2.25, 2.26, and 2.27. As K_1 increases the frequency of response goes up.

The effect of servo constant K_2, which provides velocity proportional force is shown in Figures 2.28, 2.29, 2.30, and 2.31. As K_2 is increased the frequency of response goes up. The amplitude of the bearing displacement also goes up with increasing K_2.

In the following chapter, the natural frequencies and mode shapes of a servomechanism controlled swinging arm actuator is calculated using finite element approach. ANSYS, a finite element package, is used to model the rotary arm as a flexible system.

TABLE 2.1

Base Configuration of Rotary Actuator

M	0.5 Kg	
J	10^{-3} Kg m^2	
l_1	0.1 m	
l_2	0.005 m	
l_3	0.09 m	
k	28.1 * 10^6 KN/m	(Ω_1= 149.93)
c	370 N s/m	(η_1= 14.8, ζ=0.05)
K_1	177 * 10^3	(Ω_2= 11.90)
K_2	141 N s/m	(η_2= 5.64)
d/a	0.1	
R	10^{-2}	

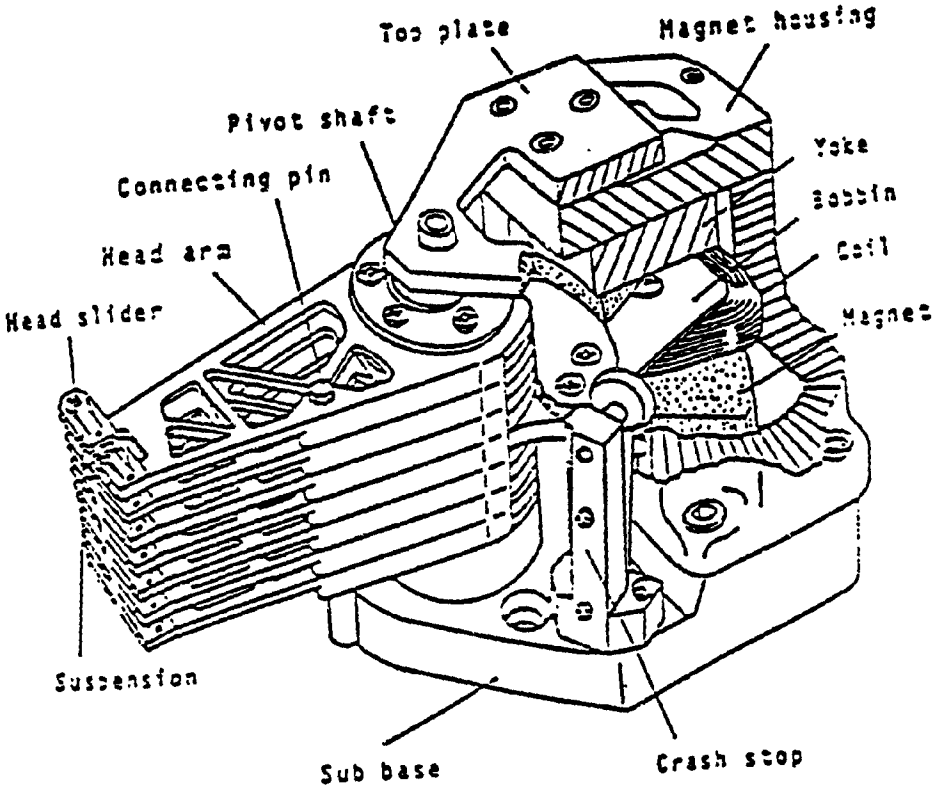

Fig. 2.1 Rotary Actuator [1]

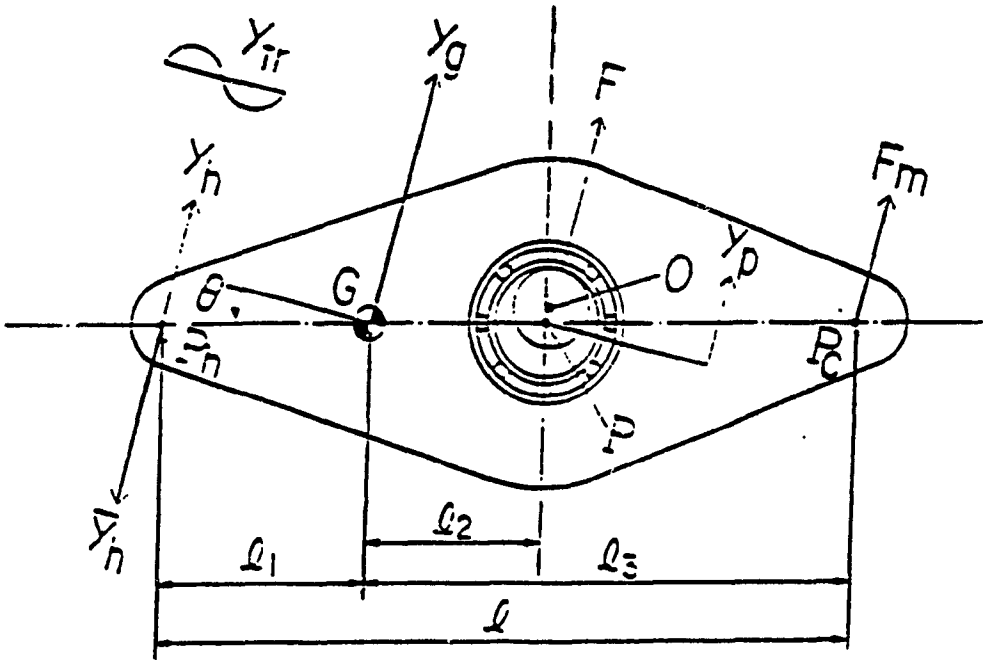

Fig. 2.2 Schematic model of the Actuator [1]

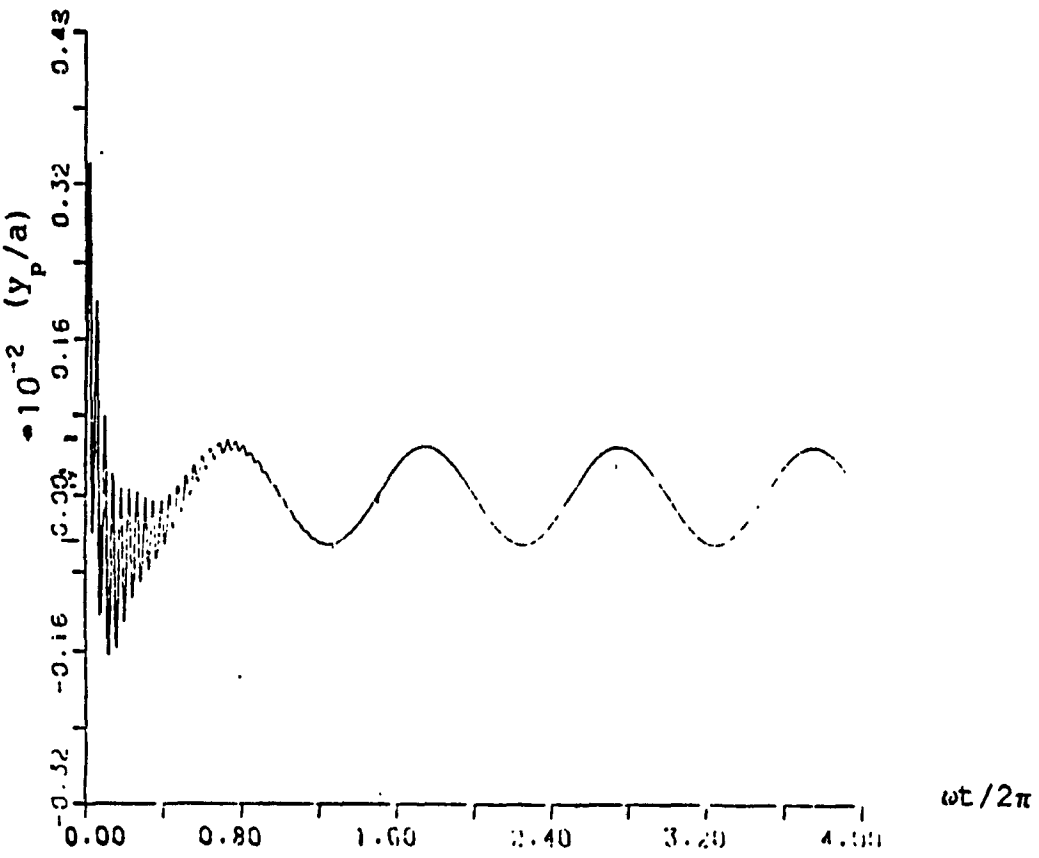

Fig. 2.3 Bearing Displacement variation with time

($R = 0$, $\Omega_1 = 149.93$, $\Omega_2 = 11.90$,
$\zeta = 0.05$, $\eta_2 = 5.64$)

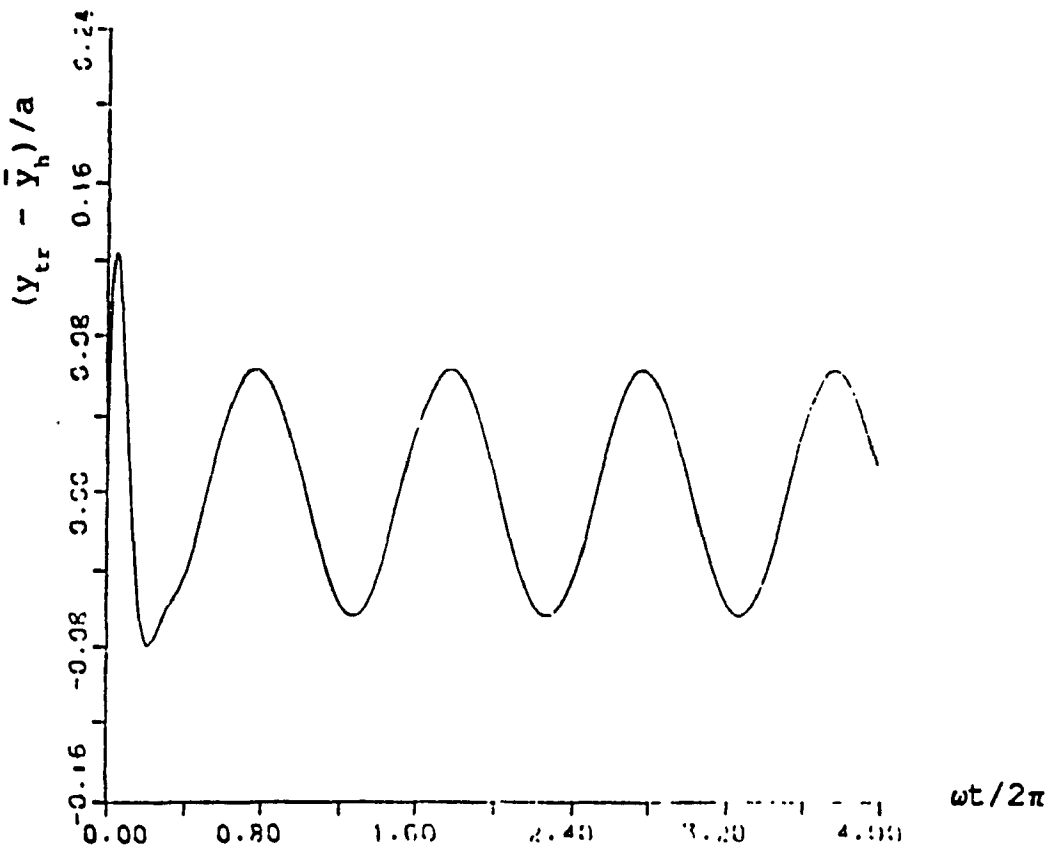

Fig. 2.4 Head positioning error variation with time

($R = 0$, $\Omega_1 = 149.93$, $\Omega_2 = 11.90$,
$\zeta = 0.05$, $\eta_2 = 5.64$)

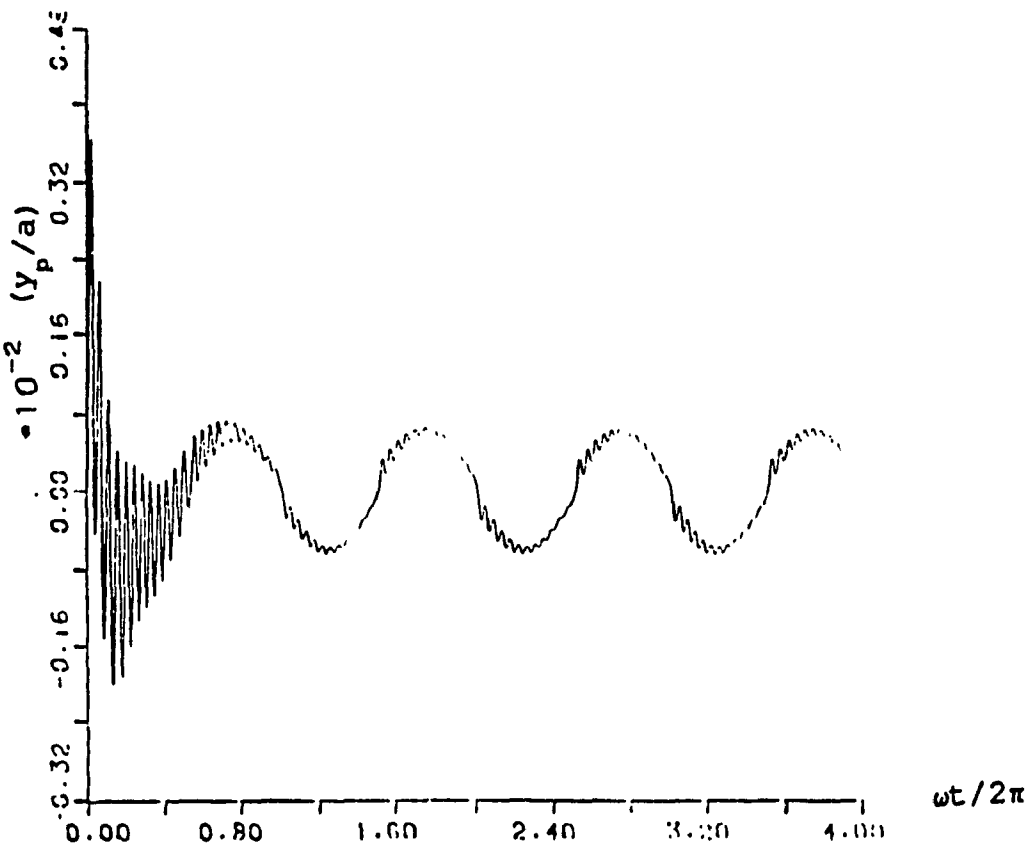

Fig. 2.5 Bearing displacement variation with time

($R = 10^{-4}$, $\Omega_1 = 149.93$, $\Omega_2 = 11.90$,
$\zeta = 0.05$, $\eta_2 = 5.64$)

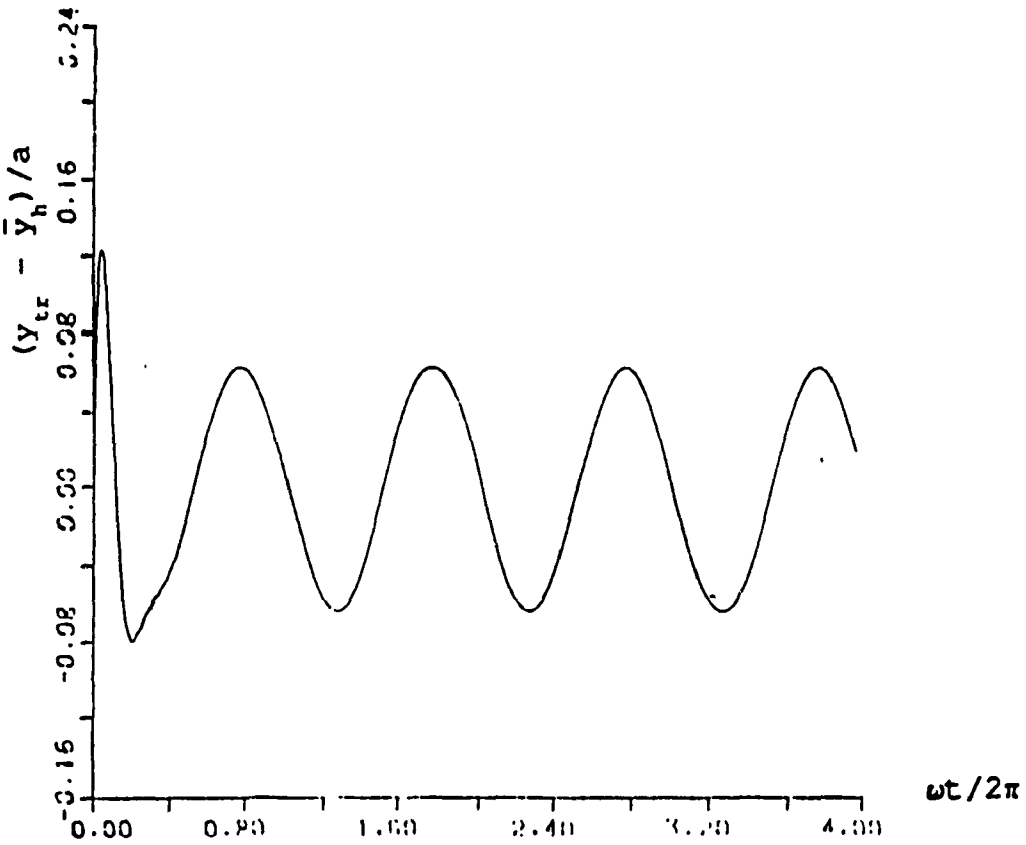

Fig. 2.6 Head positioning error variation with time

($R = 10^{-4}$, $\Omega_1 = 149.93$, $\Omega_2 = 11.90$,
$\zeta = 0.05$, $\eta_2 = 5.64$)

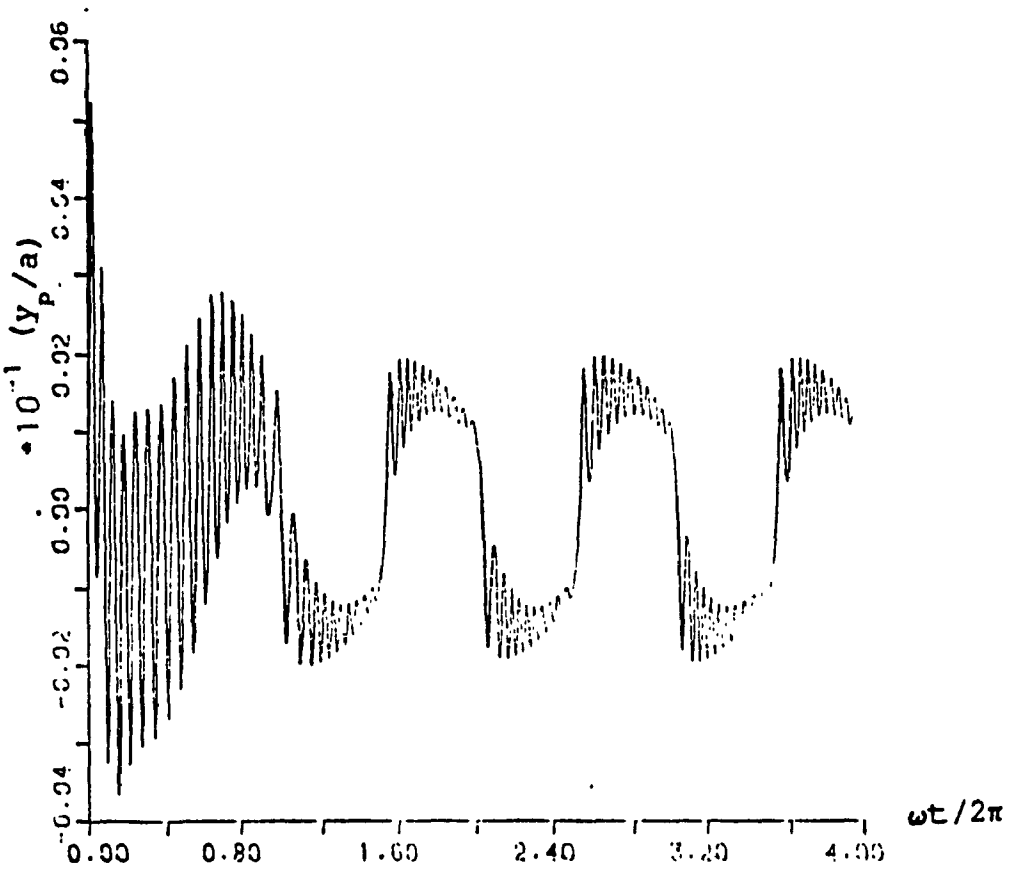

Fig. 2.7 Bearing displacement variation with time

($R = 10^{-3}$, $\Omega_1 = 149.93$, $\Omega_2 = 11.90$,
$\zeta = 0.05$, $\eta_2 = 5.64$)

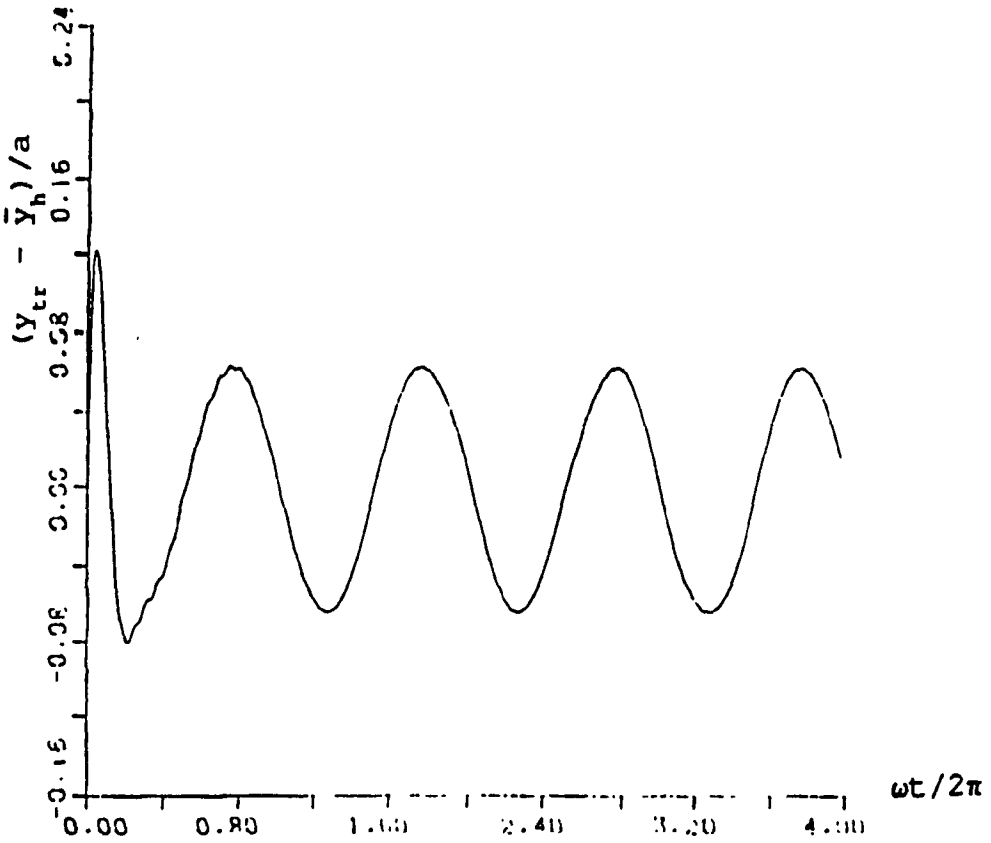

Fig. 2.8 Head positioning error variation with time

($R = 10^{-3}$, $\Omega_1 = 149.93$, $\Omega_2 = 11.90$,
$\zeta = 0.05$, $\eta_2 = 5.64$)

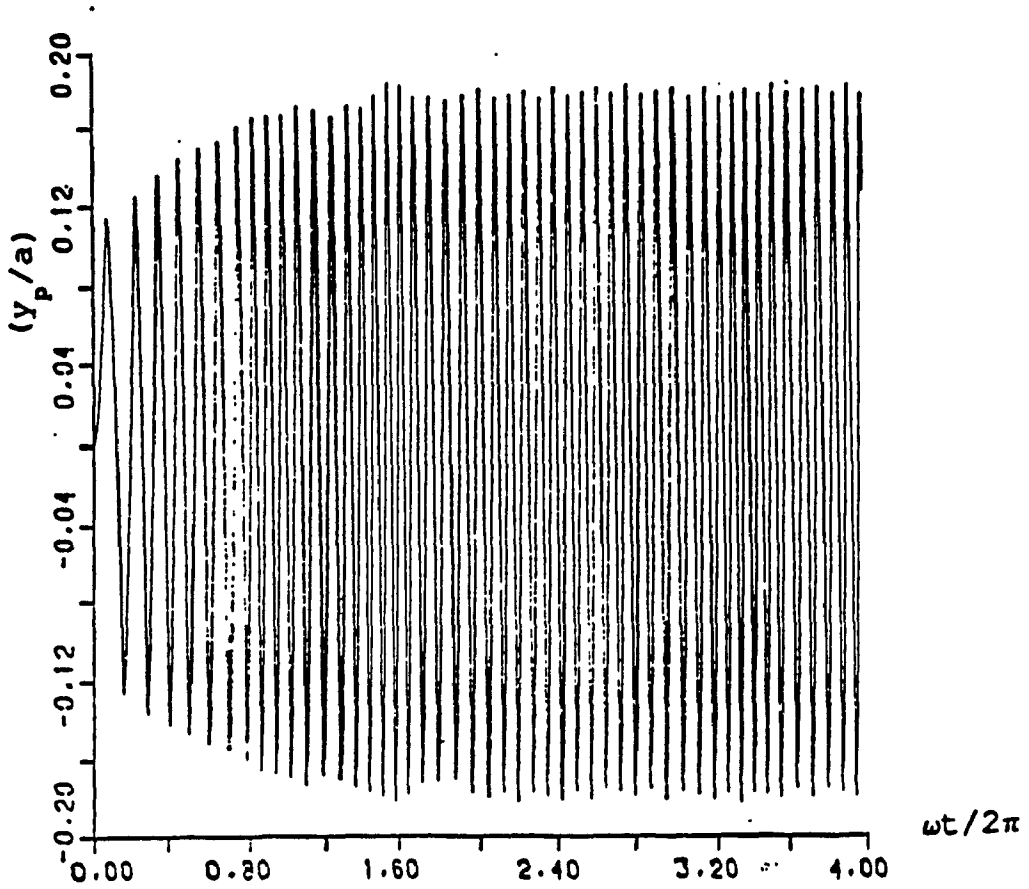

Fig. 2.9 Bearing displacement variation with time

($\Re = 10^{-1}$, $\Omega_1 = 149.93$, $\Omega_2 = 11.90$,
$\zeta = 0.05$, $\eta_2 = 5.64$)

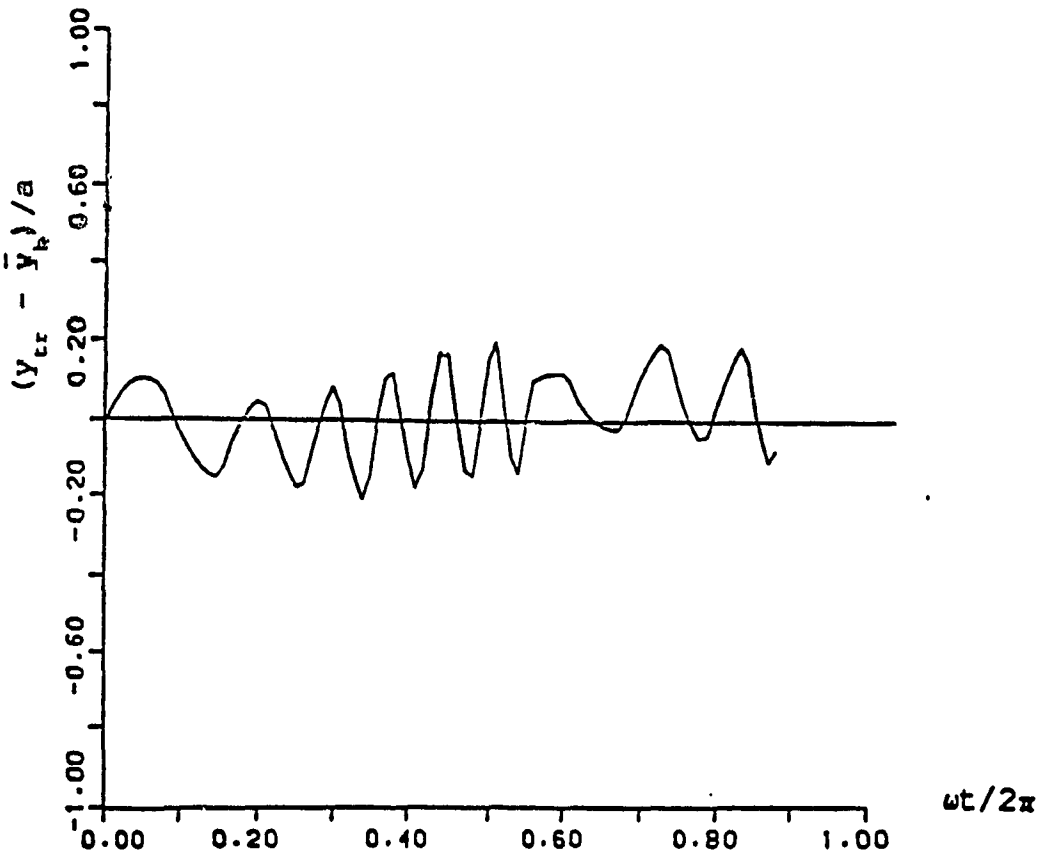

Fig. 2.10 Head positioning error variation with time

($R = 10^{-1}$, $\Omega_1 = 149.93$, $\Omega_2 = 11.90$,
$\zeta = 0.05$, $\eta_2 = 5.64$)

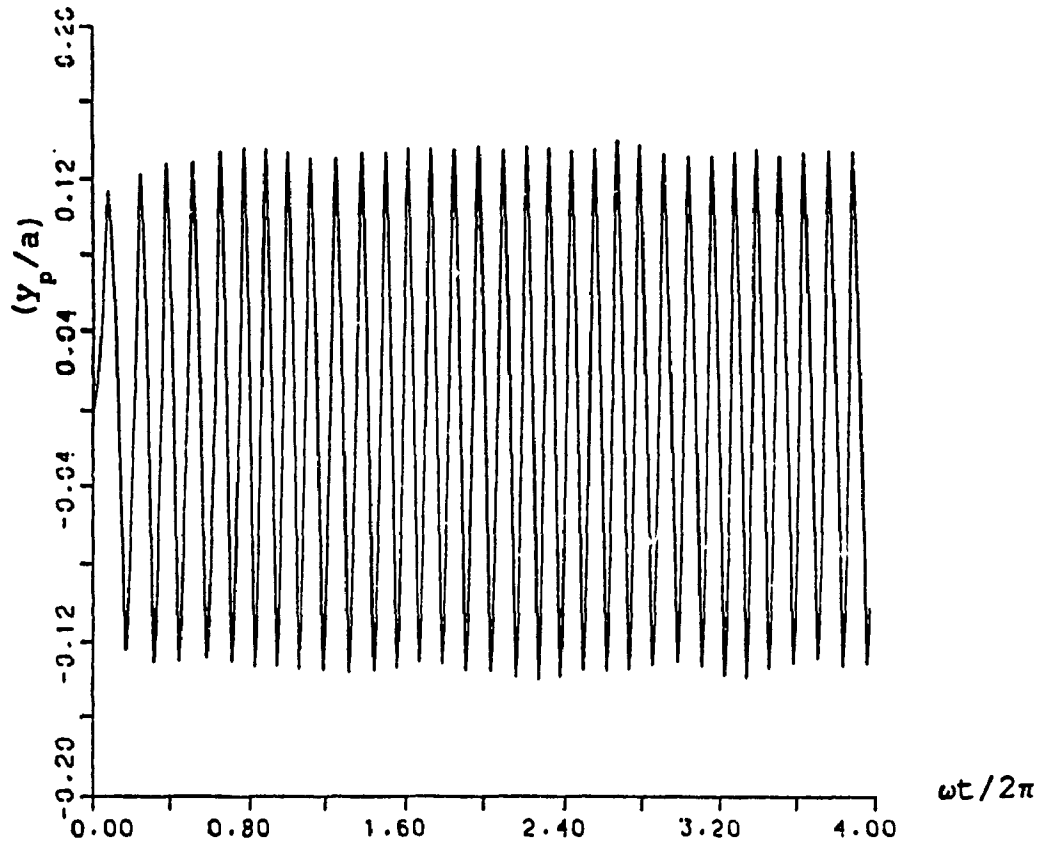

Fig. 2.11 Bearing displacement variation with time
($R = 10^{-1}$, $\Omega_1 = 149.93$, $\Omega_2 = 11.90$,
$\zeta = 0.1$, $\eta_2 = 5.64$)

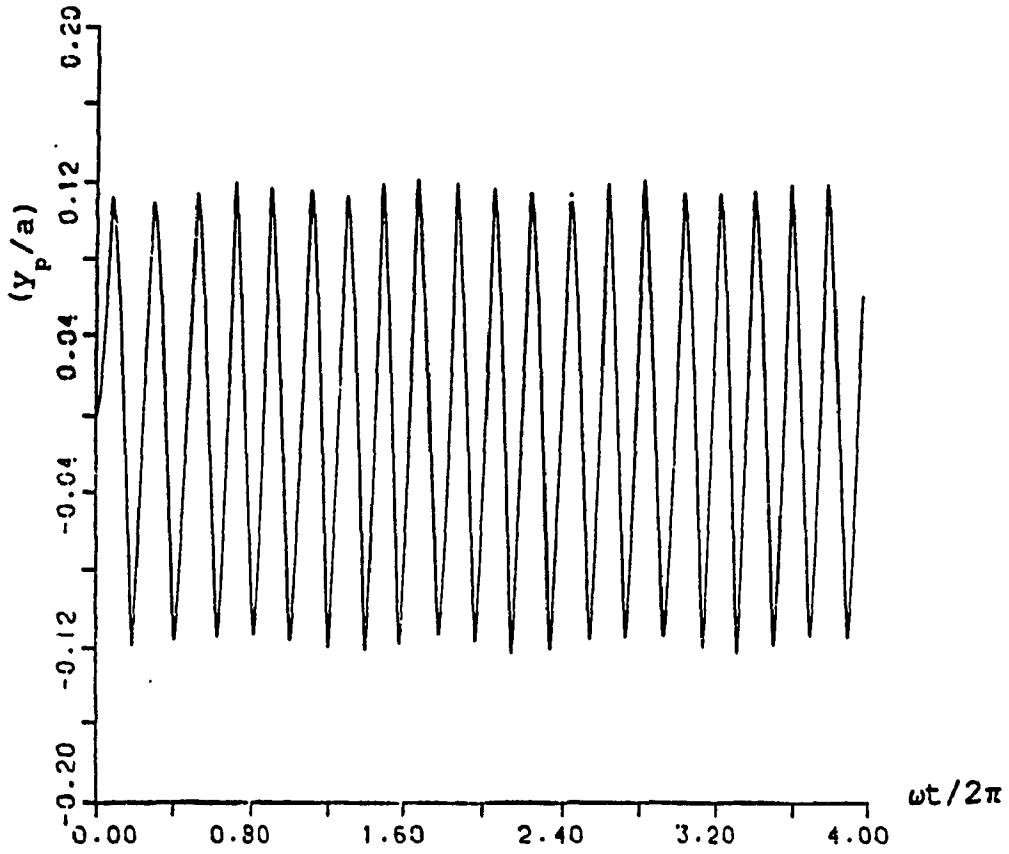

Fig. 2.12 Bearing displacement variation with time

($R = 10^{-1}$, $\Omega_1 = 149.93$, $\Omega_2 = 11.90$,
$\zeta = 0.2$, $\eta_2 = 5.64$)

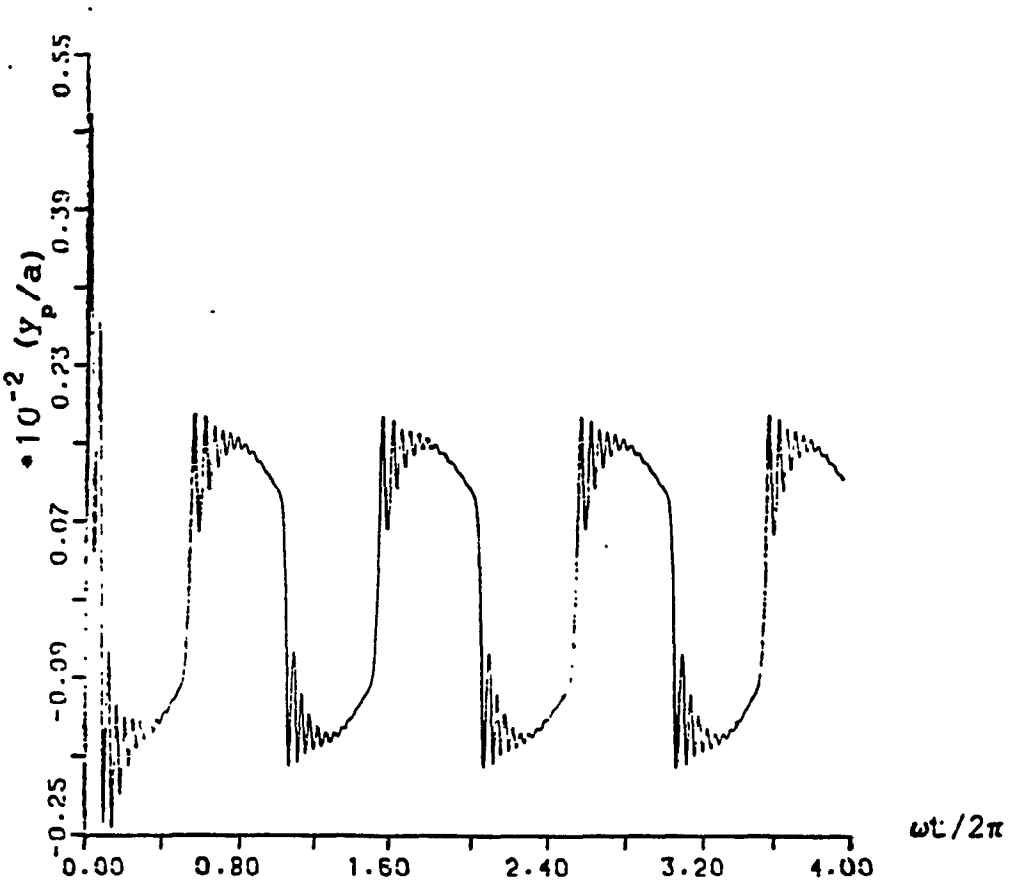

Fig. 2.13 Bearing displacement variation with time
($R = 10^{-3}$, $\Omega_1 = 149.93$, $\Omega_2 = 11.90$,
$\zeta = 0.1$, $\eta_2 = 5.64$)

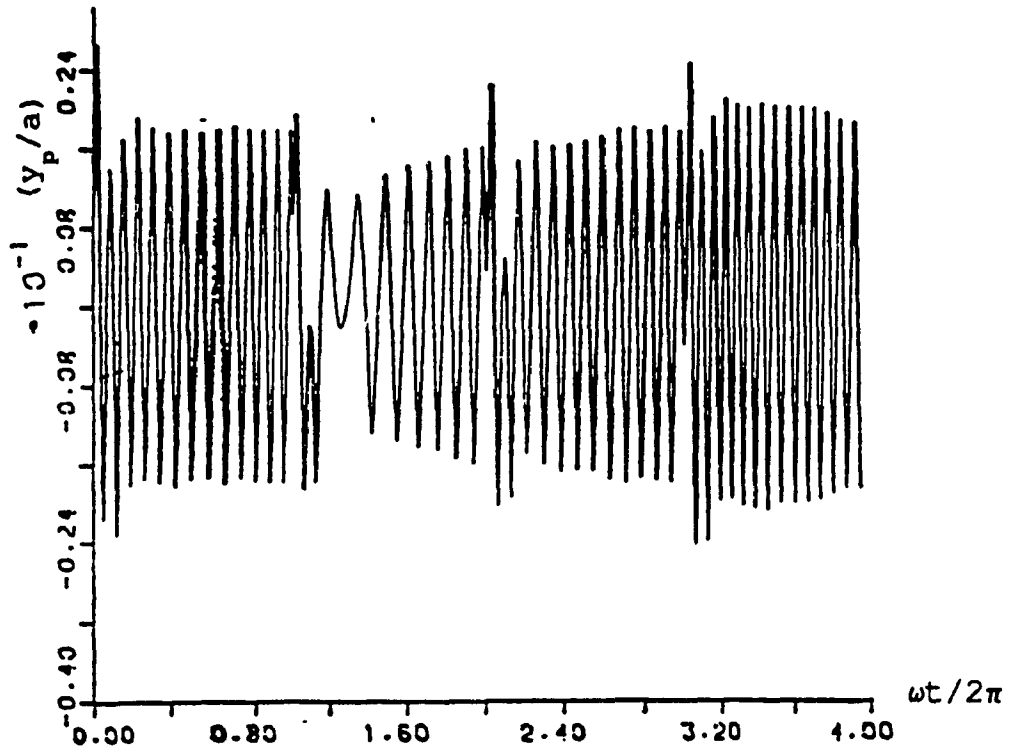

Fig. 2.14 Bearing displacement variation with time ($R = 10^{-2}$, $\Omega_1 = 149.93$, $\Omega_2 = 11.90$, $\zeta = 0.05$, $\eta_2 = 5.64$)

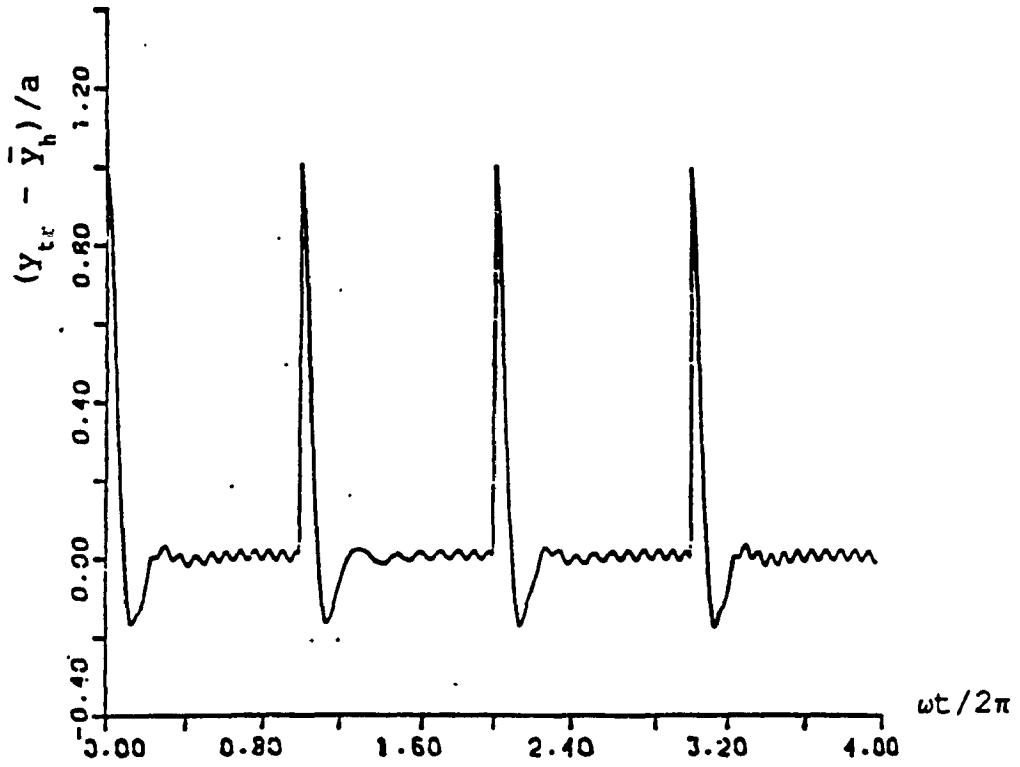

Fig. 2.15 Head positioning error variation with time ($R = 10^{-2}$, $\Omega_1 = 149.93$, $\Omega_2 = 11.90$, $\zeta = 0.05$, $\eta_2 = 5.64$)

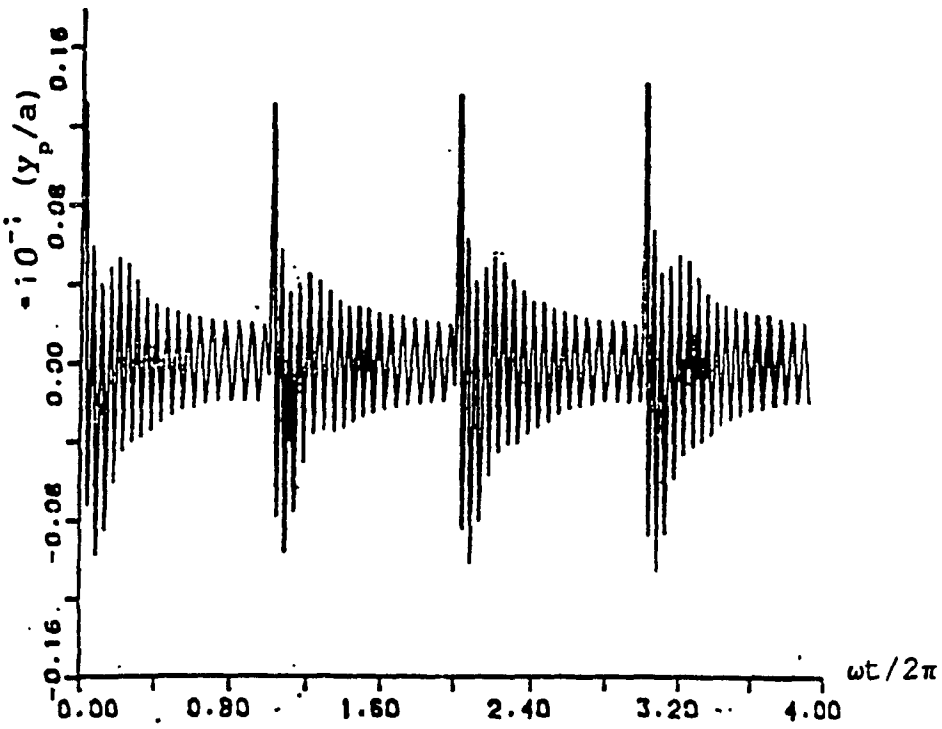

Fig. 2.16 Bearing displacement variation with time ($R = 10^{-3}$, $\Omega_1 = 149.93$, $\Omega_2 = 11.90$, $\zeta = 0.05$, $\eta_2 = 5.64$)

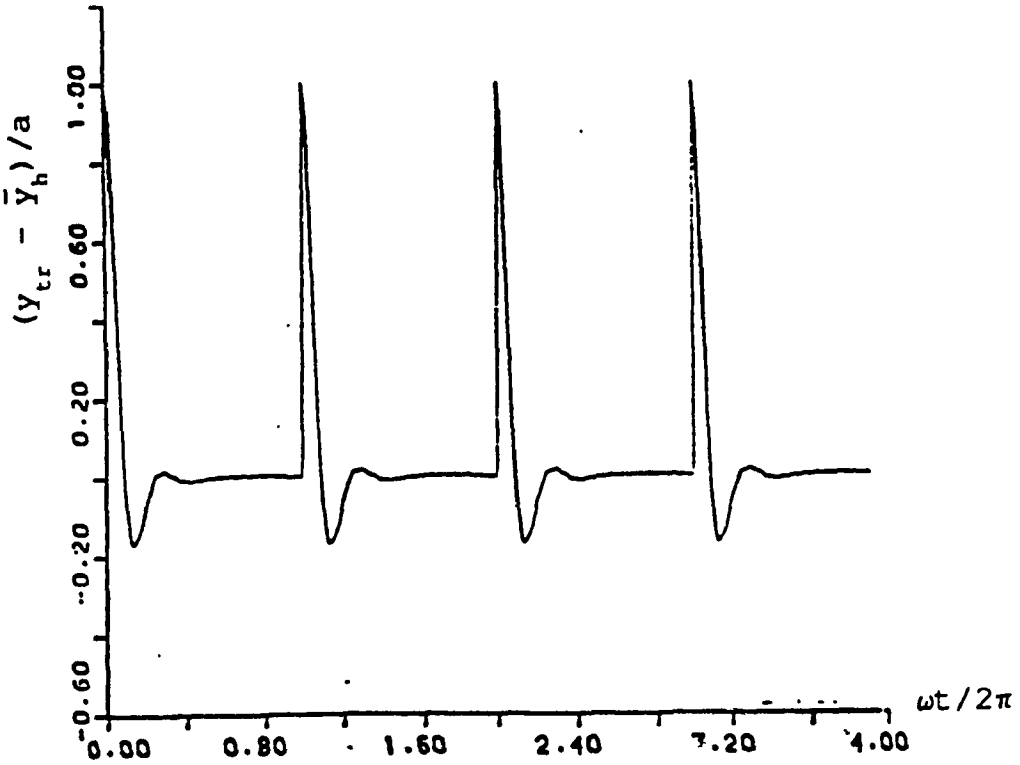

Fig. 2.17 Head position error variation with time ($R = 10^{-3}$, $\Omega_1 = 149.93$, $\Omega_2 = 11.90$, $\zeta = 0.05$, $\eta_2 = 5.64$)

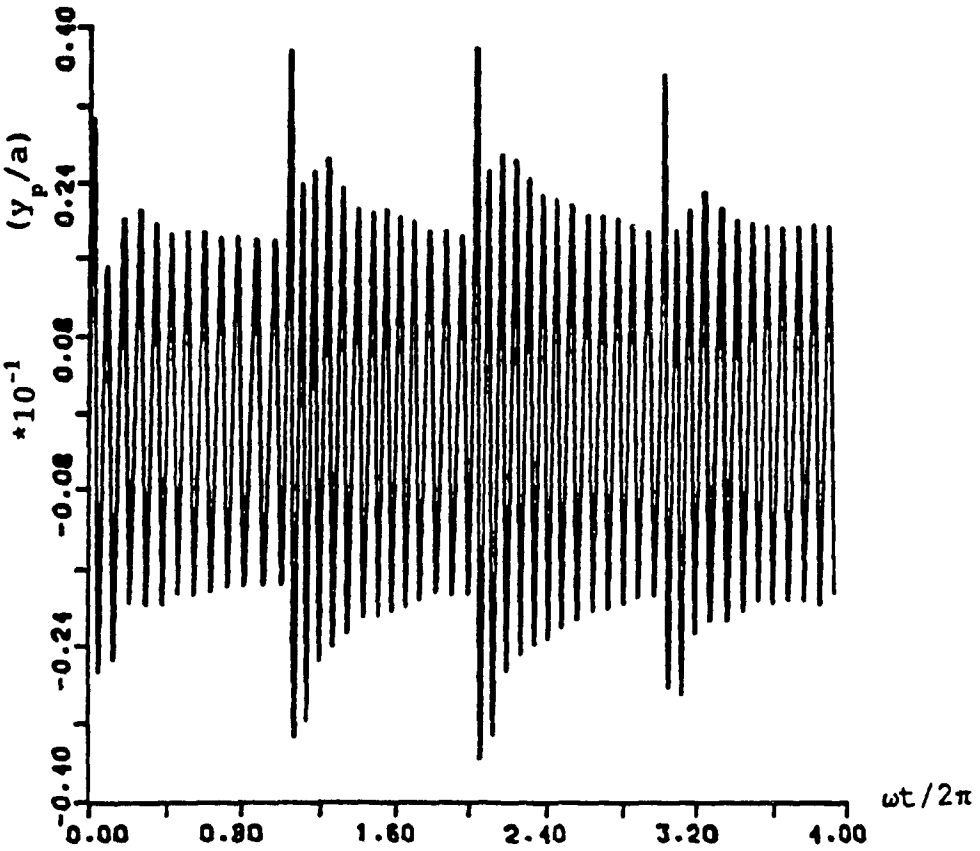

Fig. 2.18 Bearing displacement variation with time
($R = 10^{-2}$, $\Omega_1 = 104.95$, $\Omega_2 = 11.90$,
$\zeta = 0.05$, $\eta_2 = 5.64$)

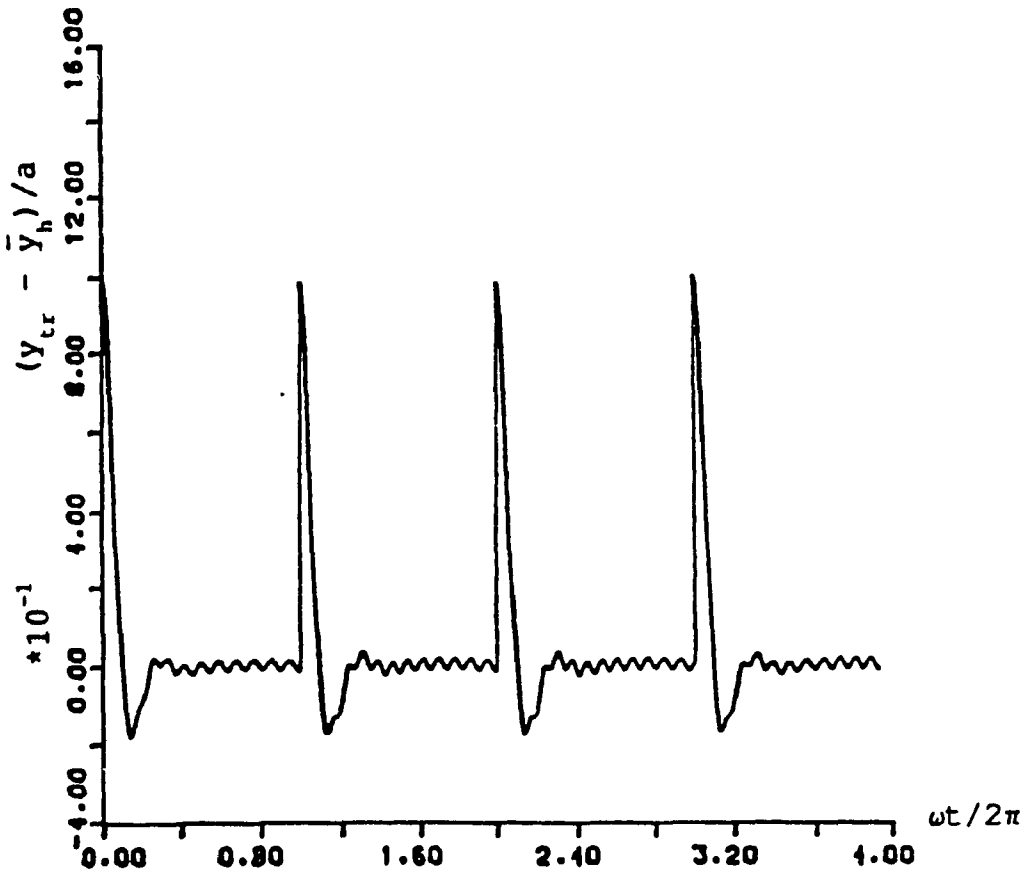

Fig. 2.19 Head positioning error variation with time ($R = 10^{-2}$, $\Omega_1 = 104.95$, $\Omega_2 = 11.90$, $\zeta = 0.05$, $\eta_2 = 5.64$)

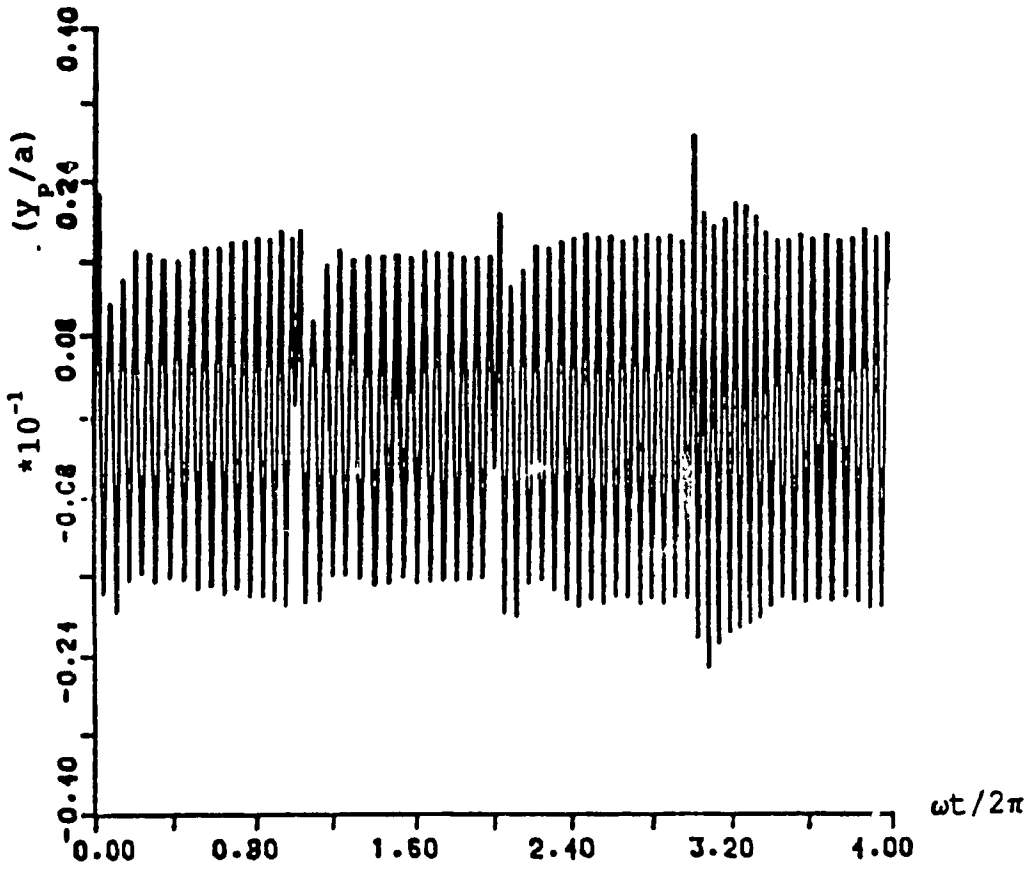

Fig. 2.20 Bearing displacement variation with time ($R = 10^{-2}$, $\Omega_1 = 224.90$, $\Omega_2 = 11.90$, $\zeta = 0.05$, $\eta_2 = 5.64$)

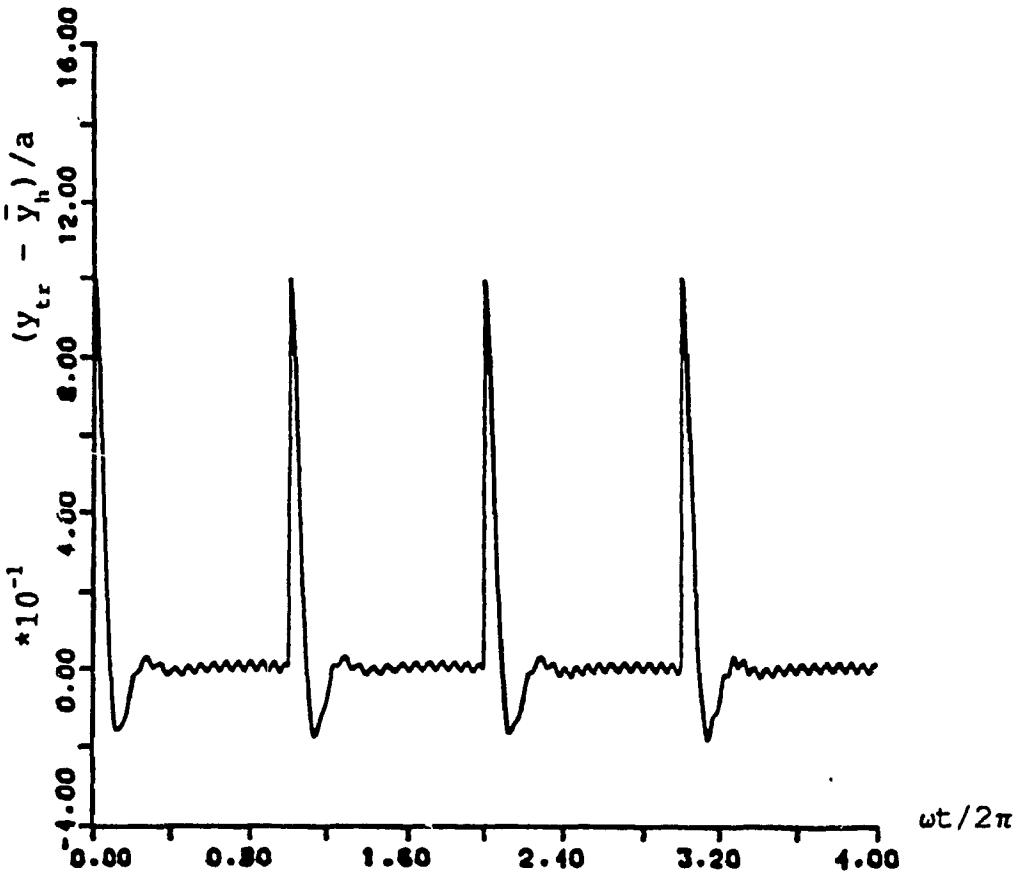

Fig. 2.21 Head positioning error variation with time
($R = 10^{-2}$, $\Omega_1 = 224.90$, $\Omega_2 = 11.90$,
$\zeta = 0.05$, $\eta_2 = 5.64$)

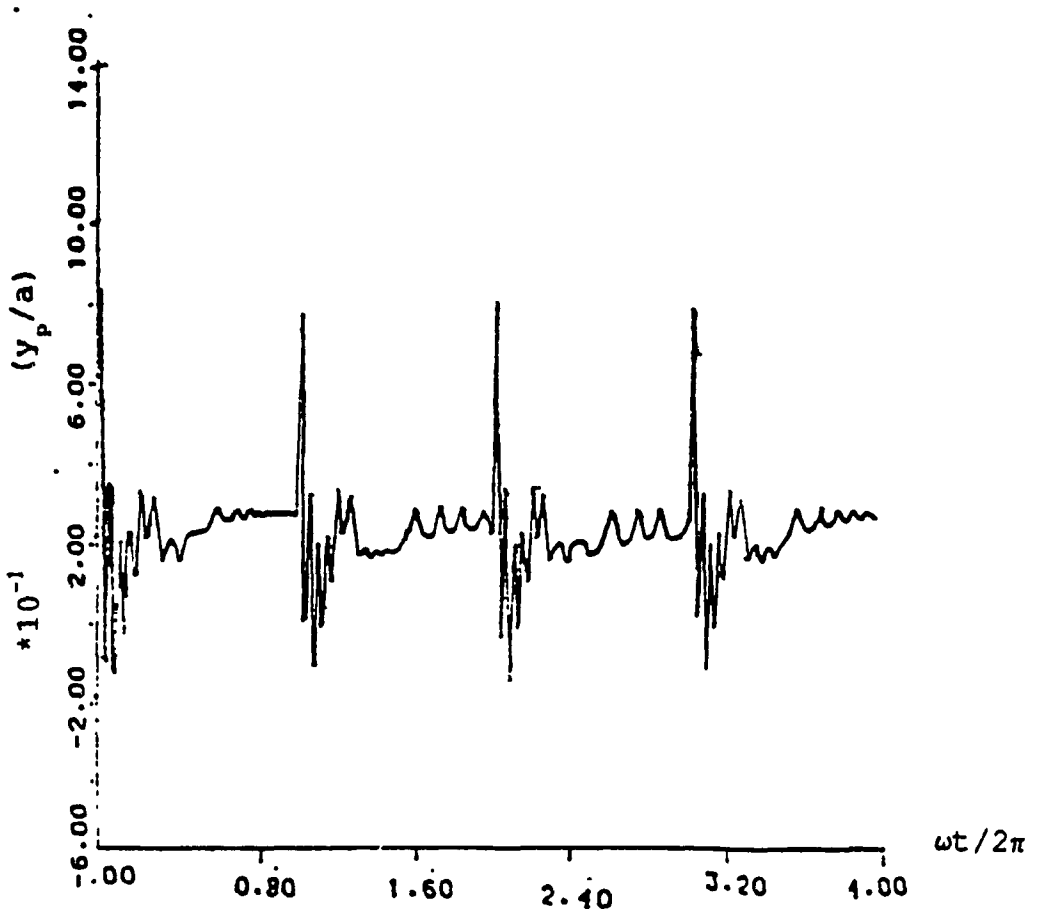

Fig. 2.22 Bearing displacement variation with time
($R = 10^{-3}$, $\Omega_1 = 149.93$, $\Omega_2 = 11.90$,
$\zeta = 0.1$, $\eta_2 = 5.64$)

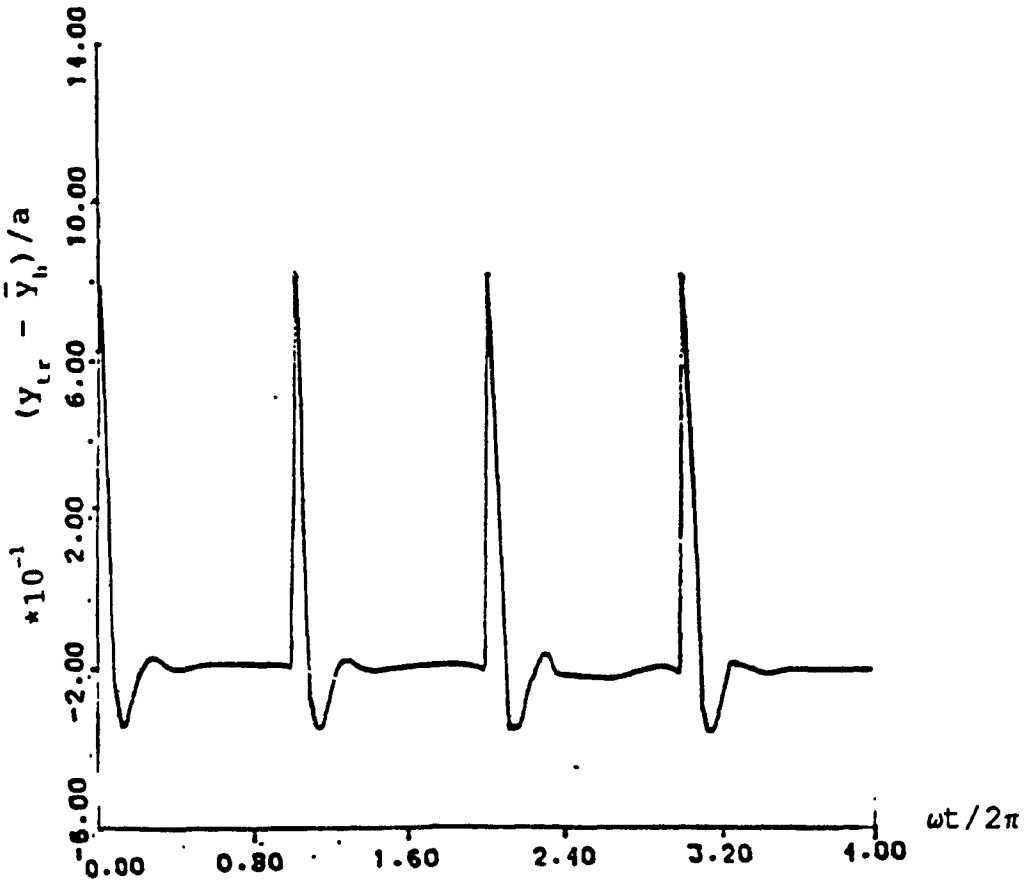

Fig. 2.23 Head positioning error variation with time
($R = 10^{-3}$, $\Omega_1 = 149.93$, $\Omega_2 = 11.90$,
$\zeta = 0.1$, $\eta_2 = 5.64$)

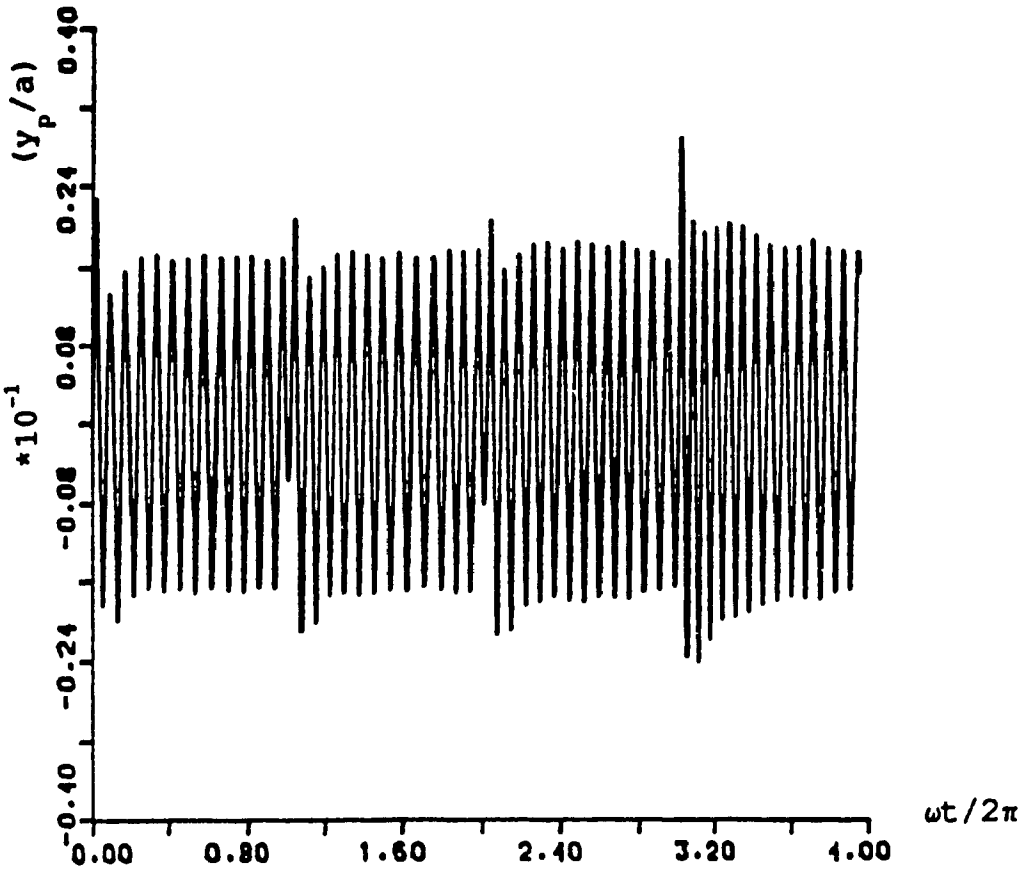

Fig. 2.24 Bearing displacement variation with time ($R = 10^{-2}$, $\Omega_1 = 149.93$, $\Omega_2 = 8.33$, $\zeta = 0.05$, $\eta_2 = 5.64$)

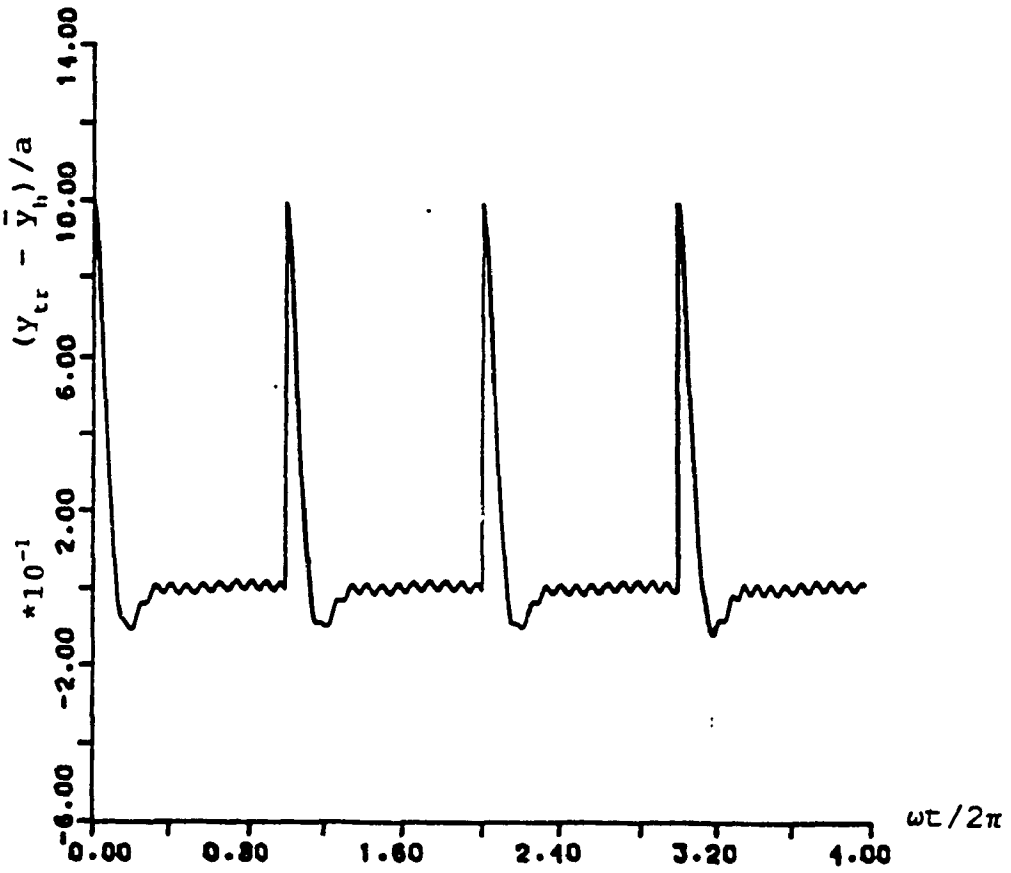

Fig. 2.25 Head positioning error variation with time ($R = 10^{-2}$, $\Omega_1 = 149.93$, $\Omega_2 = 8.33$, $\zeta = 0.05$, $\eta_2 = 5.64$)

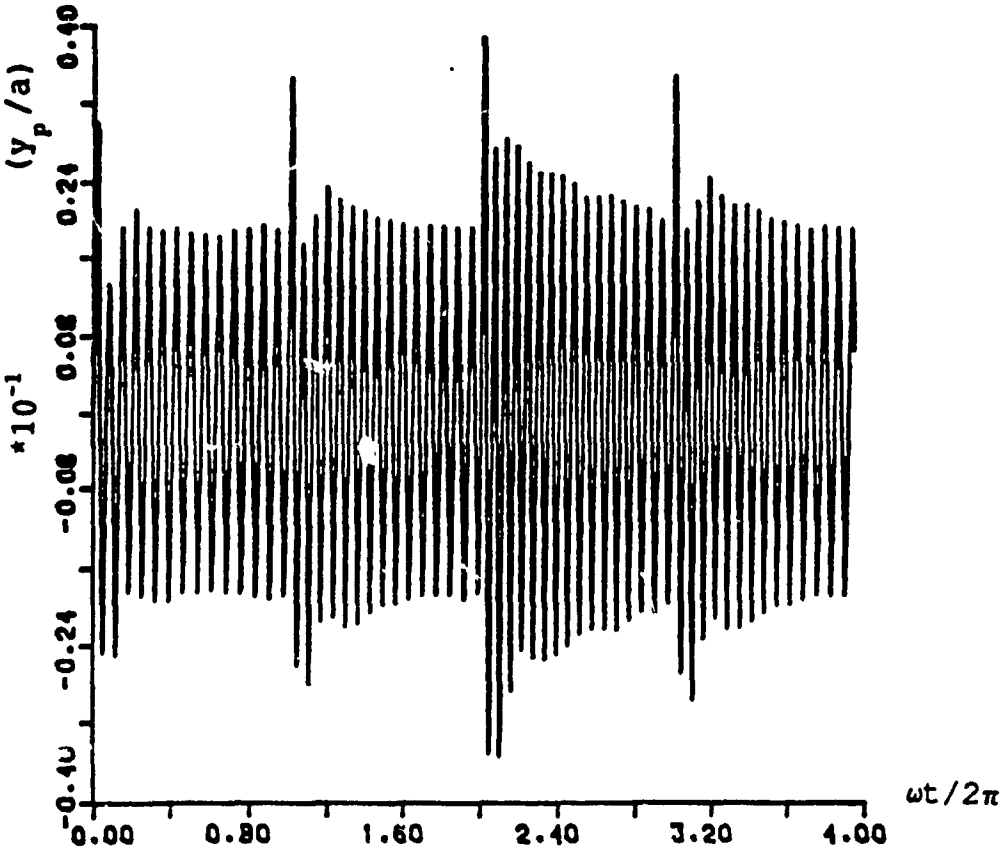

Fig. 2.26 Bearing displacement variation with time
($R = 10^{-2}$, $\Omega_1 = 149.93$, $\Omega_2 = 15.47$,
$\zeta = 0.05$, $\eta_2 = 5.64$)

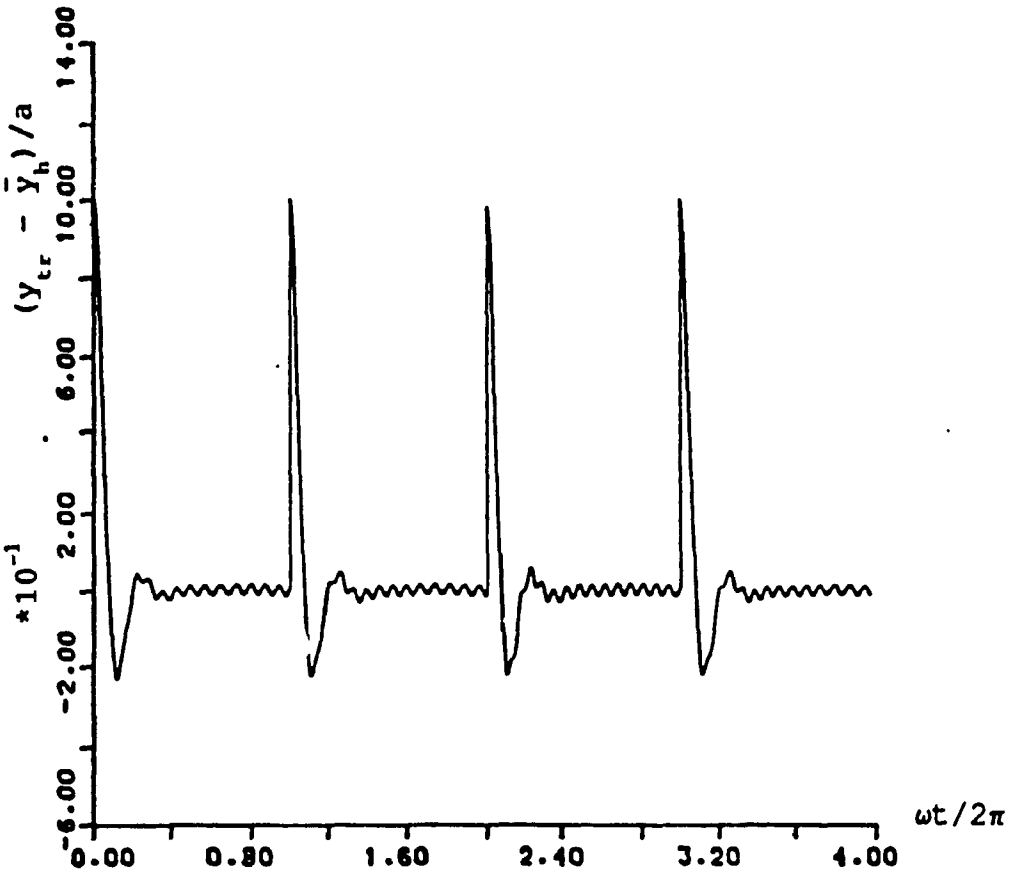

Fig. 2.27 Head positioning error variation with time
($R = 10^{-2}$, $\Omega_1 = 149.93$, $\Omega_2 = 15.47$,
$\zeta = 0.05$, $\eta_2 = 5.64$)

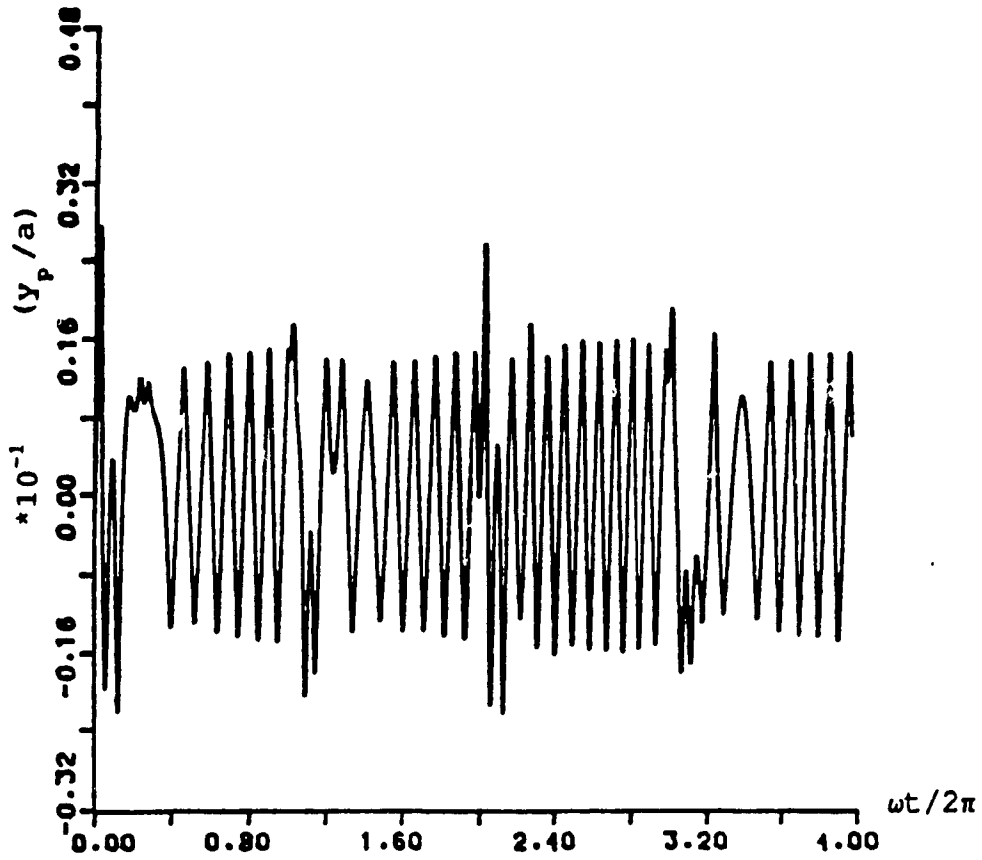

Fig. 2.28 Bearing displacement variation with time ($R = 10^{-2}$, $\Omega_1 = 149.93$, $\Omega_2 = 11.90$, $\zeta = 0.05$, $\eta_2 = 3.95$)

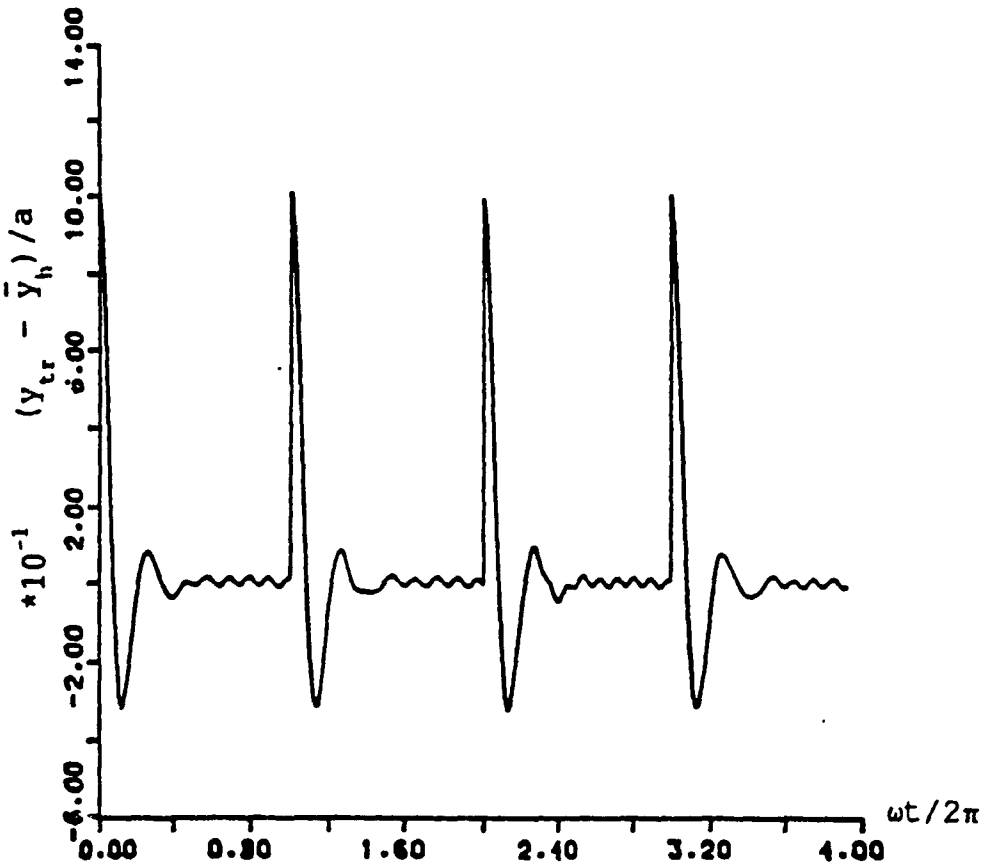

Fig. 2.29 Head positioning error variation with time
($R = 10^{-2}$, $\Omega_1 = 149.93$, $\Omega_2 = 11.90$,
$\zeta = 0.05$, $\eta_2 = 3.95$)

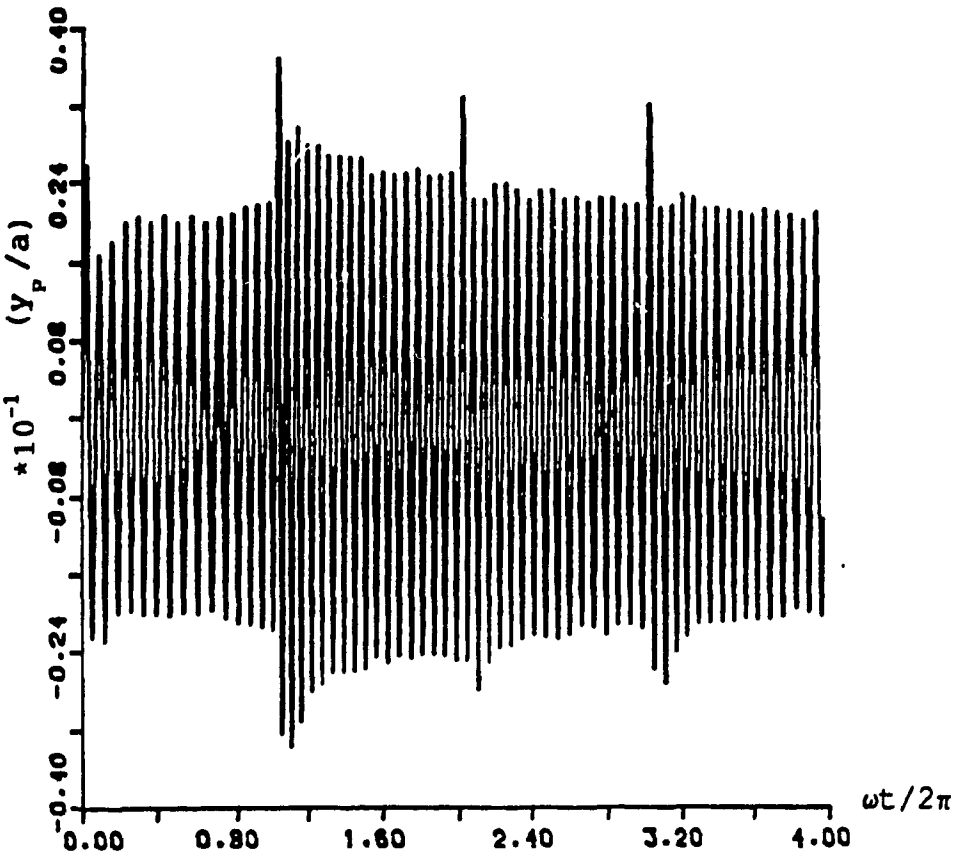

Fig. 2.30 Bearing displacement variation with time
($R = 10^{-2}$, $\Omega_1 = 19.93$, $\Omega_2 = 11.90$,
$\zeta = 0.05$, $\eta_2 = 7.33$)

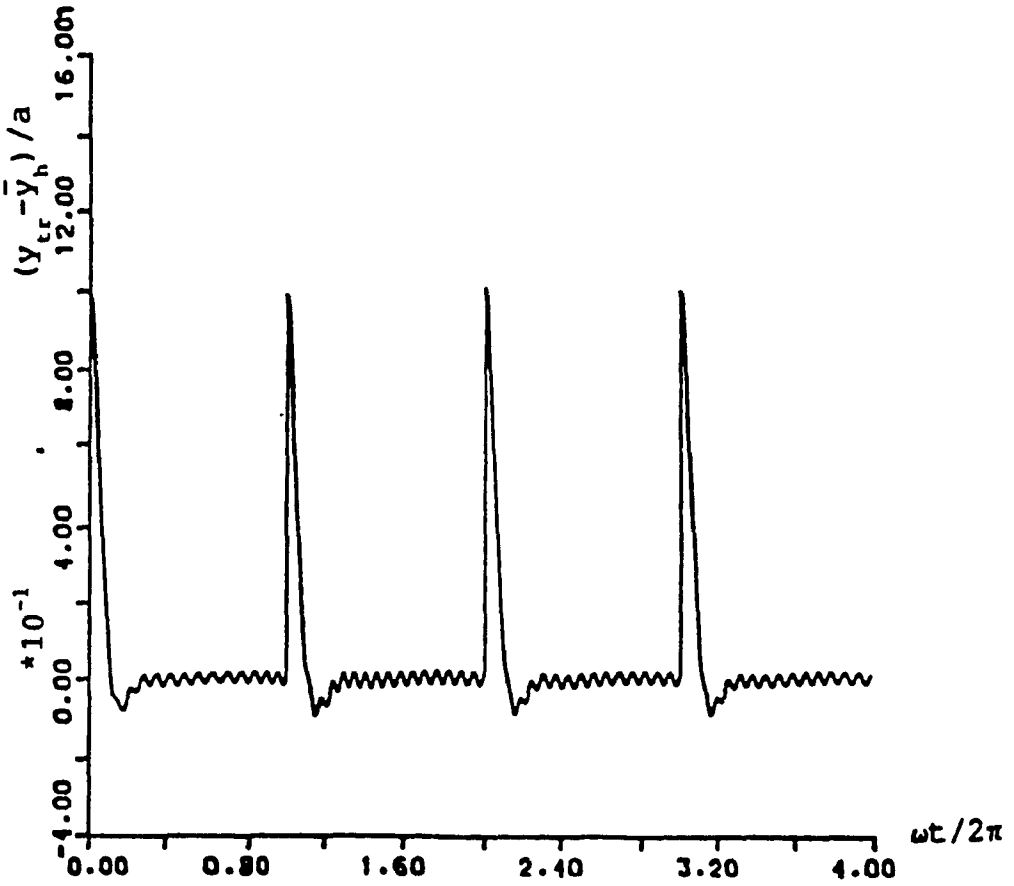

Fig. 2.31 Head positioning error variation with time
($R = 10^{-2}$, $\Omega_1 = 149.93$, $\Omega_2 = 11.90$,
$\zeta = 0.05$, $\eta_2 = 7.33$)

CHAPTER 3

FINITE ELEMENT MODELLING OF THE ROTARY ACTUATOR

CHAPTER 3

FINITE ELEMENT MODELLING OF THE ROTARY ACTUATOR ARM

3.1 Introduction

The swinging arm actuator was modelled as a rigid link rotating about a flexible pivot and analyzed in Chapter 2. However, from the point of view of the submicron accuracy needed in a head positioning mechanism in a disk storage device, it is proper to treat the swinging arm as a flexible component. A complete dynamic analysis assuming a flexible swinging arm model is beyond the scope of this study. In this chapter, a finite element model of the swinging arm is carried out and analyzed for its natural frequencies and mode shapes, to demonstrate its flexible nature. A software package called ANSYS is used for this study.

The ANSYS software is a large scale general purpose finite element program which has capabilities for linear and non-linear static and dynamic analysis. It can handle small and large displacements as well as solve problems involving elastic, plastic creep and swelling effects. It utilizes the matrix displacement method for the analysis and the wavefront solution method for the actual equation solution. Over a hundred linear and non-linear elements are available in its library for modelling purposes. There are basically three phases involved in an ANSYS solution. Figure 3.1 shows a flow chart of the analysis method for any type of problem.

3.2 Finite Element Model of a Swinging Arm Actuator

Figure 3.2 show the finite element model of the arm structure. The arm structure is composed of 18 nodes, 26 beam elements, 1 plate, 4 facets, and 4 masses. The finite element model to define the arm structure is shown in table 1.

3.3 Material Properties

The arm structure is made of Aluminium, Magnesium, Gephenolic, the detail of which is given in Table 1. For the analysis purpose all material properties were input into Ansys model. The following material properties were used for the analysis.

TABLE 1

Designation	Density (ρ)	Modulus of Elasticity (E)	Poisons ratio υ
Gephenolic	1020	3.45E9	0.3
Aluminium	2700	6.90E10	0.3
Magnesium	1310	2.42E10	0.3

3.4 Analysis

The Analytical model of the arm structure is shown in Figure. 3.3. The Modal Analysis is used to extract the natural frequencies and mode shapes of a linear structure.

The following assumptions are made

i) There is no damping.

ii) Mass and Stiffness matrices are constant.

iii) No loads (such as forces, non-zero displacements, pressures or temperatures) are allowed; i.e., free vibration are assumed.

The governing equation for free, undamped vibration is:

$$M \ddot{X} + K X = 0 \qquad (3.1)$$

where M and K are the assembled mass and stiffness matrices, respectively. For linear structure the displacements are harmonic of the form:

$$X = X_0 \cos \omega t \qquad (3.2)$$

Subsituting for X in equation (3.1) gives the eigen value equation.

$$(K - \omega^2 M) X_0 = 0 \qquad (3.3)$$

For non-trivial solutions ($X_0 = 0$), the determinant of ($K - \omega^2 M$) must vanish.

$$| K - \omega^2 M | = 0 \qquad (3.4)$$

If n is the order of the matrices, then this equation results in a polynomial of order n, which should have n roots:

These roots are the eigen values of the equation. When substituted in Equation (3.1), n corresponding vectors X_0 can be calculated:

$$X_1, X_2, \ldots\ldots, X_n$$

These are known as the eigen vectors.

3.5 Discussion of the Results

In the analysis in chapter 2, the response was calculated by assuming that rotary actuator arm is rigid. Considering mass and moment of inertia of the rigid arm and the bearing stiffness, the natural frequency of the actuator is found to be 1200 Hz. However, the rotary arm is a structure made up of linkages and plates having distributed mass and elasticity. It could have its own natural frequencies and mode shapes. Since, even very small motion of the actuator will effect the accuracy of the head positioning, it is important that the rotary arm is also modelled as a flexible system. For an accurate analysis, the response of the system must be evaluated considering the rotary arm as a flexible system, however, in the present study only the natural frequencies and mode shapes of the arm with the pivot point assumed to be fixed are presented.

Two cases are considered in obtaining the natural frequencies and mode shapes. In one case all the 6 degree's of freedom at a node are taken into account. In the second case only the inplane translational degree's of freedom are considered. Table 3.1 shows the result of this study. Figures 3.4, 3.5, 3.6 and 3.7 show the four mode shapes at 1559 Hz, 1968 Hz, 3887 Hz, and 4650 Hz corresponding to 1, 2, 3, and 4 mode shapes where 1 d.o.f are considered.

In the next chapter, the dynamic behaviour of the disk rotating mechanism is studied. The natural frequencies and mode shapes are presented, and the response of the system to unbalance

excitations is obtained by solving the non homogenous problem using modal analysis.

TABLE 3.1

Natural Frequencies of Flexible Rotary Arm

using Finite Element Method

1 d.o.f (Hz)	6 d.o.f (Hz)
1559	597
1968	805
3887	911
4650	1217
6934	1457

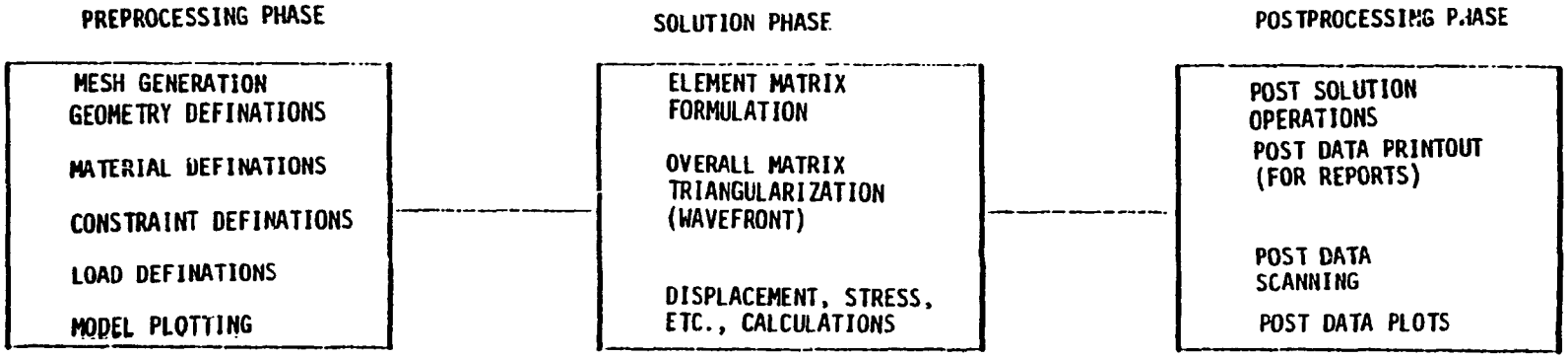

Fig. 3.1 Typical Phases of an Ansys Analysis

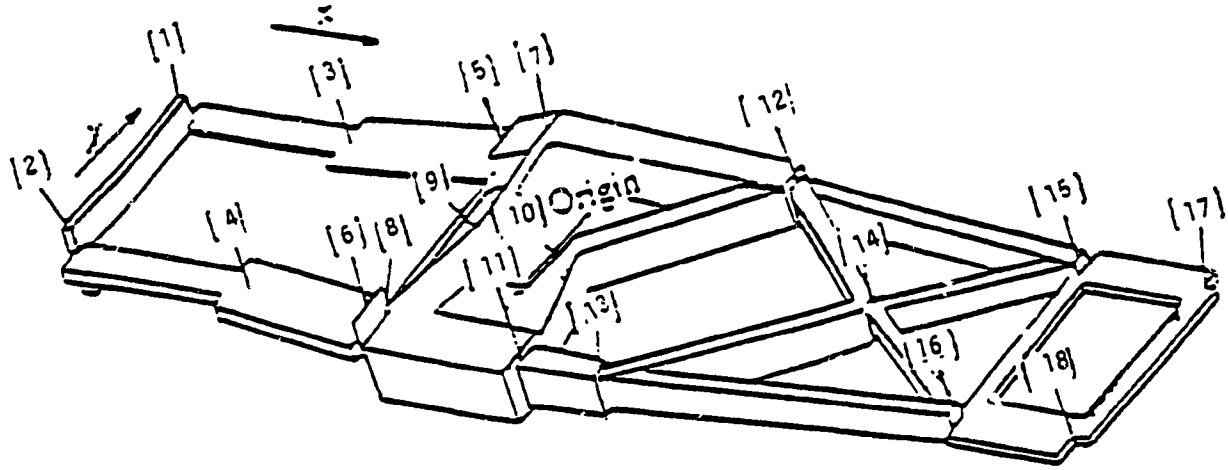

Fig. 3.2 Finite element model of arm structure [3]

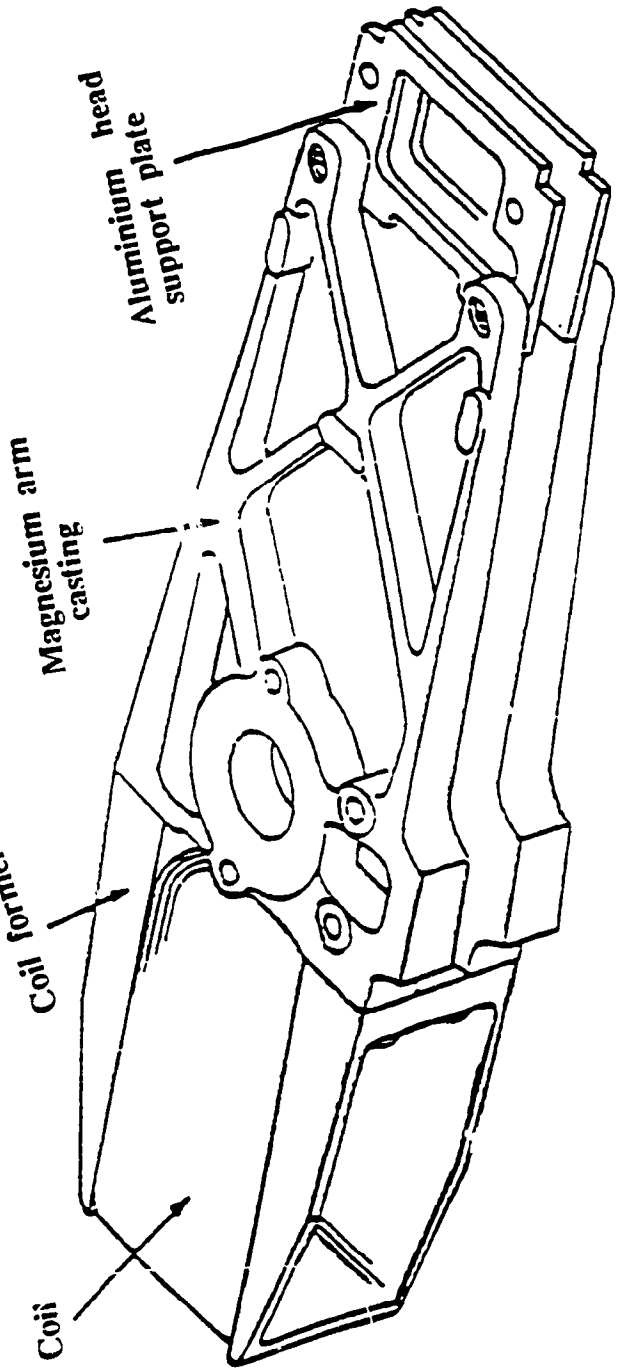

Fig. 3.3 Analytical model of the arm structure [3]

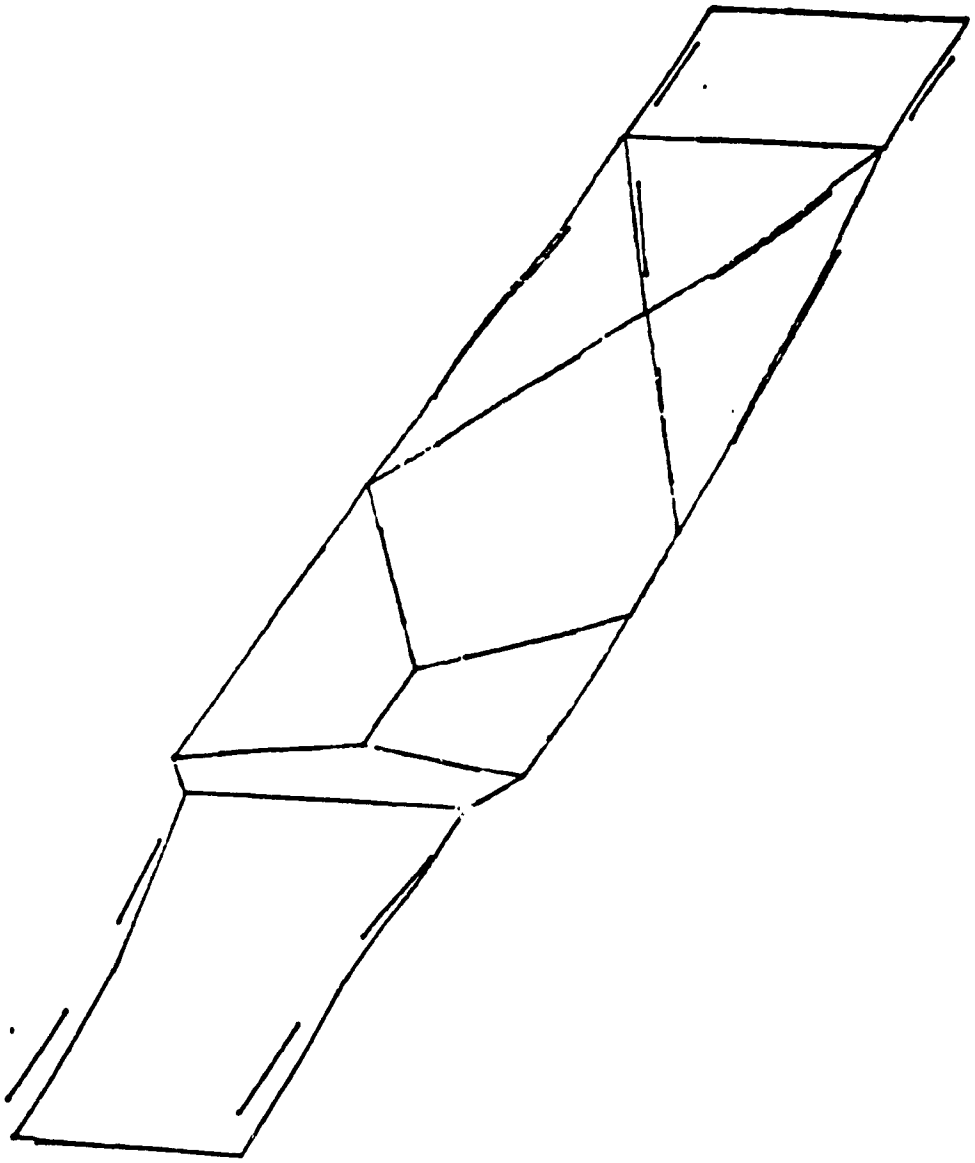

Fig. 3.4 First mode shape of the swinging arm
(f_1 = 1559 Hz)

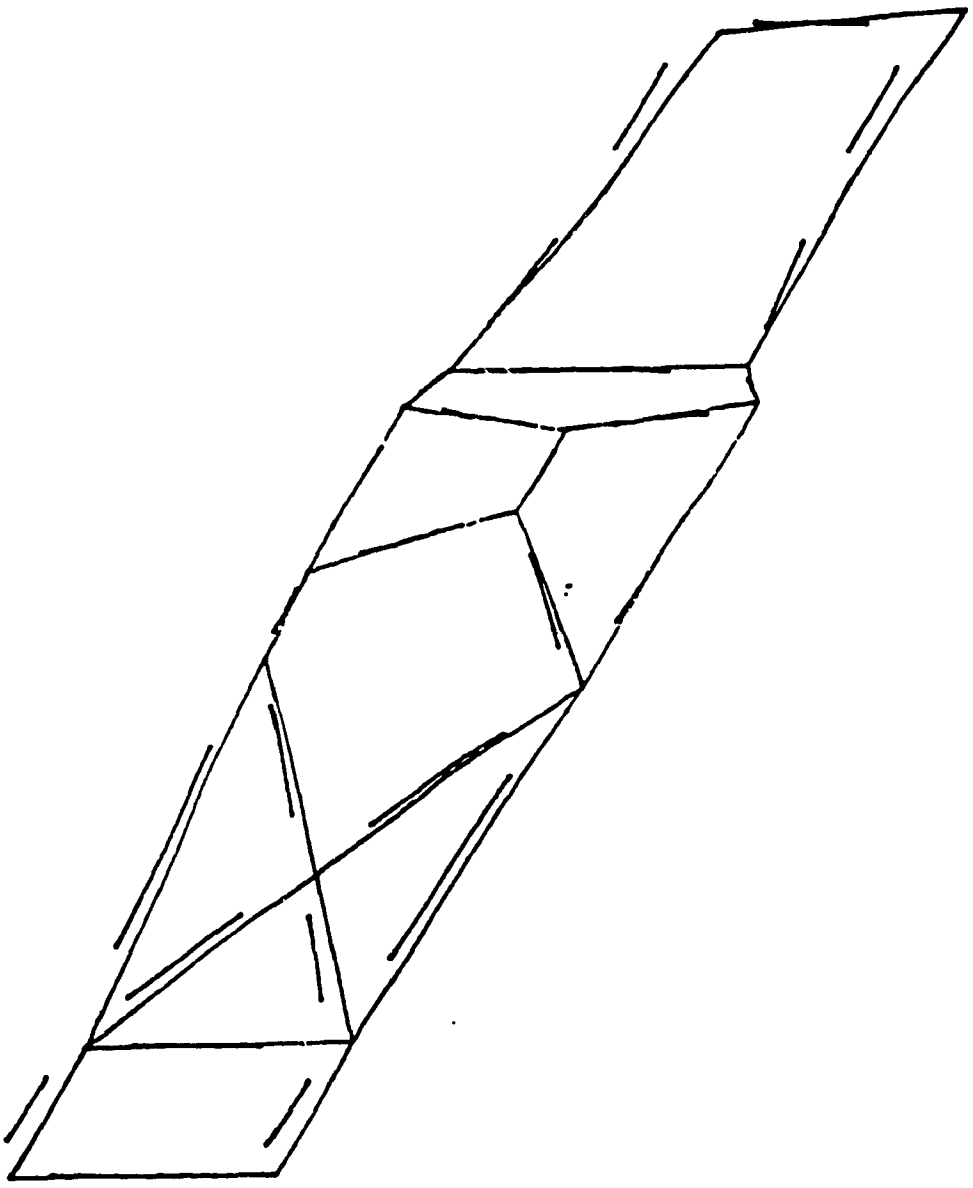

Fig. 3.5 Second mode shape of the swinging arm
(f_2 = 1968 Hz)

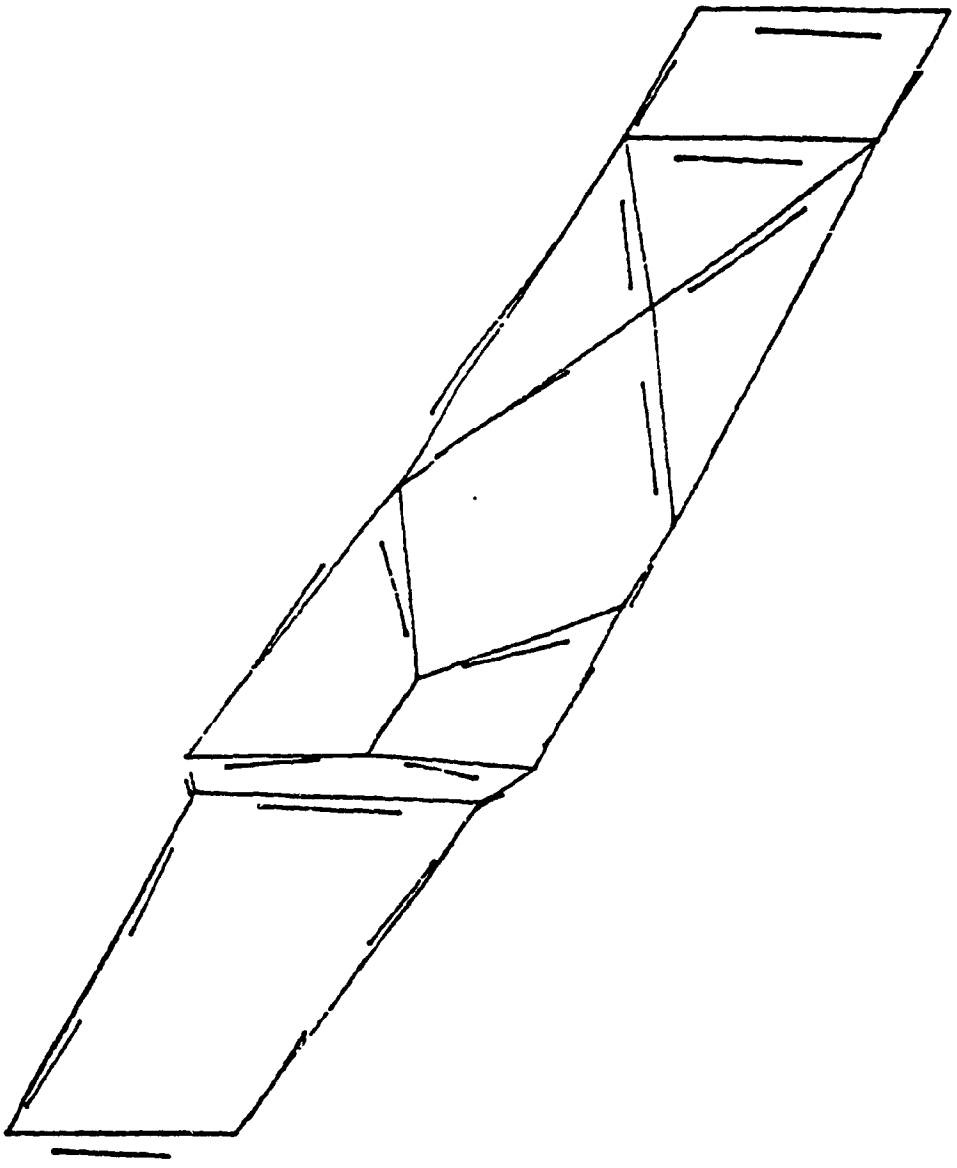

Fig. 3.6 Third mode shape of the swinging arm (f_3 = 3887 Hz)

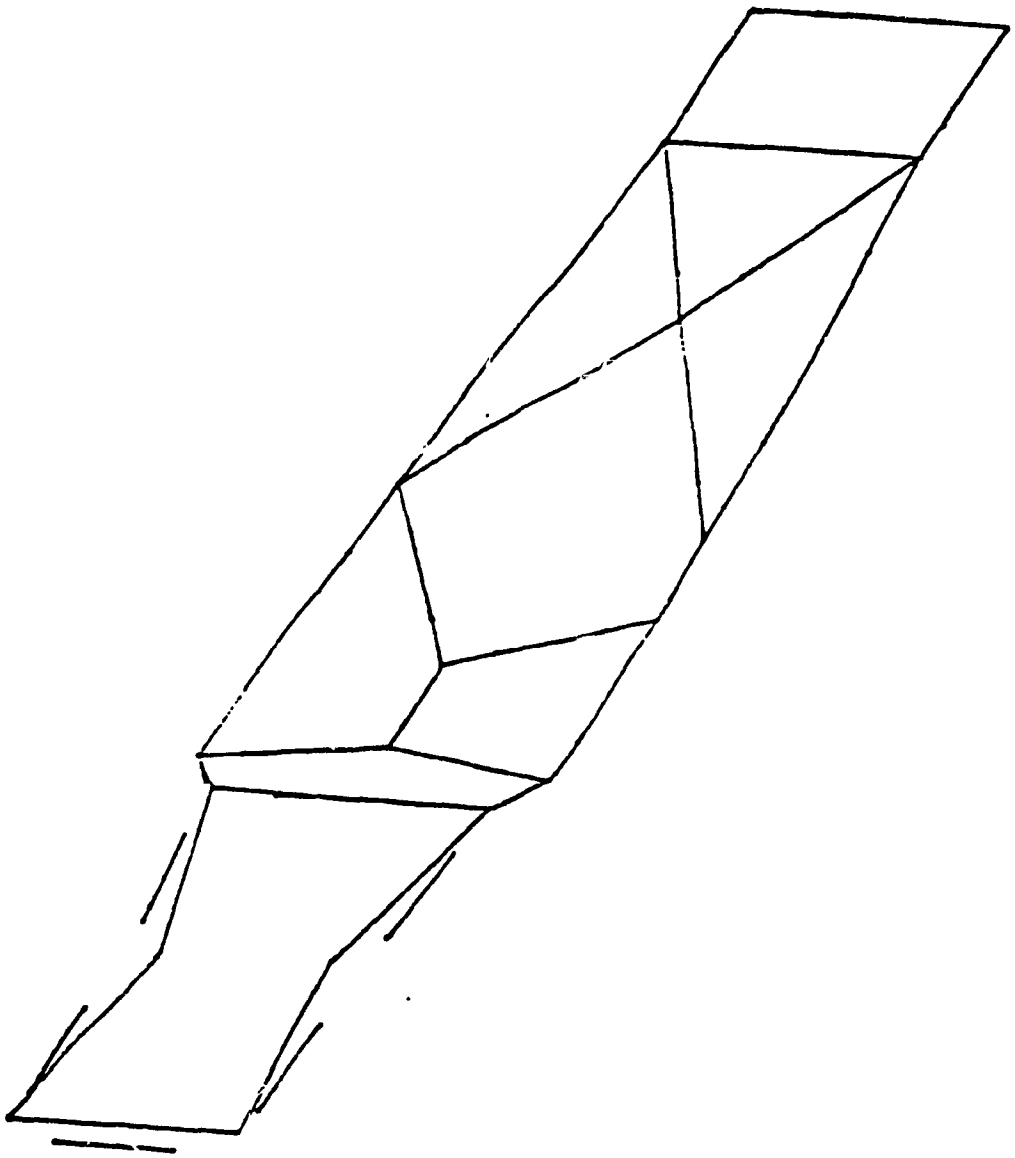

Fig. 3.7 Fourth mode shape of swinging arm (f_4 = 4650 Hz)

CHAPTER 4

DYNAMIC ANALYSIS OF A SPINDLE FOR A HARD DISK DRIVE

CHAPTER 4

DYNAMIC ANALYSIS OF A SPINDLE FOR A HARD DISK DRIVE

4.1 Introduction

Dynamic behavior of a disk rotating mechanism is of interest because the rotating shaft and disk assemblycan undergo whirling motion due to mass unbalance and torsional vibration during starting and stopping of the motor. The main performance measures in magnetic disk storage devices are access performance and areal recording density. Higher speeds and higher densities can be achieved if the performance of the disk drive assembly, can be improved by reducing the dynamic responses.

In this chapter, the dynamics of the disk rotating mechanism is studied by solving the resulting homogenous simultaneous equations, the natural frequencies and the mode shapes are obtained. The response of the system is obtained by solving the non homogenous problem using modal analysis.

4.2 CONSTRUCTION OF THE DRIVE

The overall construction of the drive is shown in Figure 4.1. The disk enclosure is supported horizontally at three points with rubber mounts for vibration and shock absorption. A shock sensor is provided on the disk enclosure to monitor for excess shock against the disk enclosure during shipping and handling. The rotary actuator is secured by a mechanical lock to prevent damage to the heads and disks during transportation. No mechanical lock is required for the spindle motor.

4.3 DISK ENCLOSURE (DE)

The mechanical configuration of the DE is shown in Figure 4.2. It is designed to provide a compact, low power consumption, and maintenance free file. It features eight 8 inch diameter disks which are supported on a spindle and are driven by the built in brushless DC motor with a rotational speed of 3000 rpm. A compact swinging arm head positioning rotary actuator is used for head positioning on to the desired track.

4.4 Spindle

The primary function of the spindle is to maintain precise and constant rotation of the assembled disks. The accuracy of rotation involves concentricity, precision, thermal, and dynamic stability, all of which become stringent as the track spacing gets denser.

4.5 Air Filtration System

The disks, read/write heads and actuator are fully enclosed in a module using an integral re-circulating air system and filter to maintain a clean environment. A separate filter permits ambient pressure equilization without entry of contaminants. The fundamental and important function of the air system is to minimize the possibility of head-disk interference. Air flows through the disk spacings from the center to outside of the disks by the pressure difference between them, induced by the rotation of disks. An absolute filter, whose efficiency is 99.97 percent

about 0.3 μ m particle size dust, is attached within the spindle hub and is rotating with the disks. Particle count goes very nearly zero in a few minutes from the start of rotation. Ferro fluidic seals are adopted to complete the elimination of air contamination.

4.6 Whirling Response of Disk Rotor

The analytical model of the disk rotating mechanism is shown in Fig. 4.3. The rotor poles in the DC motorgenerate torque by the revolving magnetic field, and are connected directly to a single shaft to which magnetic disks are attached.

The flexural motion of the spindle carrying the disks is described by:

$$m_1\ddot{x}_1 + K_1x_1 + K_2(x_1 - x_2) + C_1\dot{x}_1 + C_2(\dot{x}_1 - \dot{x}_2) = m_1e_1\omega^2\sin(\omega t + \varphi_1) \quad (4.1)$$

$$m_2\ddot{x}_2 + K_2(x_2 - x_1) + K_3(x_2 - x_3) + C_2(\dot{x}_2 - \dot{x}_1) + C_3(\dot{x}_2 - \dot{x}_3) = m_2e_2\omega^2\sin(\omega t + \varphi_2) \quad (4.2)$$

$$m_3\ddot{x}_3 + K_3(x_3 - x_2) + K_4(x_3 - x_4) + C_3(\dot{x}_3 - \dot{x}_2) + C_4(\dot{x}_3 - \dot{x}_4) = m\, e_3\omega^2\sin(\omega t + \varphi_3) \quad (4.3)$$

$$m_4\ddot{x}_4 + K_4(x_4 - x_3) + K_5(x_4 - x_5) + C_4(\dot{x}_4 - \dot{x}_3) + C_5(\dot{x}_4 - \dot{x}_5) = m\, e_4\omega^2\sin(\omega t + \varphi_4) \quad (4.4)$$

$$m_5\ddot{x}_5 + K_5(x_5 - x_4) + K_6(x_5 - x_6) + C_5(\dot{x}_5 - \dot{x}_4) + C_6(\dot{x}_5 - \dot{x}_6) = m_5e_5\omega^2\sin(\omega t + \varphi_5) \quad (4.5)$$

$$m_6\ddot{x}_6 + K_6(x_6 - x_5) + K_7(x_6 - x_7) + C_6(\dot{x}_6 - \dot{x}_5) + C_7(\dot{x}_6 - \dot{x}_7) = m_6 e_6 \omega^2 \sin(\omega t + \varphi_6) \quad (4.6)$$

$$m_7\ddot{x}_7 + K_7(x_7 - x_6) + K_8(x_7 - x_8) + C_7(\dot{x}_7 - \dot{x}_8) + C_8(\dot{x}_7 - \dot{x}_8) = m_7 e_7 \omega^2 \sin(\omega t + \varphi_7) \quad (4.7)$$

$$m_8\ddot{x}_8 + K_8(x_8 - x_7) + C_8(\dot{x}_8 - \dot{x}_7) + K_9 x_8 + C_9 \dot{x}_8 = m_8 e_8 \omega^2 \sin(\omega t + \varphi_8) \quad (4.8)$$

Divide Eqn's (4.1) to (4.8) by m_1, and introducing the following quantities.

$$\alpha_i = \frac{m_i}{m_1}$$

$$\omega_i^2 = \frac{K_i}{m_1}$$

$$\zeta_i = \frac{C_i}{2 m_1 \omega_1} \qquad i = 1,2 \ldots\ldots 8$$

$$\alpha_1 \frac{\ddot{x}_1}{e_1} + \omega_1^2 \frac{x_1}{e_1} + 2 \zeta_1 \omega_1 \frac{\dot{x}_1}{e_1} + \omega_2^2 \frac{(x_1 - x_2)}{e_1} + 2 \zeta_2 \omega_1 \frac{(\dot{x}_1 - \dot{x}_2)}{e_1} = \alpha_1 \omega^2 \sin(\omega t + \varphi_1) \quad (4.9)$$

$$\alpha_2 \frac{\ddot{x}_2}{e_2} + \omega_2^2 \frac{(x_2 - x_1)}{e_2} + 2 \zeta_2 \omega_1 \frac{(\dot{x}_2 - \dot{x}_1)}{e_2} + \omega_3^2 \frac{(x_2 - x_3)}{e_2} + 2 \zeta_3 \omega_1 \frac{(\dot{x}_2 - \dot{x}_3)}{e_2} = \alpha_2 \omega^2 \sin(\omega t + \varphi_2) \quad (4.10)$$

$$\alpha_3 \frac{\ddot{x}_3}{e_3} + \omega_3^2 \frac{(x_3 - x_2)}{e_3} + 2 \zeta_3 \omega_1 \frac{(\dot{x}_3 - \dot{x}_2)}{e_3} + \omega_4^2 \frac{(x_3 - x_4)}{e_3} + 2 \zeta_4 \omega_1 \frac{(\dot{x}_3 - \dot{x}_4)}{e_3} = \alpha_3 \omega^2 \sin(\omega t + \varphi_3) \quad (4.11)$$

$$\alpha_4 \frac{\ddot{x}_4}{e_4} + \omega_4^2 \frac{(x_4 - x_3)}{e_4} + 2\,\zeta_4\,\omega_1 \frac{(\dot{x}_4 - \dot{x}_3)}{e_4} + \omega_5^2 \frac{(x_4 - x_5)}{e_4}$$

$$+ 2\,\zeta_5\,\omega_1 \frac{(\dot{x}_4 - \dot{x}_5)}{e_4} = \alpha_4\,\omega^2 \sin(\omega t+\varphi_4) \qquad (4.12)$$

$$\alpha_5 \frac{\ddot{x}_5}{e_5} + \omega_5^2 \frac{(x_5 - x_4)}{e_5} + 2\,\zeta_5\,\omega_1 \frac{(\dot{x}_5 - \dot{x}_4)}{e_5} + \omega_6^2 \frac{(\dot{x}_5 - \dot{x}_4)}{e_5}$$

$$+ 2\,\zeta_6\,\omega_1 \frac{(\dot{x}_5 - \dot{x}_6)}{e_5} = \alpha_5\,\omega^2 \sin(\omega t+\varphi_5) \qquad (4.13)$$

$$\alpha_6 \frac{\ddot{x}_6}{e_6} + \omega_6^2 \frac{(x_6 - x_5)}{e_6} + 2\,\zeta_6\,\omega_1 \frac{(\dot{x}_6 - \dot{x}_5)}{e_6} + \omega_7^2 \frac{(x_6 - x_7)}{e_6}$$

$$+ 2\,\zeta_7\,\omega_1 \frac{(\dot{x}_6 - \dot{x}_7)}{e_6} = \alpha_6\,\omega^2 \sin(\omega t+\varphi_6) \qquad (4.14)$$

$$\alpha_7 \frac{\ddot{x}_7}{e_7} + \omega_7^2 \frac{(x_7 - x_6)}{e_7} + 2\,\zeta_7\,\omega_1 \frac{(\dot{x}_7 - \dot{x}_6)}{e_7} + \omega_8^2 \frac{(x_7 - x_8)}{e_7}$$

$$+ 2\,\zeta_8\,\omega_1 \frac{(\dot{x}_7 - \dot{x}_8)}{e_7} = \alpha_7\,\omega^2 \sin(\omega t+\varphi_7) \qquad (4.15)$$

$$\alpha_8 \frac{\ddot{x}_8}{e_8} + \omega_8^2 \frac{(x_8 - x_7)}{e_8} + 2\,\zeta_8\,\omega_1 \frac{(\dot{x}_8 - \dot{x}_7)}{e_8}$$

$$= \alpha_8\,\omega^2 \sin(\omega t+\varphi_8) \qquad (4.16)$$

$$\alpha_i = \frac{x_i}{e_i}$$

The elements of mass, stiffness, and damping matrices are given in appendix III.

4.7 Torsional Vibration of Disk Rotor

The equations of motion for torsional vibrations are described by:

$$I_1\ddot{\theta}_1 + K_{t1}\theta_1 + K_{t2}(\theta_1 - \theta_2) = T_m \quad (4.17)$$

$$I_2\ddot{\theta}_2 + K_{t2}(\theta_2 - \theta_1) + K_{t3}(\theta_2 - \theta_3) = 0.0 \quad (4.18)$$

$$I_3\ddot{\theta}_3 + K_{t3}(\theta_3 - \theta_2) + K_{t4}(\theta_3 - \theta_4) = 0.0 \quad (4.19)$$

$$I_4\ddot{\theta}_4 + K_{t4}(\theta_4 - \theta_3) + K_{t5}(\theta_4 - \theta_5) = 0.0 \quad (4.20)$$

$$I_5\ddot{\theta}_5 + K_{t5}(\theta_5 - \theta_4) + K_{t6}(\theta_5 - \theta_6) = 0.0 \quad (4.21)$$

$$I_6\ddot{\theta}_6 + K_{t6}(\theta_6 - \theta_5) + K_{t7}(\theta_6 - \theta_7) = 0.0 \quad (4.22)$$

$$I_7\ddot{\theta}_7 + K_{t7}(\theta_7 - \theta_6) + K_{t8}(\theta_7 - \theta_8) = 0.0 \quad (4.23)$$

$$I_8\ddot{\theta}_8 + K_{t8}(\theta_8 - \theta_7) = 0.0 \quad (4.24)$$

where damping is not considered.

The elements of torsional mass and stiffness matrices are given in appendix.

The equations for flexural and torsional motion freedom can be put independently in the matrix form as:

$$[M] \{ \ddot{X} \} + [C] \{ \dot{X} \} + [K] \{ X \} = \{ F \} \quad (4.25)$$

For torsional motions, it can be seen that [C] is considered as zero.

Equation of motion can be written in the form

$$[M] \{ \ddot{X} \} + [C] \{ \dot{X} \} + [K] \{ X \} = \mathrm{Im} \{ \alpha_i \omega^2 e^{i(\omega t + \psi_i)} \} \quad (4.26)$$

Assuming the solution in the form for the complex response.

$$\{ X \} = \{ \dot{X} \} e^{i\omega t} \quad (4.27)$$

Subsequently, the actual response is obtained as Im (X).

From Equation's (4.26) and (4.27), we get

$$\{ - [M] \omega^2 + i \omega [C] + [K] \} \dot{X} = \{ \alpha_i \omega^2 e^{i\Psi_i} \}$$

Expressing $\{ \dot{X} \}$ in terms of modal coordinate $\{ \dot{P} \}$.

$$\{ \dot{X} \} = [\phi] \{ \dot{P} \} \tag{4.28}$$

The equation of motion can be written as:

$$\{ - [M] \omega^2 + i \omega [C] + [\kappa] \} [\phi] \{ \dot{P} \} = \{ \alpha_i \omega^2 e^{i\Psi_i} \} \tag{4.29}$$

Premultiplying Equation (4.29) by $[\phi]^T$

$$- \omega^2 [\phi]^T [M] [\phi] \{ \dot{P} \} + i \omega [\phi]^T [C] [\phi] + [\phi]^T [\kappa] [\phi] \{ \dot{P} \} = [\phi]^T \{ \alpha_i \omega^2 e^{i\Psi_i} \} \tag{4.30}$$

From Equation (4.30), we have

$$\begin{aligned} [\phi]^T [M] [\phi] &= [\mu_i] \\ [\phi]^T [K] [\phi] &= [\kappa_i] \\ [\phi]^T [C] [\phi] &= [\gamma_i] \end{aligned} \tag{4.31}$$

Since the matrices [M] and [K] are symmetrical, the matrices [μ] and [κ] are diagonalized matrices. In general, [γ] is not diagonal for a general damping [C]. However if [C] can be expressed in terms of [M] and/ or [K], than [γ] is also diagonal. Here [γ] is assumed as diagonalized. With this the Equations (4.30) to (4.31) can be written as:

$$\{ -\omega^2 [\mu_i] + i \omega [\gamma_i] + [\kappa_i] \} \{ \dot{P} \} = [\phi]^T \{ \alpha_i \omega^2 e^{i\Psi_i} \}$$

Denoting,

$$\eta = \frac{\omega}{\omega_1}$$

Equation can be written as:

$$-\eta^2 [\mu_i] + i\eta [\dot{\gamma}_i] + [\kappa_i] \{\dot{P}\}$$

$$= [\phi]^T \eta^2 \{\alpha_i e^{i\Psi_i}\}$$

$$\{\dot{P}\} = [A]^{-1} [\phi]^T \eta^2 \{\alpha_i e^{i\Psi_i}\} \quad (4\ 32)$$

where,

$$[A] = -\eta^2 [\mu_i] + i\eta [\dot{\gamma}_i] + [\dot{\kappa}_i]$$

Equation's (4.28) and (4.32), results in,

$$\{\dot{X}\} = [\phi] [A]^{-1} [\phi]^T \eta^2 \{\alpha_i e^{i\Psi_i}\} \quad (4.33)$$

The response of the system can be found from Equation (4.33).

4.8 Dynamic Response Using Modal Analysis

The linear equations of motion in flexure and torsion are described by Eqn. (4.25). Inorder to obtain the system dynamic response, the original equations of motion are transformed into an independent set of equations by use of the undamped or damped modes. This procedure is called modal analysis.

The homogenous part of the equation neglecting damping is given by,

$$[M] \{\ddot{X}\} + [K] \{X\} = 0 \quad (4.34)$$

which is solved to obtain the eigen values λ_i and eigen vectors ψ_i of the undamped system.

Expressing the response { X } in terms of the modal coordinates [P] as:

$$\{ X \} = [\phi] \{ P \} \tag{4.35}$$

where [ϕ] is the modal matrix formed by concatenating the eigen vectors [ψ_i] and { P } areprincipal coordinates. Using equation (4.35) in Equation (4.25) and pre-multiplying by [ϕ]^T results in uncoupled equations in the modal coordinates of the form,

$$\mu_i (\ddot{P}) + \gamma_i (\dot{P}) + K_i (P) = (\sigma_i) \tag{4.36}$$

where μ_i and K_i are the elements of diagonal matrices [μ] and [K] given by,

$$[\mu] = [\phi]^T [M] [\phi] \tag{4.37}$$

$$[K] = [\phi]^T [K] [\phi] \tag{4.38}$$

and γ_i is the equivalent damping co-efficient in each mode.The generalized force vector { σ_i }, given by

$$\{ \sigma_i \} = [\phi]^T \{ F \} \tag{4.39}$$

The solution of equation (4.28) yields.

$$(P_i) = \frac{(\sigma_i)}{(-\omega_k^2 \mu_i + K_i) + j (\gamma_i \omega_k)} \tag{4.40}$$

Using Equation's (4.35) and (4.40), we obtain the system dynamic response [X].

4.9 Discussion of the Results

The above analysis has been applied on a disk rotating system and numerical results obtained are given in Table 4.2.

Two cases are considered in obtaining the natural frequencies and mode shapes. In one case only flexural degree of freedom of rotor is taken into account. In the second case the torsional degree of fre dom are considered. Table 4.2 shows the natural frequencies in bending and torsion.

The critical speeds in whirling as well as torsion are much higher than the operational speed which is 50 Hz. Hence the dynamic response due to whirling as well as torsion will be quite negligible. The mode shapes in bending are shown in Figs. 4.5 to 4.12.

The mode shapes in torsion are shown in Figs. 4.13 to 4.20.

In the final chapter, conclusions, recommendations and scope for future work are presented.

TABLE 4.1

Details of the Disk Rotating Mechanism

D	0.0635	m
E	68.6E9	Pa
G	26.5E9	Pa
L1	0.032	m
L2	0.028	m
R	0.105	m
Density	2710.	Kg/m3
Thickness	0.00066	m

TABLE 4.2

Natural Frequencies of Flexible Rotor

Whirling (Hz)	Torsion (Hz)
.1931E+05	.1921E+04
.5767E+05	.5705E+04
.9493E+05	.9315E+04
.1298E+06	.1263E+05
.1607E+06	.1554E+05
.1863E+06	.1793E+05
.2054E+06	.1970E+05
.2172E+06	.2080E+05

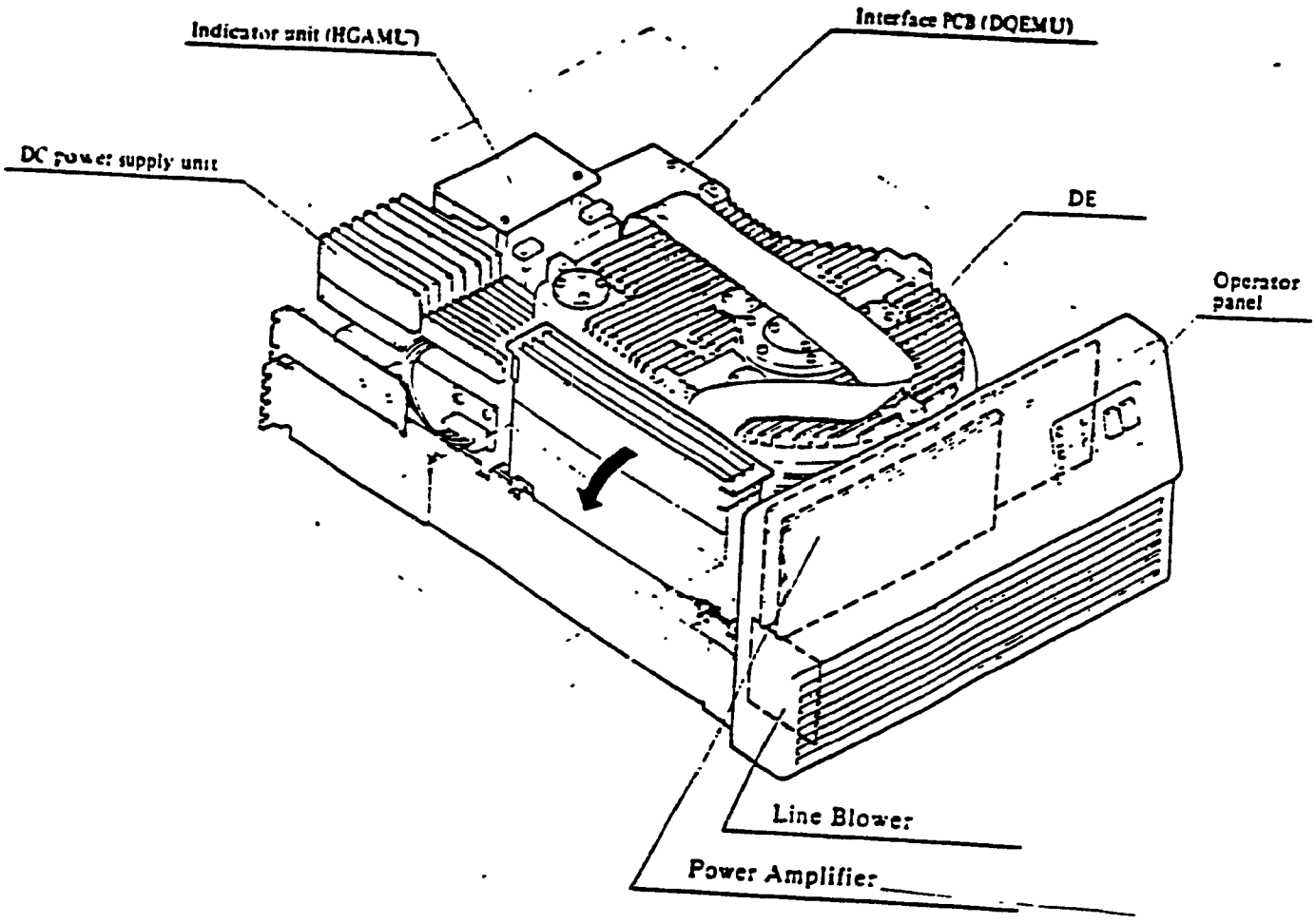

Fig. 4.1 Construction of the drive

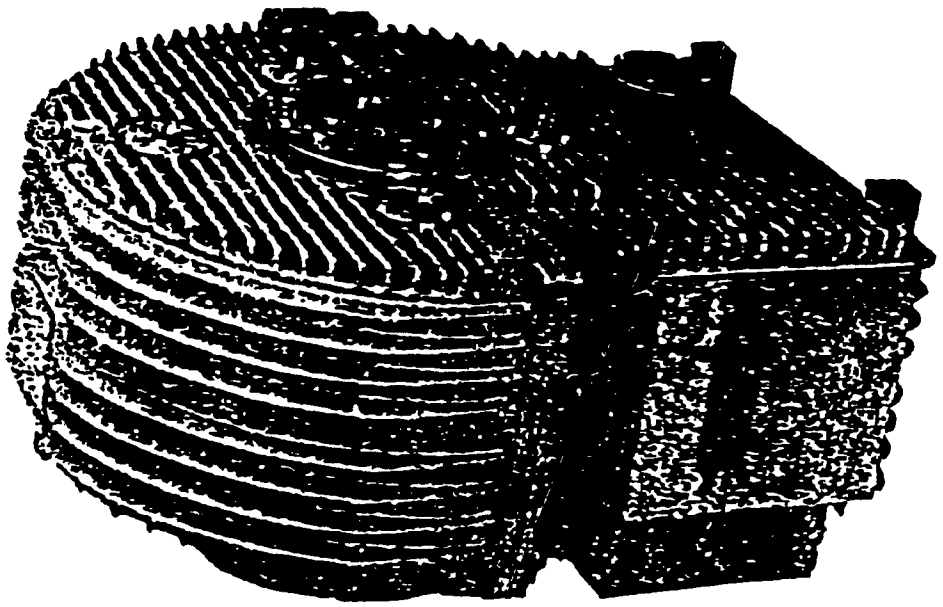

Fig. 4.2 Outerview of the DE

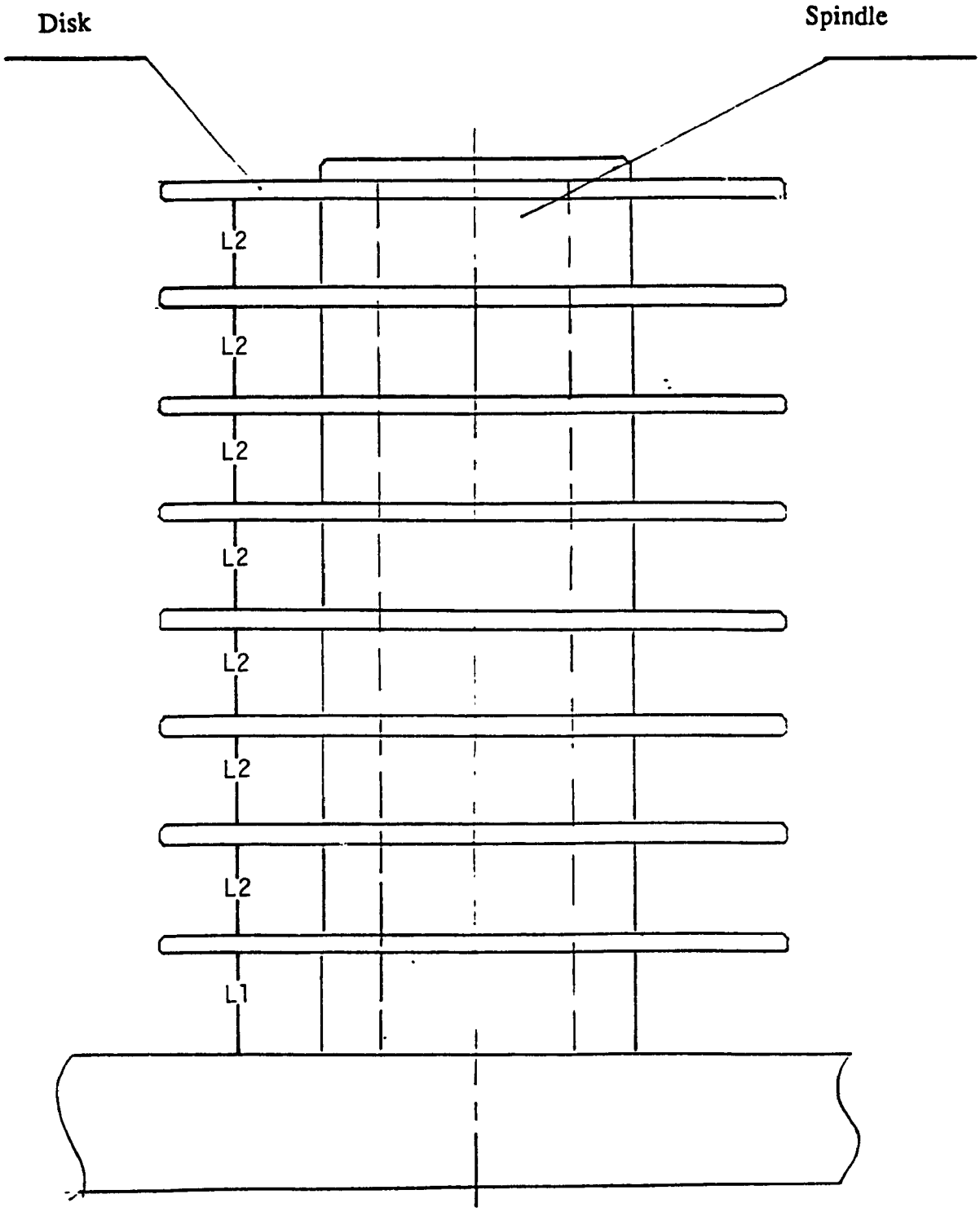

Fig. 4.3 Analytical model of disk rotating mechanism

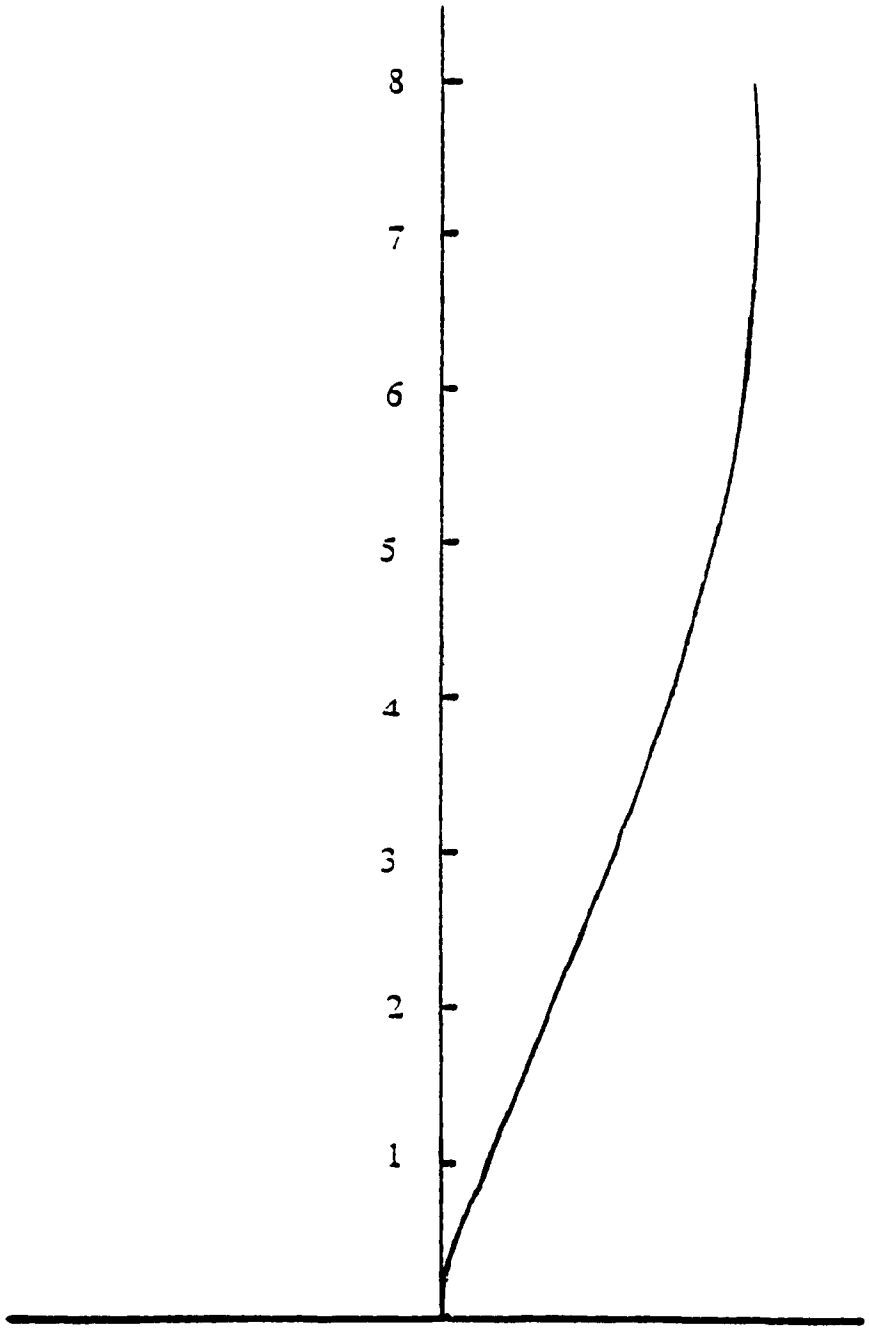

Fig. 4.4 Bending mode shape of the rotor, first mode (f_1 = .1931E+5, numbers are disc locations)

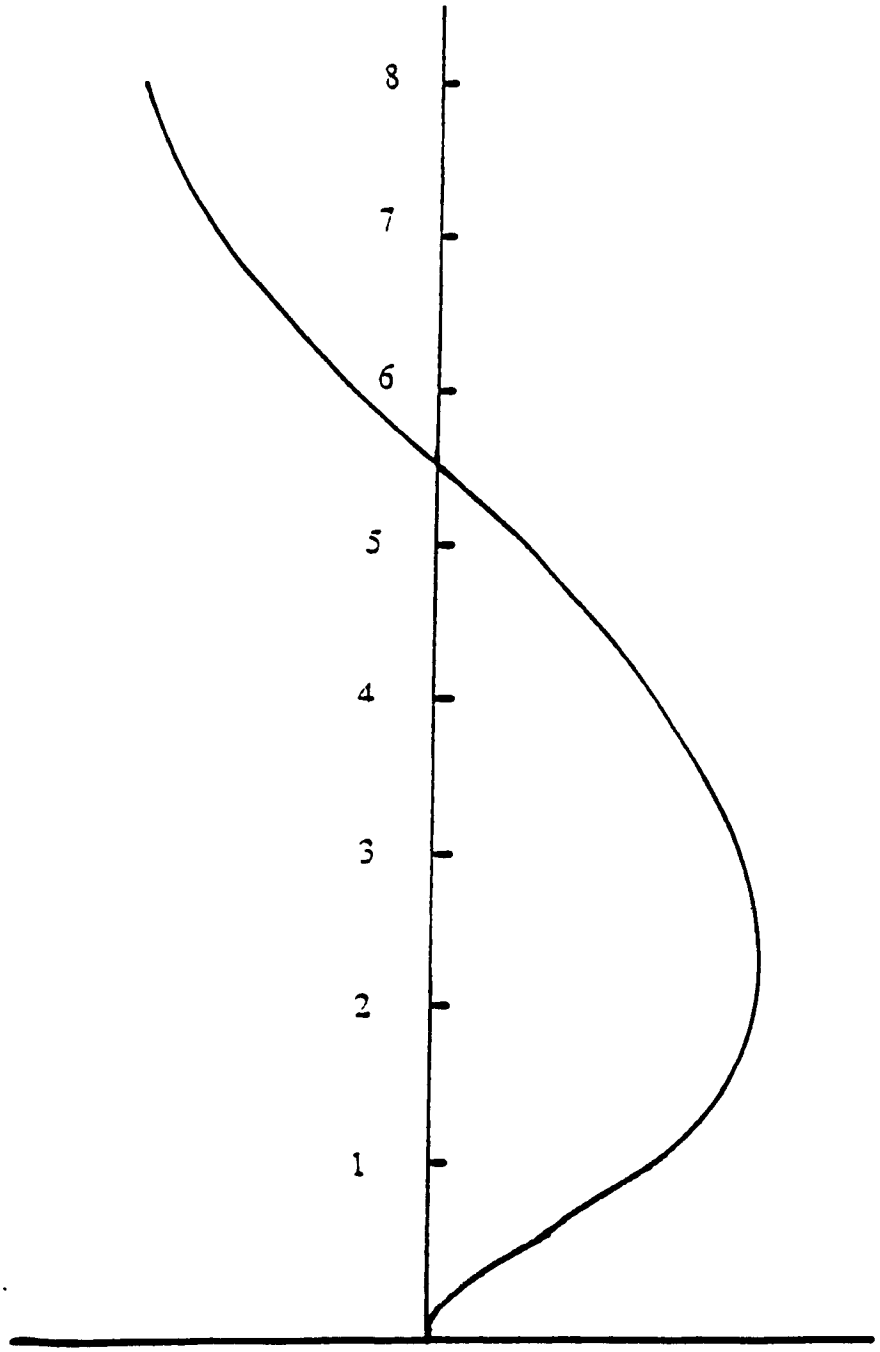

Bending Deflection

Fig. 4.5 Bending mode shape of the rotor, second mode (f_2 = .5767E+5, numbers are disc locations)

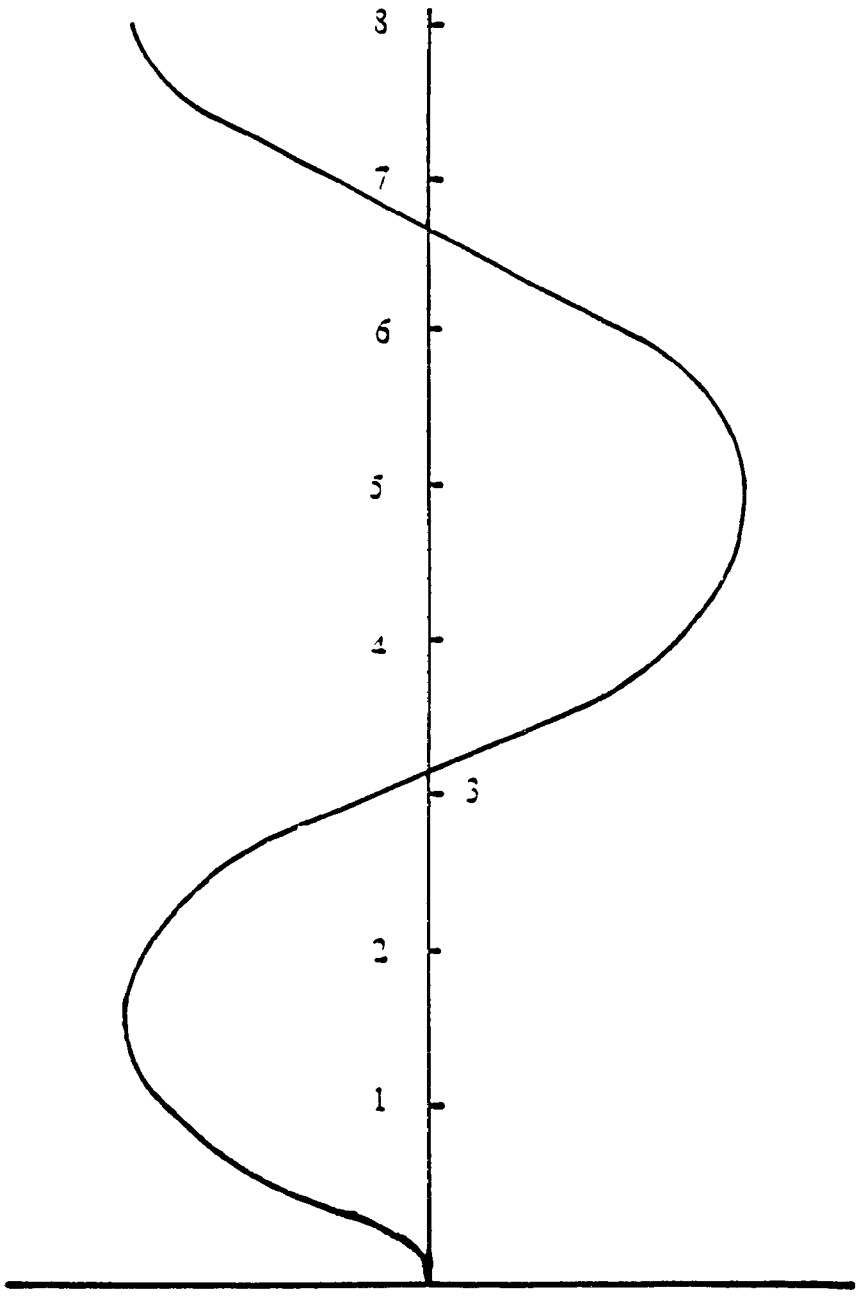

Bending Deflection

Fig. 4.5 Bending mode shape of the rotor, third mode (f_3 = .9493E+5, numbers are disc locations)

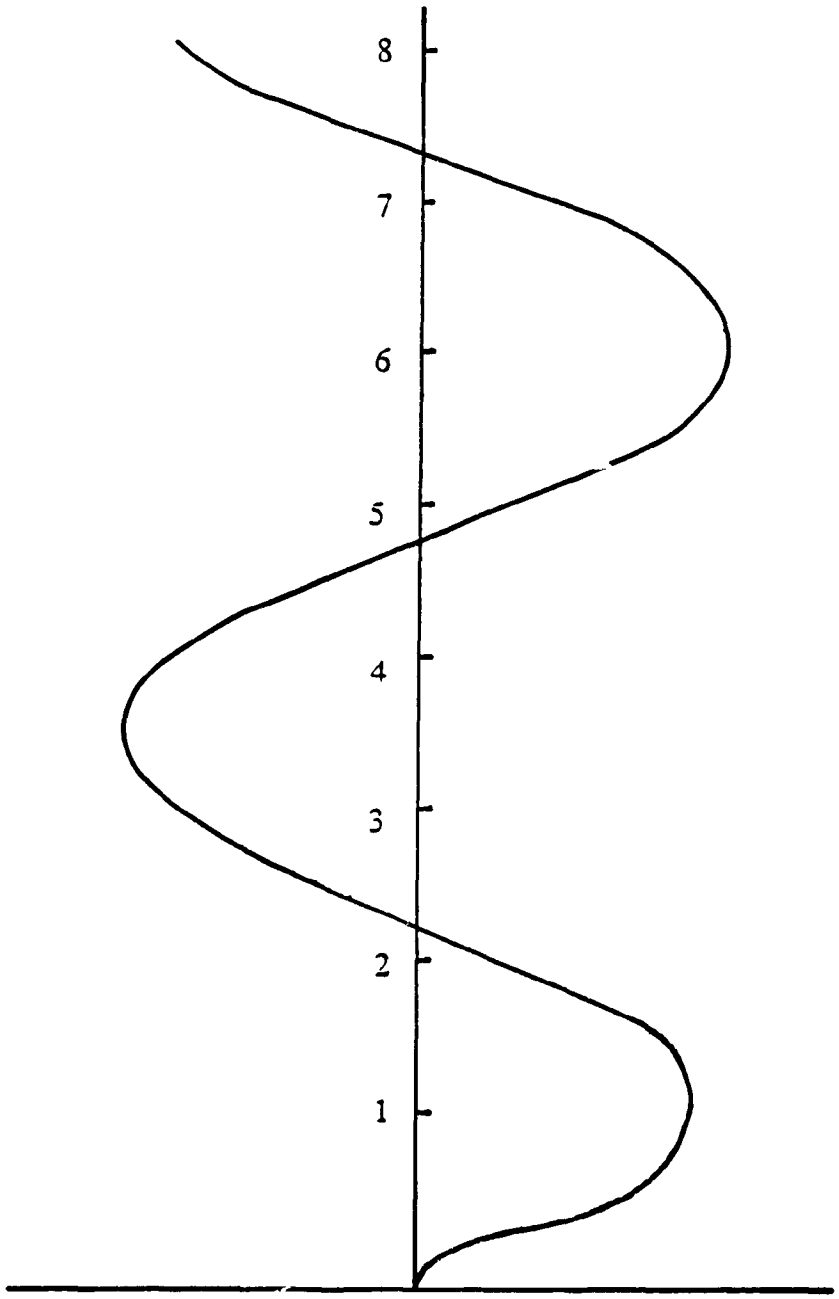

Fig. 4.7 Bending mode shape of the rotor, fourth mode (f_4 = .1298E+6, numbers are disc locations)

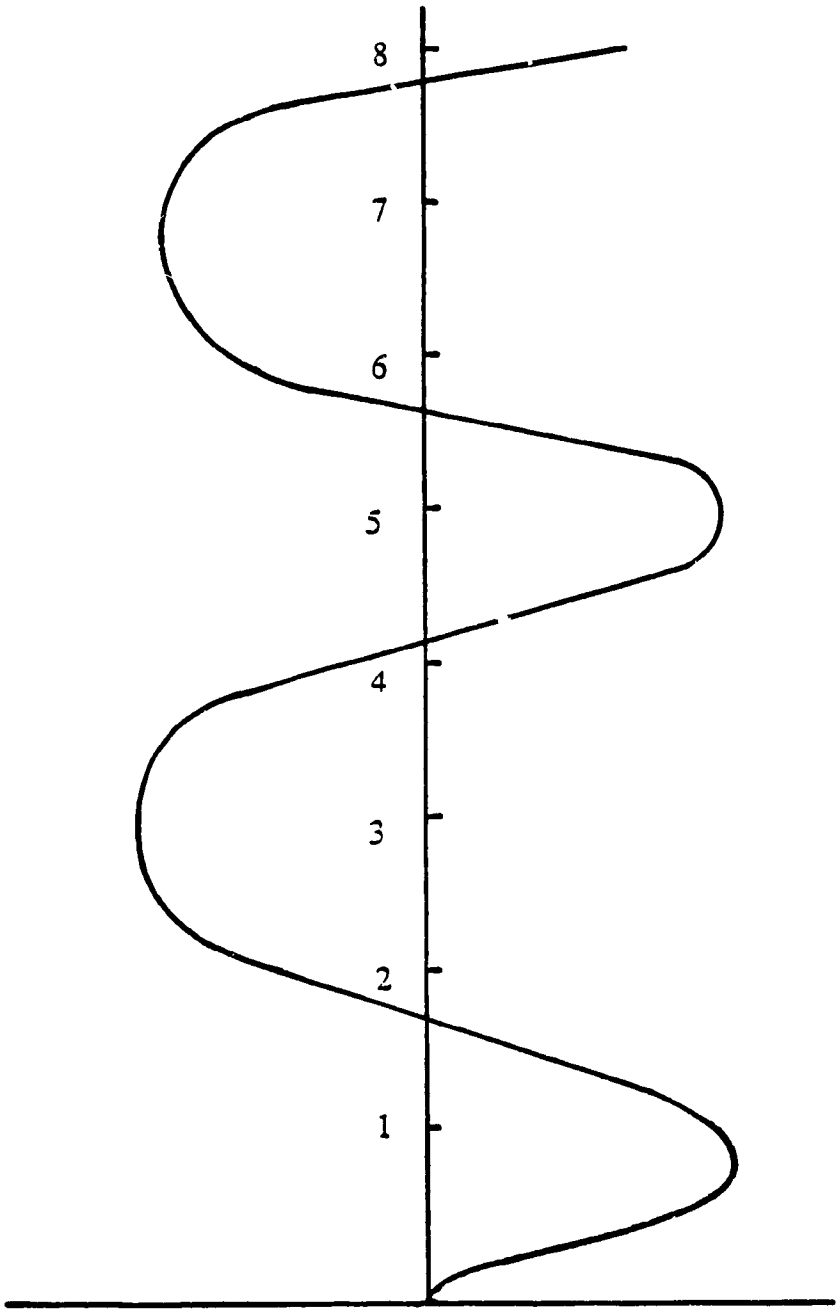

Fig. 4.8 Bending mode shape of the rotor, fifth mode (f_5 = .1607E+6, numbers are disc locations)

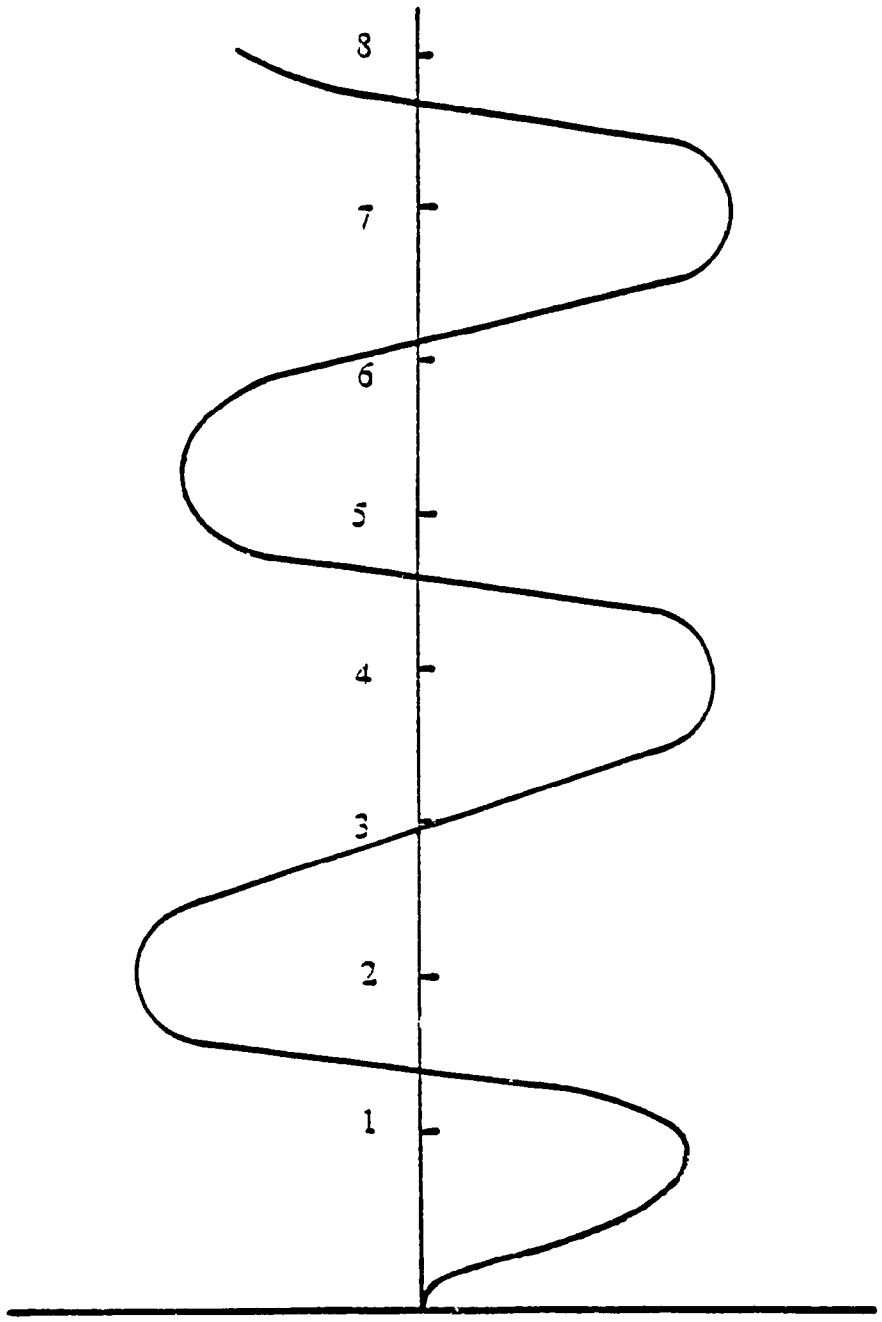

Bending Deflection

Fig. 4.9 Bending mode shape of the rotor, sixth mode (f_6 = .1863E+6, numbers are disc locations)

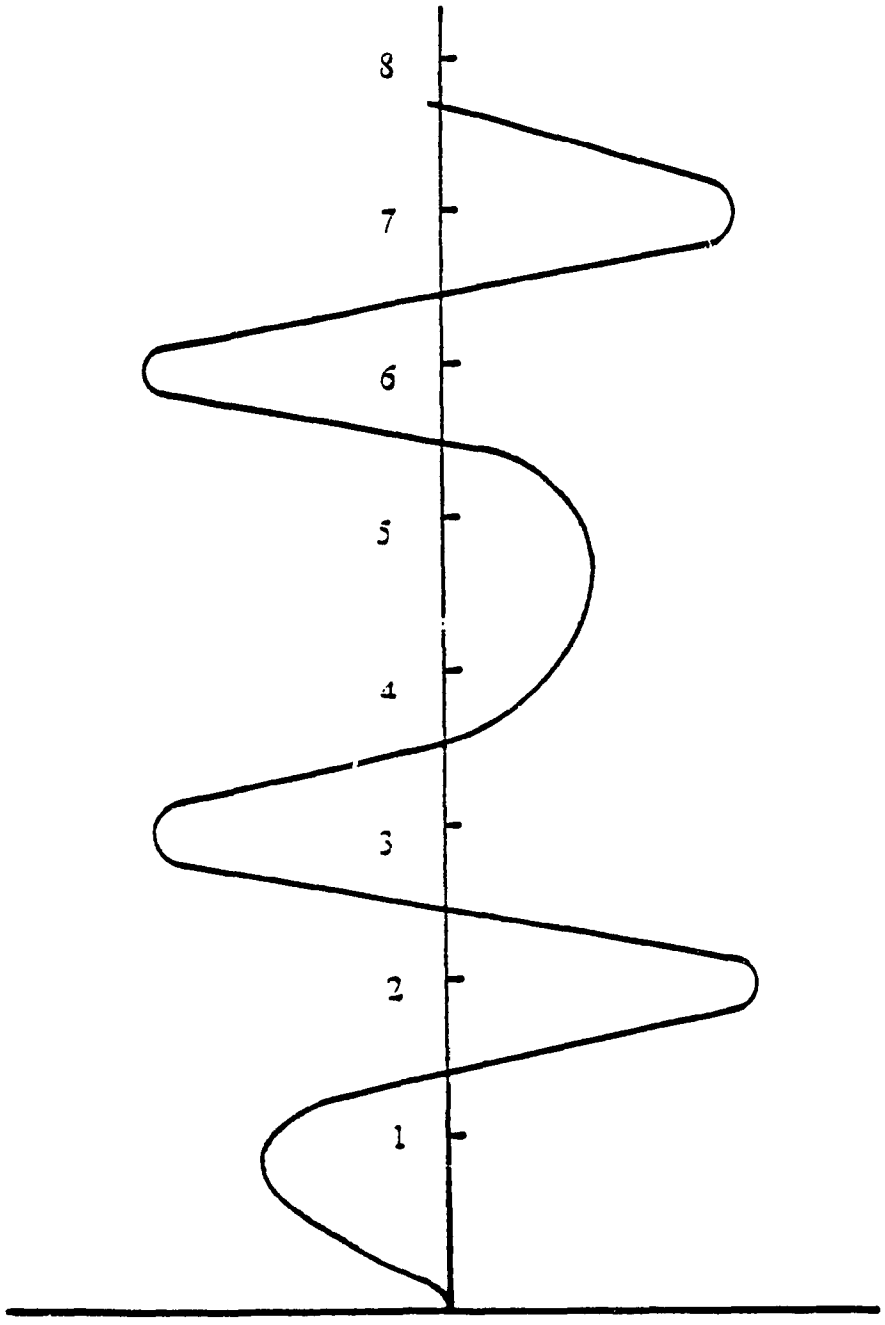

Fig. 4.10 Bending mode shape of the rotor, seventh mode (f_7 = .2054E+6, numbers are disc locations)

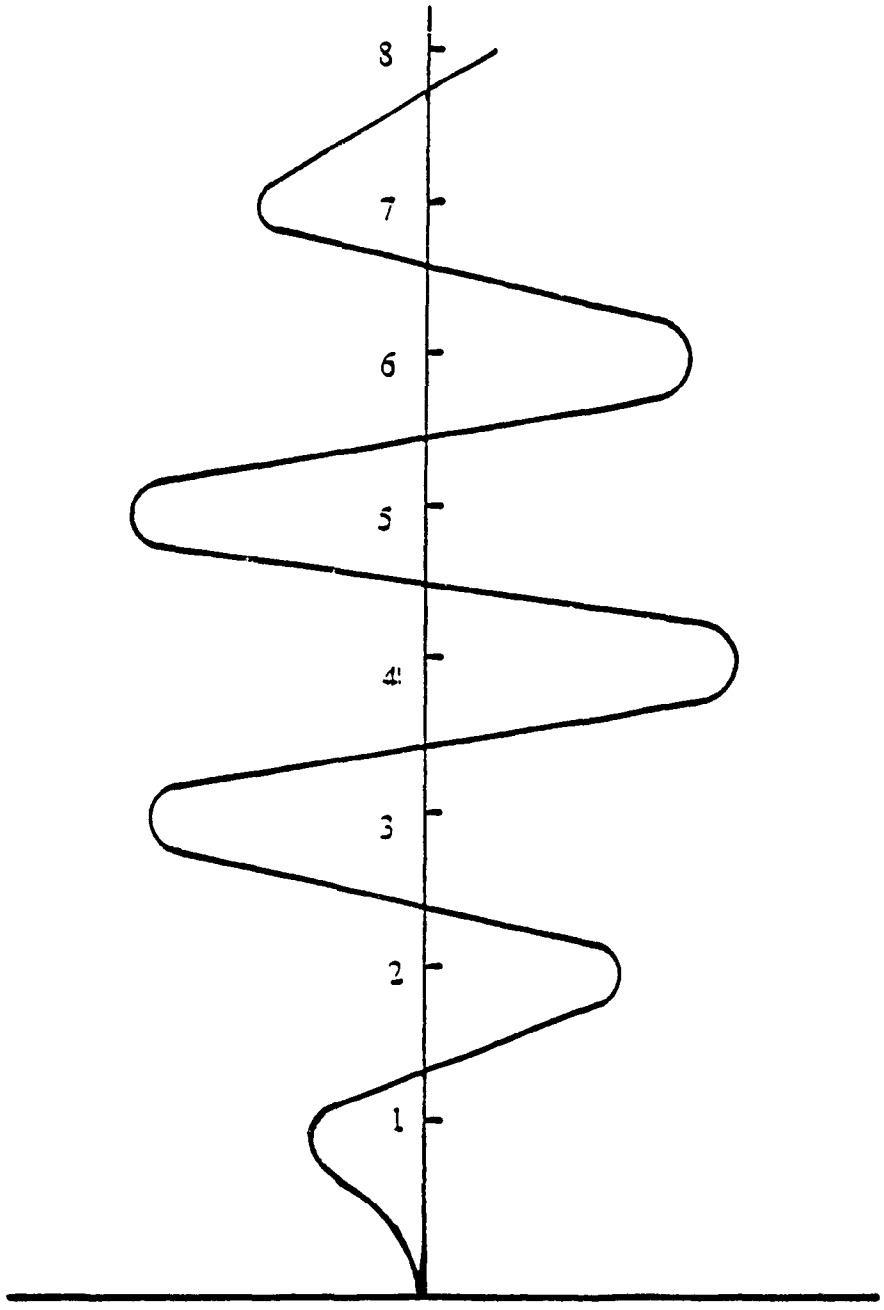

Fig. 4.11 Bending mode shape of the rotor, eighth mode (f_8 = .2172E+6, numbers are disc locations)

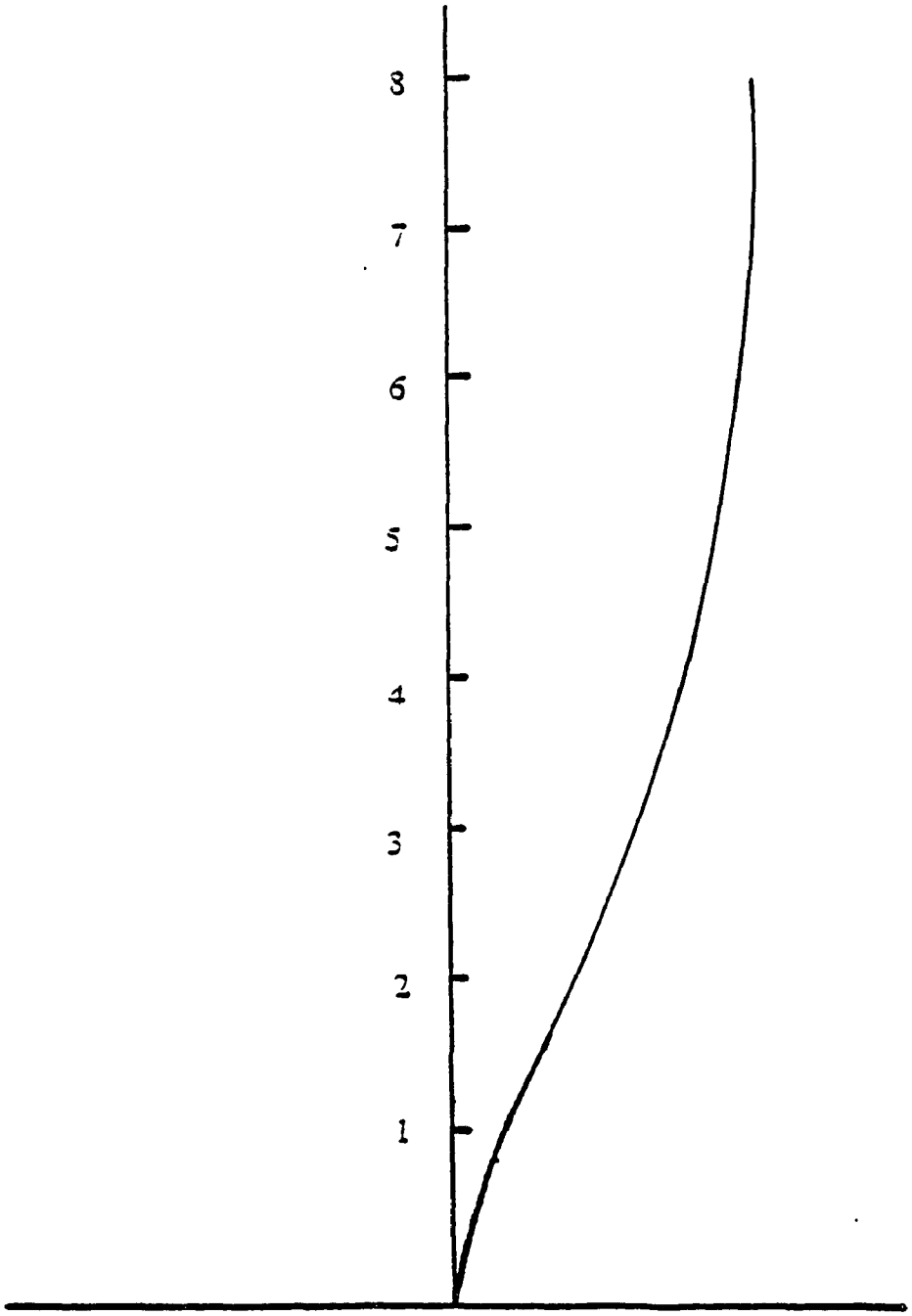

Fig. 4.12 Torsion mode shape of the rotor, first mode (f_1 = .1921E+4, numbers are disc locations)

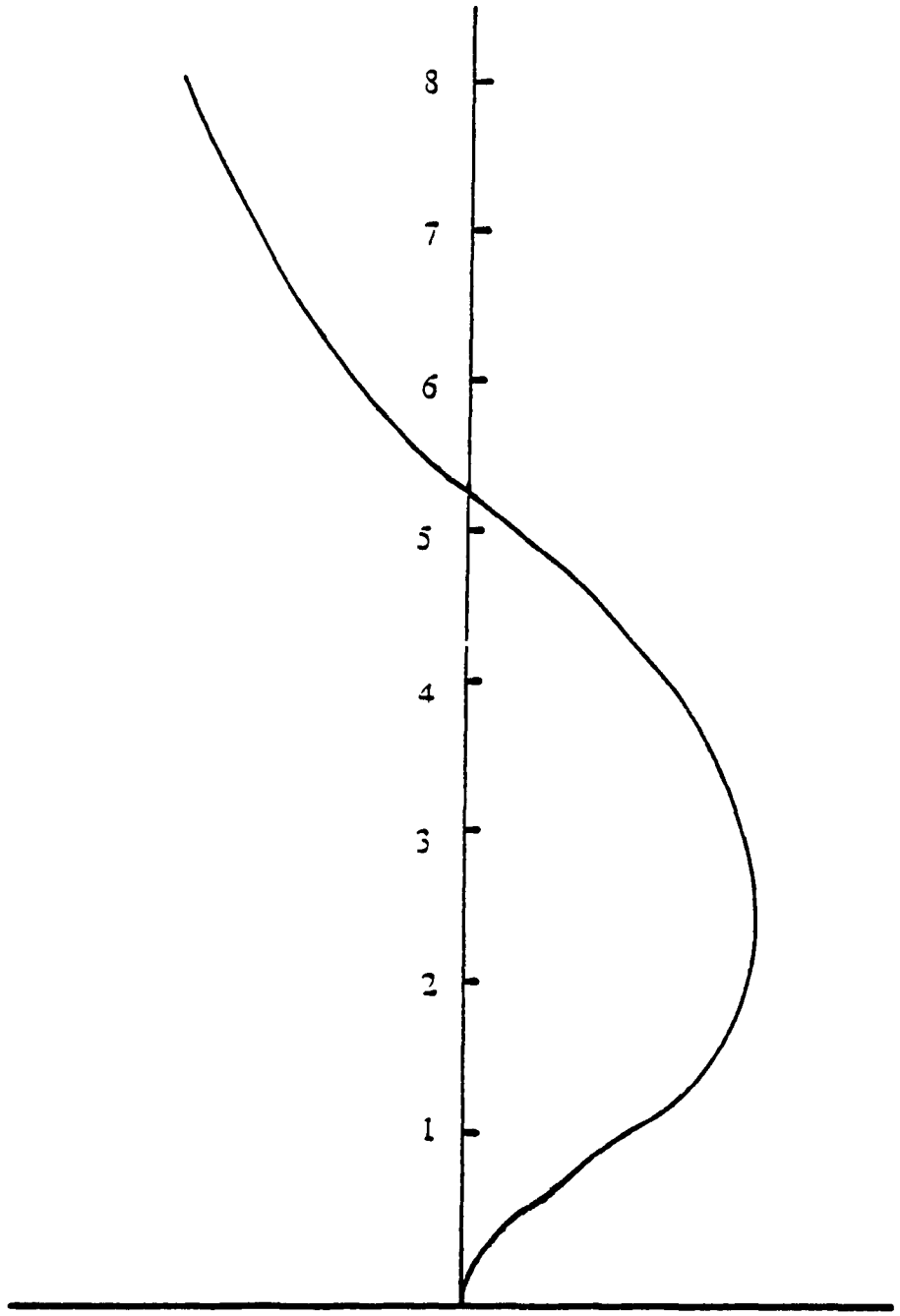

Fig. 4.13 Torsion mode shape of the rotor, second mode (f_2 = .5705E+4, numbers are disc locations)

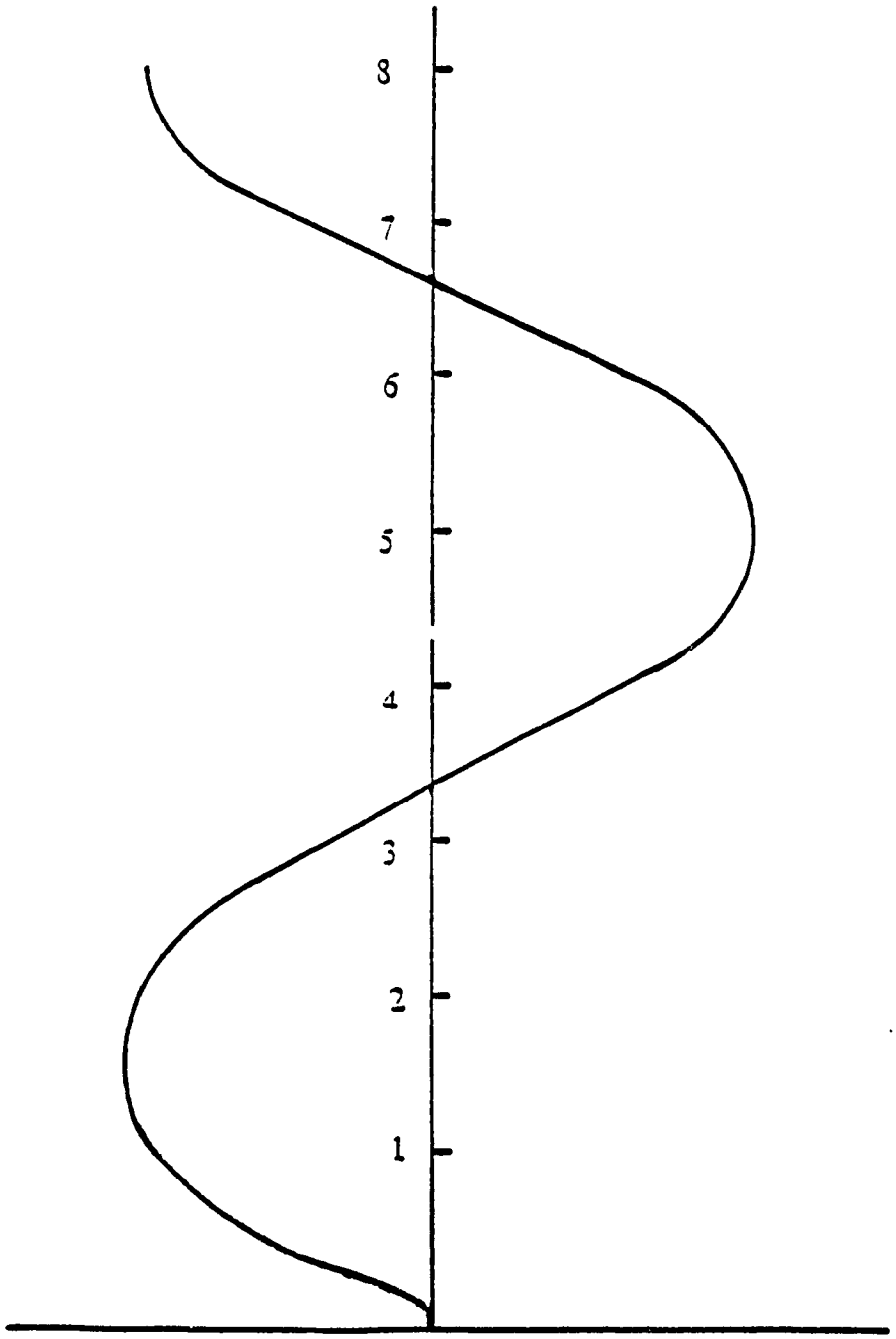

Fig. 4.14 Torsion mode shape of the rotor, third mode (f_3 = .9315E+4, numbers are disc locations)

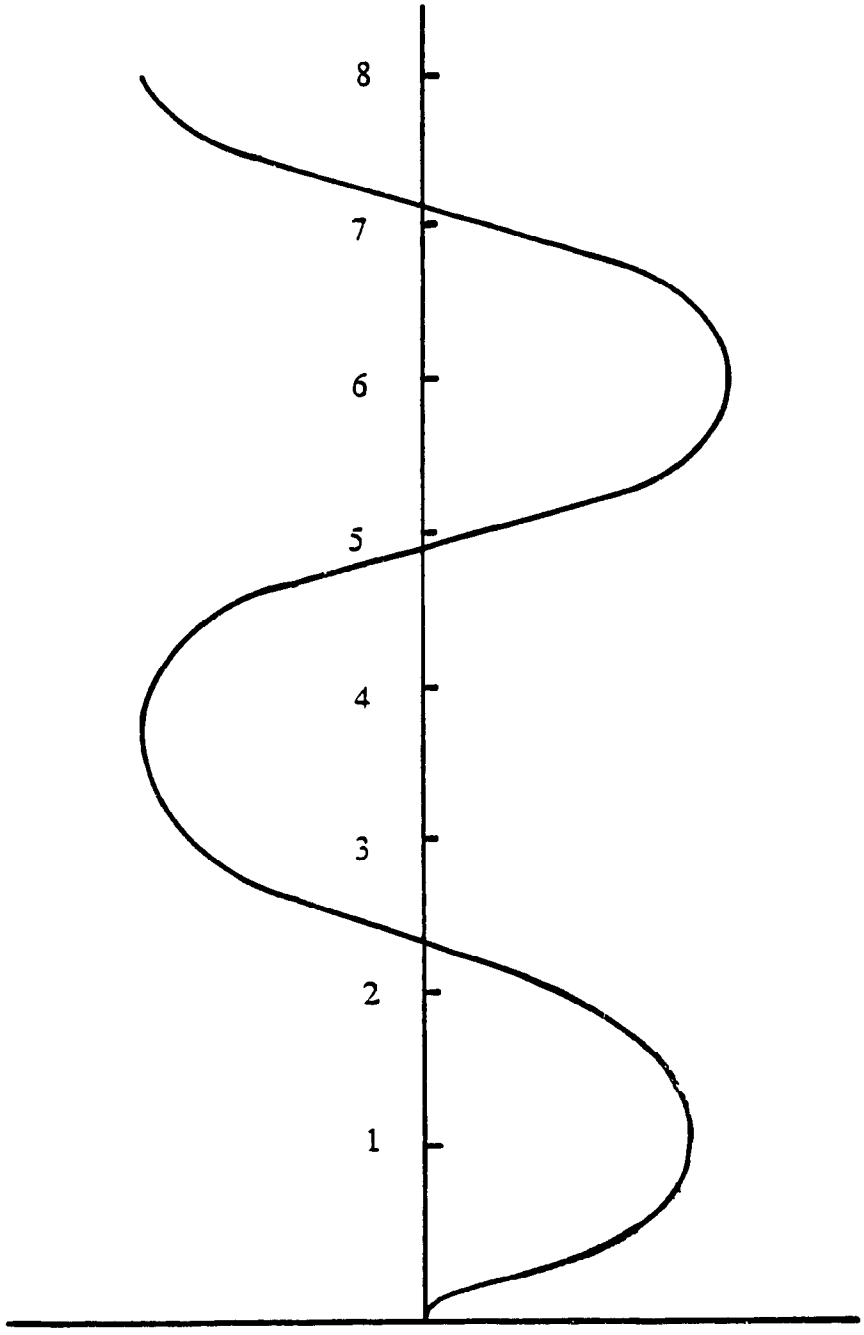

Fig. 4.15 Torsion mode shape of the rotor, fourth mode (f_4 = .1263E+5, numbers are disc locations)

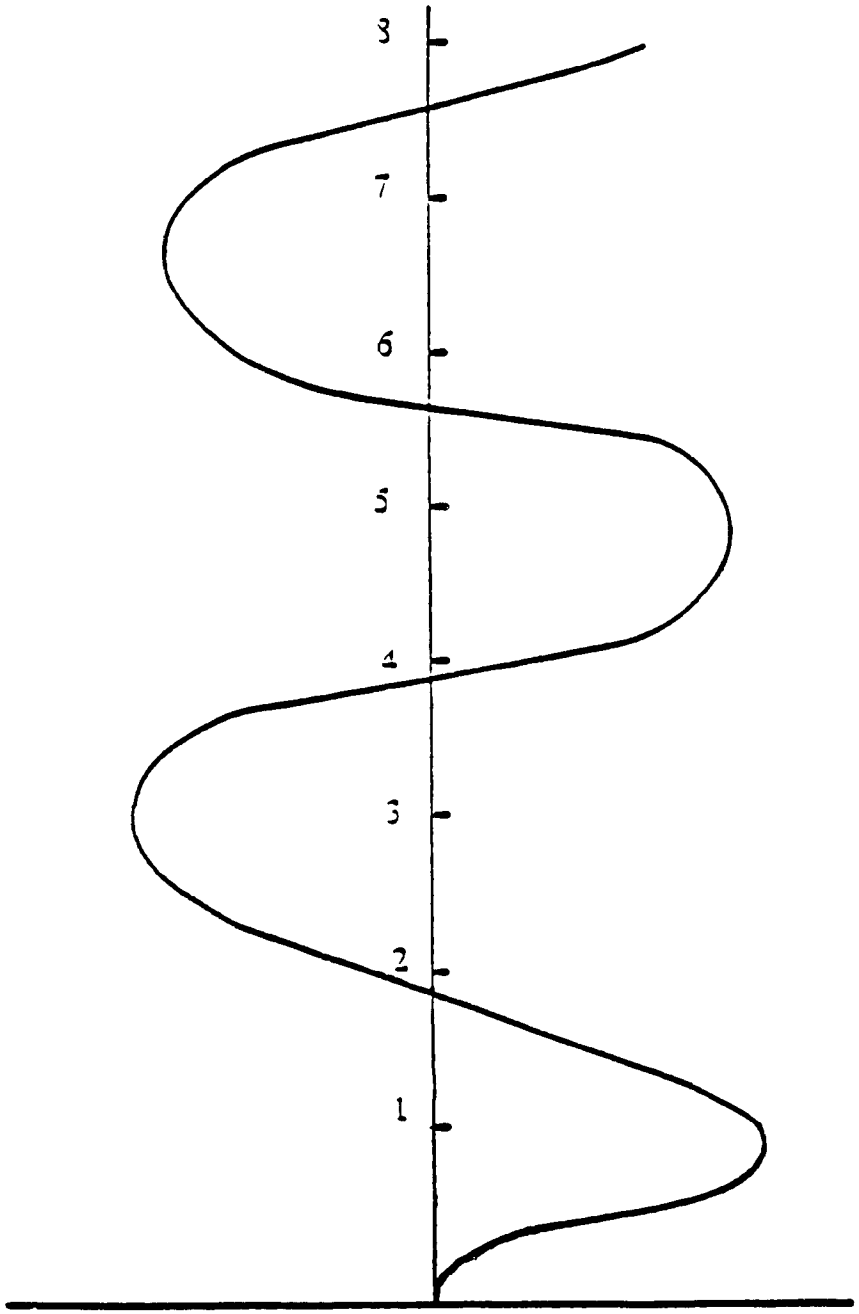

Torsional Deflection

Fig. 4.16 Torsion mode shape of the rotor, fifth mode (f_5 = .1554E+5, numbers are disc locations)

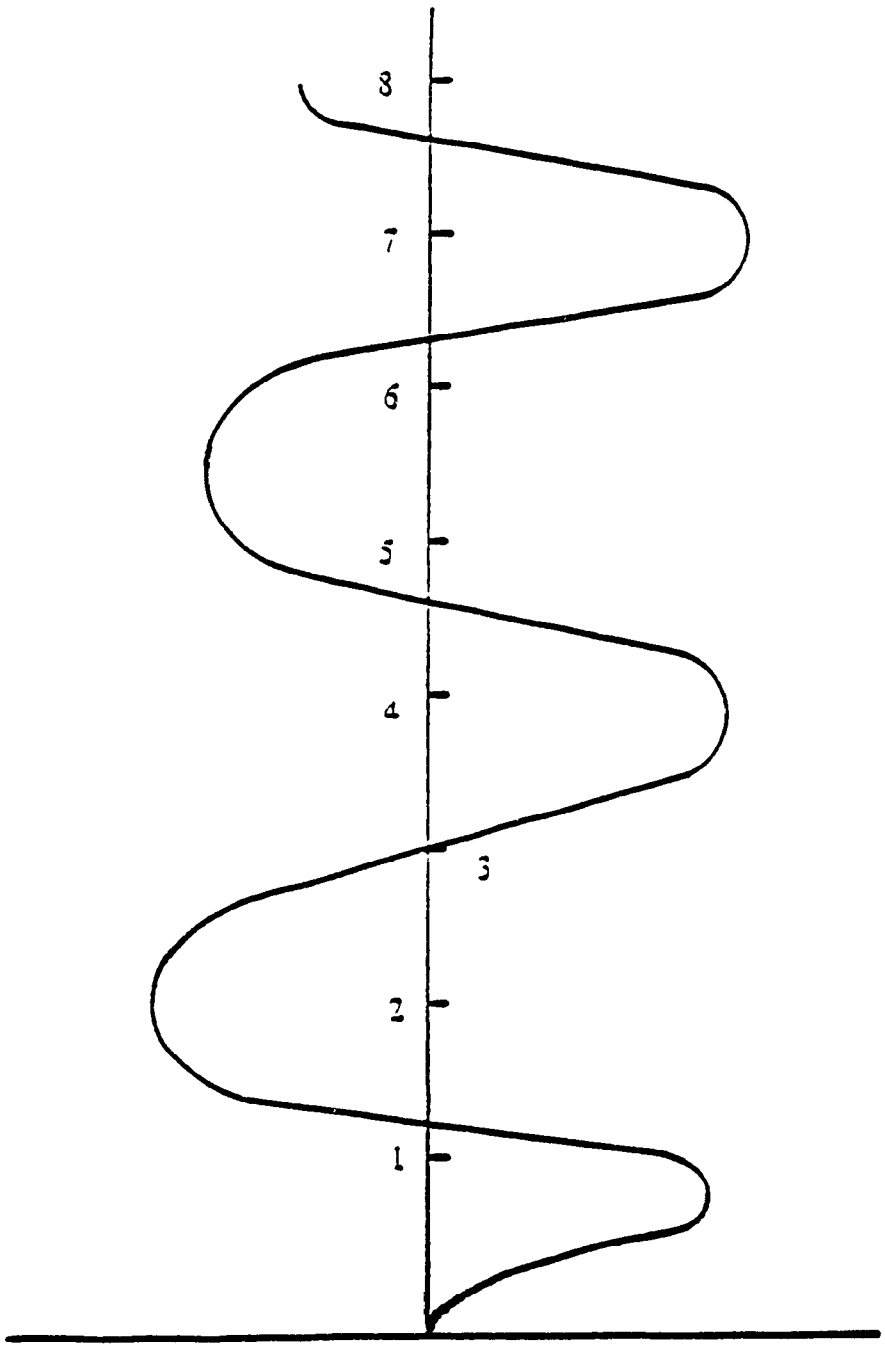

Fig. 4.17 Torsion mode shape of the rotor, sixth mode (f_6 = .1793E+5, numbers are disc locations)

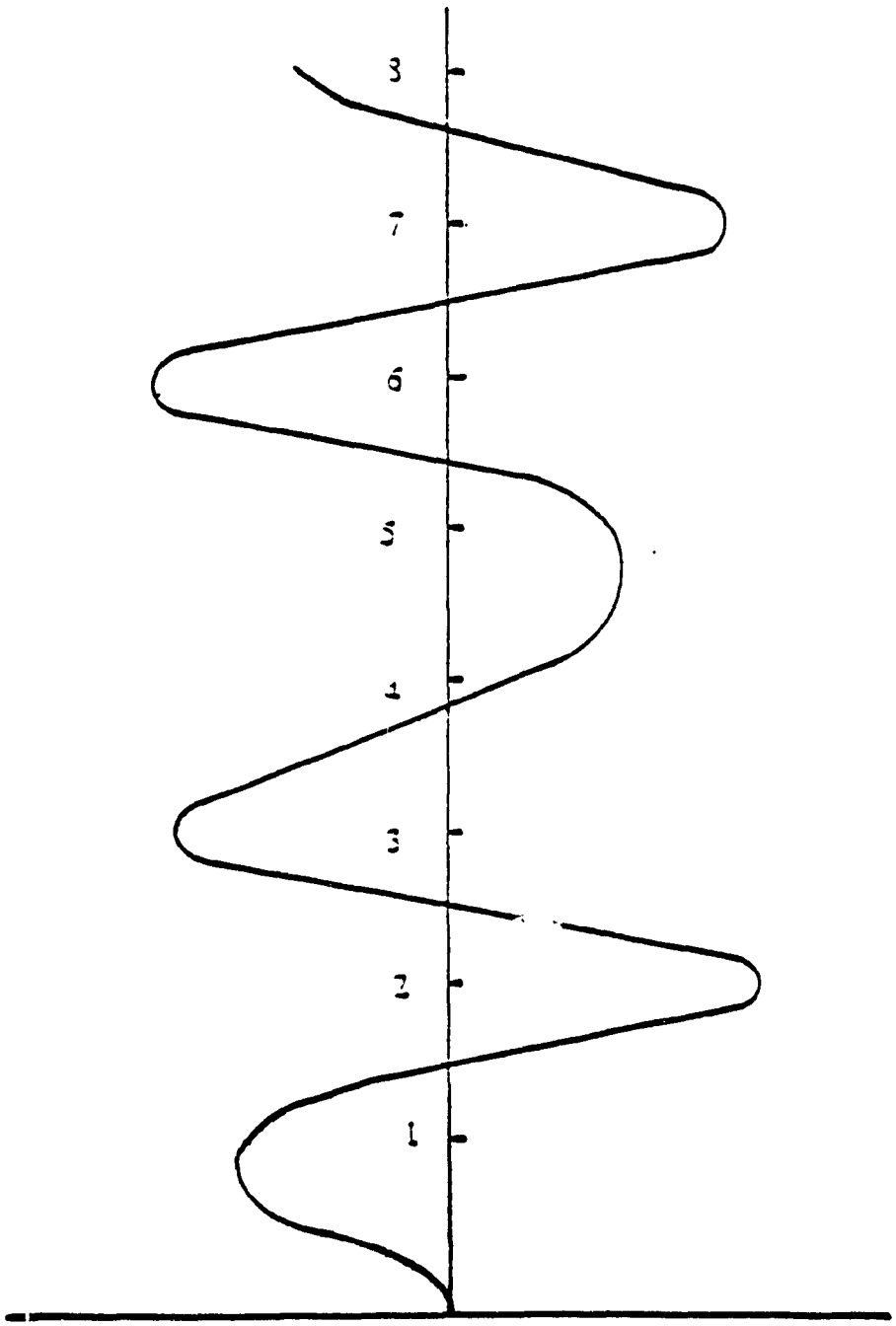

Torsional Deflection

Fig. 4.18 Torsion mode shape of the rotor, seventh mode
(f_n = .1970E+5, numbers are disc locations)

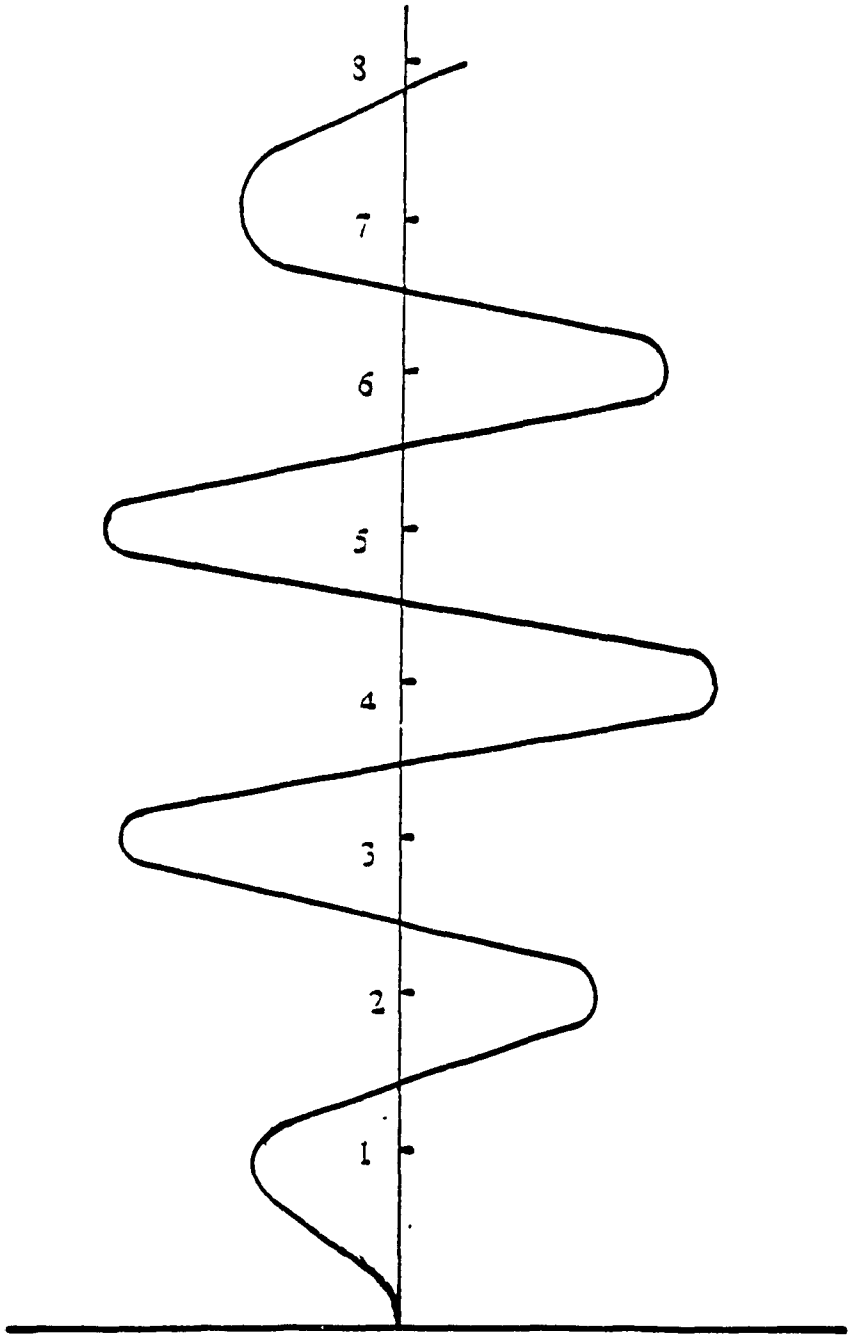

Fig. 4.19 Torsion mode shape of the rotor, eighth mode (f_8 = .2080E+5, numbers are disc locations)

CHAPTER 5

CONCLUSIONS AND RECOMMENDATIONS

CHAPTER 5

CONCLUSIONS AND RECOMMENDATIONS

The dynamic behaviour of a computer hard disk drive was studied in this thesis.

The rotary actuator is modelled taking into account the flexibility of the bearing and the pivot clearance. The natural frequencies, mode shapes, and dynamic response of a disk rotating mechanism were obtained by modal analysis. Modelling of the rotary actuator arm using finite element approach are presented.

The rotary actuator was analysed first using the non-linear model considering the backlash since the arm of the rotary actuator on which the heads are mounted rotates in a ball bearing about a pivot shaft. A radial clearance called the pivot clearance, exists between the pivot shaft and the inner race of the bearing. In this formulation the effect of clearance on bearing displacement and head positioning error are presented.

The finite element program ANSYS has been used to model the rotary actuator arm. The natural frequencies and mode shapes for the arm structure were obtained.

The torsional and flexural degree's of freedom of a disk rotating mechanism containing eight disks, supported on a vertical spindle and driven by a D.C motor are considered. This disk rotating mechanism acts like a large capacity random access memory. By solving the resulting homogenous simultaneous equations, the natural frequencies ω_i and mode shapes ψ_i are

obtained. The response of the system is obtained by solving the non homogenous problem using modal analysis.

5.1 Conclusions

The conclusion arrived on the basis of the results of this work in the different chapter of this thesis are summarized and given below:

1) The effect of pivot clearance on head positioning of a rotary actuator for magnetic disk storage is quite significant.

a) When the pivot clearance is small there is no head positioning error but as it value increases its becomes difficult for the head to read the desired track.

b) Pivot bearing damping can reduce the number of impacts on the pivot shaft.

2) It is seen that there is a significent reduction in the vibration amplitude as the radial clearance is decreased.

3) The frequency of the arm increases with arm stiffness.

4) The damping reduces the vibration amplitude.

5) The frequency of response goes up as value of servo constants increases.

6) The rotary arm has its own natural frequencies and mode shapes.

7) Critical speed in whirling and torsion are much higher than the operational speed of 50 Hz.

There are limitations imposed by the manufacturing process on the bearing clearance and similarly, the bearing stiffness and damping depend on the material used. Hence, even though the above

conclusions suggest reduction of clearance and increase of bearing damping, these can be carried out only to the extent practically possible.

5.2 Recommendation for Future Work

Some suggestions for possible future work are given below:

1) The response of the rotary arm system should be evaluated considering it as a flexible system.

2) Experimental modal analysis of the arm structure, can be carried out to identify the modal parameters of the system.

3) The dynamic response in whirling due to unbalances in the disks can be obtained.

4) Experimental measurement of the dynamic response of the rotary arm. A larger scale model of the arm may be used to facilitate measurements.

REFERENCES

REEFERENCES

1. Kakizaki, T., "Effect of Pivot Clearance on Head Positioning of a Rotary Actuator for Magnetic Disk Storage",ASME_Journal_of__Mechanisms,__Transmissions,__and Automation_in_Design, Vol. 108, Dec. 1986, pp. 556-561.
2. Khan, B.M., Neriya, S.V., and Bhat, R.B., "Response of servomechanism controlled Rotary Actuator Subjected to Step Input and a Sinusoidal Track Runout", Pan American Congress of Applied Mechanics., Rio de Janeiro, Jan, 3-6, 1989, pp. 194-197.
3. Heath, J.S., "Design of a Swinging Arm Actuator for a Disk File", IBM_J.Res._Develop., July. 1976, pp. 389-397.
4. Oswald, R.K., "Design of a Disk File Head Positioning Servo", IBM J. Res. Develop., Nov. 1974., pp. 506-512.
5. Kakizaki, T., et al., "Design and Dynamics Analysis of a High Performance Rotary Actuator for a disk storage", Proc. of 1st ISDS Conf. July. 1984, pp. 813-818.
6. Dubowsky, S., "On Predicting the Dynamic Effects of Clearances in One Dimensional Closed Loop System", ASME JOURNAL_of_Engineering_for_Industry, Vol. 96, No 1, Feb.1974, pp. 324-329.
7. Dubowsky, S., "On Predicting the Dynamic Effects of Clearances in Planar Mechanisms", ASME___Journal___of Engineering_for_Industry, Vol. 96, No. 1, Feb. 1974, pp.317-323.

8. Funabashi, H., et al., "A Dynamic Analysis of Mechanisms with Clearances", Bull._JSME, Vol. 21, No. 161, Nov. 1978, pp. 1652-1659.

9. Shimojima, H., et al., Bull. JSME, Vol. 18, No. 118, 1975, p.426.

10. Furuhashi, T., et al., Bull. JSME, Vol. 21, No 153, 1978, p.518.

11. Funabashi, H., et al., "A Dynamic Analysis of the Plane Crank-and-Rocker Mechanisms with Clearances", Bull._JSME, Vol. 23, No. 177, Mar. 1980, pp. 446-452.

12. Bapat, C.N., and Popplewell, N., "Stable Periodic Motions of an Impact-Pair", Journal_of_Sound__and__Vibration, Vol. 87, No. 1, 1983, pp. 19-40.

13. Dubowsky, S., and Freudenstein., "Dynamic Analysis of Mechanical Systems with Clearances, Part 1 : Formation of Dynamic Model: Part 2: Dynamic Response", ASME_Journal__of Engineering_for_Industry, Vol. 93, No. 1, Feb. 1971, pp.305-316.

14. R.B. Mulvany, "Engineering Design of a Disk Storage Facility with Data Modules", IBM_J._Res._Develop, 1974, pp. 489-

15. Douglas, F., et al., "Application of Finite Element Analysis, Component mode Synthesis and Modal Test Data in the Development of a Rotary Actuators in high performance, 5.25 inch Winchester disk drives.

16. Radwan, H.R., and Chokshi, J.V., "Use of non-contact measurements for Modal Analysis of Disk Drive Components.

17. Radwan, H.R., et al., "Use of Finite Element Analysis for improving Disk drive servo performance.

18. Lennemann. E., "Aerodynamic aspects of Disk File", IBM_J._Res._Develop,. Nov. 1974, pp. 480-488.

19. Bouchard, G., et al., "An experimental Comparison of the Head/Disk interface dynamics in 5 1/4 and 8-inch disk drives", IBM_J._Res._Develop., Vol. 29, No. 3., May. 1985, pp. 316-323.

20. Mulvany, R.B., and Thompson, L.H, "Innovations in disk file manufacturing", IBM_Journal._Res._Develop, Vol. 25, No. 5., Sept. 1981, pp. 711-723.

21. Noyes, T., and Dickinson, W.E., "The Random-Access Memory Accounting Machine", IBM_Journal., Jan. 1957, pp. 72-75.

22. Ciskowski, R.D., et al, "System identification An experimental verification", IBM_J._Res._Develop., Vol. 31, No. 5, Sept, 1987, pp. 571-584.

23. Mizoshita, Y., et al, "Dynamic Characteristics of a magnetic head slider", IEEE_Trans_on_Magnetics, Vol. MAG-21, No. 5, Sept 1985, pp. 1509-1511.

24. Morris, F., and Chou, Y.S., "Effect of flying height variation on off track data handling", IEEE_ Trans__on Magnetics, Vol. Mag-17, No. 4, July 1981, pp. 1372-1375.

25. Mizochita, Y., et al, "Mechanical and servo design of a 10 inch disk drive", Trans_on_Magnetics, Vol. Mag-17, No. 4, July. 1981, pp. 1387-1391.

26. Scranton, R.A., et al, "A novel high performance, low mass

disk head actuator", IEEE_Trans_on_Magnetics, Vol. Mag-19, No. 5, Sept. 1983, pp. 1692-1694.

27. Naruse, J., et al, "Design of a large Capacity disk drive with two actuators", IEEE_Trans_on_Magnetics, Vol. Mag-19, No. 5, Sept. 1983, pp. 1695-1697.

28. Winfrey, R.C., et al, "Design of a high performance rotary positioner for a magnetic disk memory", IEEE Trans on Magnetics, Vol. Mag-17, No. 4, Sept. 1983, pp. 1689-1691.

29. Tagawa, N., and Hashimoto, M., "Submicron Spacing dynamics for flying head slider mechanisms using building block approach", IEEE Trans on Magnetics, Vol. Mag-21, No. 5, Sept 1985, pp. 1506-1508.

30. Harker, J.M., et al, "A Quarter Century of Disk File Innovation", IBM. J. Res. Develop,. vol. 25, No. 5, September, 1981, pp.

31. Bahar, L.Y., and Sinha, A.K., "Matrix Exponential Approach to Dynamic Response", Computers and Structures, 1975, Vol. 5, No. 5, pp. 159-165.

32. Wilson, E.L., "A computer programme for the Dynamic Stress Analysis of Underground Structures", Report No. 68-1, University of California at Berkeley, Berkeley, California, 1969.

33. Kaneko, R., and Yoshi, S., "3.2 G Byte Multi-Device Disk Storage Development", Review of the ECL, Vol. 30, No. 1, 1982, pp. 1-7.

34. Takanami, S., et al, "Storage control for 3.2 GByte

multi-device disk storage", Review of the ECL, Vol. 30, No. 1, 1982, pp. 8-13.

35. Nakanishi, T., et al, "Recording Characteristic of 3.2 GByte multi-device disk storage", Review of the ECL, Vol. 30, No. 1, 1982, pp. 14-23.

36. Koguri, K., et al, "Mechanical Characteristics of flying head and recording media for 3.2 GByte multi-device storage", Review of the ECL, Vol. 30, No. 1, 1982, pp. 36-45.

37. Mitsuya, Y., et al, "Mechanisms for 3.2 GByte multi-device disk storage", Review of the ECL, Vol. 30, No. 1, 1982, pp. 46-56.

38. Ito, Y., et al, "800 Mega Byte disk storage system development", Review of the ECL, Vol. 28, No's 5-6, May-June, 1980, pp. 361-367.

39. Keneko, R., et al, "Development of 800 Mega Byte disk drive", Review of the ECL, Vol. 28, No's 5-6, May-June, 1980, pp. 368-380.

APPENDIX I

ELEMENT OF MATRICES

This appendix gives the elements a_{nk}, b_{nk}, of matrices [A] and [B] as discussed in Section 2.2 of Chapter 2.

The elements a_{nk}, b_{nk} of matrices [A], [B] are given as:

$$A(1,1) = 1.$$

$$A(2,1) = - \Omega_1^2 \delta + \Omega_2^2$$

$$A(2,2) = -\eta_1 \delta + \eta_2$$

$$A(2,3) = - \Omega_1^2 L_2 \delta - \Omega_2^2 L_1$$

$$A(2,4) = - \eta_1 L_2 \delta - \eta_1 L_1$$

$$A(3,4) = 1.$$

$$A(4,1) = \frac{- \Omega_1^2 L_2 \delta + \Omega_2^2 L_3}{\alpha}$$

$$A(4,2) = \frac{- \eta_1 L_2 \delta + \eta_2 L_3}{\alpha}$$

$$A(4,3) = \frac{- \Omega_1^2 L_2^2 \delta - \Omega_2^2 L_3}{\alpha}$$

$$A(4,4) = \frac{- \eta_1 L_2^2 \delta - \eta_2 L_1 L_3}{\alpha}$$

$$B(2) = - \lambda \delta R \Omega_1^2 + \Omega_2^2 * 10 + \Omega_2^2 \sin 2\pi\tau + 2 \pi \eta_2 \cos 2\pi\tau$$

$$B(4) = - \frac{L_2 \delta \lambda R \Omega_1^2}{\alpha} + \frac{L_3}{\alpha} \Omega_2^2 * 10 + \frac{L_3}{\alpha} 2 \pi \eta_2 \cos 2\pi\tau + \frac{L_3}{\alpha} \Omega_2^2 \sin 2\pi\tau$$

APPENDIX II

ELEMENT OF MATRICES

This appendix gives the elements of mass matrix, stiffness matrix, damping matrix, and force vector as mentioned in Section 4.4 of chapter 4.

The elements a_{nk}, b_{nk}, and c_{nk} of matrices [A], [B], and [C] are given by :

$$A(1,1) = \alpha_1$$
$$A(2,2) = \alpha_2$$
$$A(3,3) = \alpha_3$$
$$A(4,4) = \alpha_4$$
$$A(5,5) = \alpha_5$$
$$A(6,6) = \alpha_6$$
$$A(7,7) = \alpha_7$$
$$A(8,8) = \alpha_8$$

$$B(1,1) = \omega_1^2 + \omega_2^2$$

$$B(1,2) = - \omega_2^2$$

$$B(2,1) = B(1,2)$$

$$B(2,2) = \omega_2^2 + \omega_3^2$$

$$B(2,3) = - \omega_3^2$$

$$B(3,2) = B(2,3)$$

$$B(3,3) = \omega_3^2 + \omega_4^2$$

$$B(3,4) = - \omega_4^2$$

$$B(4,3) = B(3,4)$$

$$B(4,4) = \omega_4^2 + \omega_5^2$$

$$B(4,5) = - \omega_5^2$$

$$B(5,4) = B(4,5)$$

$$B(5,5) = \omega_5^2 + \omega_6^2$$

$$B(5,6) = - \omega_6^2$$

$$B(6,5) = B(5,6)$$

$$B(6,6) = \omega_6^2 + \omega_7^2$$

$$B(6,7) = -\omega_7^2$$

$$B(7,6) = B(6,7)$$

$$B(7,7) = \omega_7^2 + \omega_8^2$$

$$B(7,8) = -\omega_8^2$$

$$B(8,7) = B(7,8)$$

$$B(8,8) = \omega_8^2$$

$$C(1,1) = 2\,\omega_1\,\{\,\zeta_1 + \zeta_2\,\}$$

$$C(1,2) = -\,2\,\omega_1\,\zeta_2$$

$$C(2,1) = C(1,2)$$

$$C(2,2) = 2\,\omega_1\,\{\,\zeta_2 + \zeta_3\,\}$$

$$C(2,3) = -\,2\,\omega_1\,\zeta_3$$

$$C(2,3) = -\,2\,\zeta_3\,\omega_1$$

$$C(3,2) = C(2,3)$$

$$C(3,3) = 2\,\omega_1\,\{\,\zeta_3 + \zeta_4\}$$

$$C(3,4) = -\,2\,\omega_1\zeta_4$$

$$C(4,3) = C(3,4)$$

$$C(4,4) = 2\,\omega_1\,\{\,\zeta_4 + \zeta_5\,\}$$

$$C(4,5) = -\,2\,\omega_1\,\zeta_5$$

$$C(5,4) = C(4,5)$$

$$C(5,5) = 2\,\omega_1\,\{\,\zeta_5 + \zeta_6\,\}$$

$$C(5,6) = -\,2\,\omega_1\,\zeta_6$$

$$C(6,5) = C(5,6)$$

$$C(6,6) = 2\,\omega_1\,\{\,\zeta_6 + \zeta_7\,\}$$

$$C(6,7) = -\ 2\ \omega_1\ \zeta_7$$

$$C(7,6) = C(6,7)$$

$$C(7,7) = 2\ \omega_1\ \{\ \zeta_7 + \zeta_8\ \}$$

$$C(7,8) = -\ 2\ \zeta_8\ \omega_1$$

$$C(8,7) = C(7,8)$$

$$C(8,8) = 2\ \omega_1\ \zeta_8$$

The force vector is given by :

$$F(1) = \alpha_1\ \omega^2\ e^{i(\omega t+\psi_1)}$$

$$F(2) = \alpha_2\ \omega^2\ e^{i(\omega t+\psi_2)}$$

$$F(3) = \alpha_3\ \omega^2\ e^{i(\omega t+\psi_3)}$$

$$F(4) = \alpha_4\ \omega^2\ e^{i(\omega t+\psi_4)}$$

$$F(5) = \alpha_5\ \omega^2\ e^{i(\omega t+\psi_5)}$$

$$F(6) = \alpha_6\ \omega^2\ e^{i(\omega t+\psi_6)}$$

$$F(7) = \alpha_7\ \omega^2\ e^{i(\omega t+\psi_7)}$$

$$F(8) = \alpha_8\ \omega^2\ e^{i(\omega t+\psi_8)}$$

The non dimensional stiffness and damping matrix are given by :

$$B(1,1) = 1 + \frac{\omega_2^2}{\omega_1^2}$$

$$B(1,2) = - \frac{\omega_2^2}{\omega_1^2}$$

$$B(2,1) = B(1,2)$$

$$B(2,2) = \frac{\omega_2^2 + \omega_3^2}{\omega_1^2}$$

$$B(2,3) = - \frac{\omega_3^2}{\omega_1^2}$$

$$B(3,2) = B(2,3)$$

$$B(3,3) = \frac{\omega_3^2 + \omega_4^2}{\omega_1^2}$$

$$B(3,4) = - \frac{\omega_4^2}{\omega_1^2}$$

$$B(4,3) = B(3,4)$$

$$B(4,4) = \frac{\omega_4^2 + \omega_5^2}{\omega_1^2}$$

$$B(4,5) = - \frac{\omega_5^2}{\omega_1^2}$$

$$B(5,4) = B(4,5)$$

$$B(5,5) = \frac{\omega_5^2 + \omega_6^2}{\omega_1^2}$$

$$B(5,6) = -\frac{\omega_6^2}{\omega_1^2}$$

$$B(6,5) = B(5,6)$$

$$B(6,6) = \frac{\omega_6^2 + \omega_7^2}{\omega_1^2}$$

$$B(6,7) = -\frac{\omega_7^2}{\omega_1^2}$$

$$B(7,6) = B(6,7)$$

$$B(7,7) = \frac{\omega_7^2 + \omega_8^2}{\omega_1^2}$$

$$B(7,8) = -\frac{\omega_8^2}{\omega_1^2}$$

$$B(8,7) = B(7,8)$$

$$B(8,8) = \frac{\omega_8^2}{\omega_1^2}$$

APPENDIX III

ELEMENTS OF MATRICES

This appendix gives the elements a_{nk}, b_{nk} of matrices [A] and [B] as mentioned in section 4.6.

The elements of matrices and force vector are given by :

$A(1,1) = I_1$

$A(2,2) = I_2$

$A(3,3) = I_3$

$A(4,4) = I_4$

$A(5,5) = I_5$

$A(6,6) = I_6$

$A(7,7) = I_7$

$A(8,8) = I_8$

$B(1,1) = K_{t1} + K_{t2}$

$B(1,2) = - K_{t2}$

$B(2,1) = B(1,2)$

$B(2,2) = K_{t2} + K_{t3}$

$B(2,3) = - K_{t3}$

$B(3,2) = B(2,3)$

$B(3,3) = K_{t3} + K_{t4}$

$B(3,4) = - K_{t4}$

$B(4,3) = B(3,4)$

$B(4,4) = K_{t4} + K_{t5}$

$B(4,5) = - K_{t5}$

$B(5,4) = B(4,5)$

$B(5,5) = K_{t5} + K_{t6}$

$$B(5,6) = - K_{t6}$$

$$B(6,5) = B(5,6)$$

$$B(6,6) = K_{t6} + K_{t7}$$

$$B(6,7) = - K_{t7}$$

$$B(7,6) = B(6,7)$$

$$B(7,7) = K_{t7} + K_{t8}$$

$$B(7,8) = - K_{t8}$$

$$B(8,7) = B(7,8)$$

$$B(8,8) = K_{t8}$$

$$F(1) = T_{m}$$